THE EFFECT OF CAPPING LAYERS, DIFFUSION BARRIERS AND STRESS ON $TiSi_2$ PHASE FORMATION.

BY

M.M. NKOSI

Dissertation presented in partial fulfillment of the requirements for the degree of

MASTER OF SCIENCE

to the

DEPARTMENT OF PHYSICS
UNIVERSITY OF ZULULAND

Promoter: Prof. O.M. Ndwandwe, Department of Physics, University of Zululand
Co-promoter: Dr. C.C. Theron, Materials Research Group, iThemba LABS, Faure

FEBRUARY 2002

Acknowledgements

This work was produced with the help and guidance of the following to whom I would like to express my sincere appreciation.

- Dr. C. C. Theron, Materials Research Group, iThemba LABS, who acted as a co-promoter, for his guidance, advice, active participation and many stimulating discussions throughout this investigation.
- Prof. O. M. Ndwandwe, Physics Department, University of Zululand, for the interest he maintained throughout the course of this investigation and the constructive discussion throughout his supervision.
- Prof. R. Pretorius, Physics Department, University of Stellenbosch, for initiating this project and for his input at the beginning of this work.
- Prof. J. Sharpey-Schafer, Director of iThemba LABS, for his encouragement and use of facilities at the iThemba LABS.
- Mr. K. Springhorn, Mr. C. Doyle, Mr. S. Marsh and Mr. L. Ashworth for their assistance during the running of experiments and maintenance of laboratory equipments.
- Mr. T. Ntsoane for his friendly assistance and efficient operation of the X-ray diffraction.
- Miss. L. Godana, Mrs. G. Stone and Mr. T. Kubeka for their help and encouragement.
- The Staff and students at the Materials Research Group, iThemba LABS.
- My Parents and the rest of the family for their moral support.
- God, my Creator, for giving me the Strength throughout this project.

Abstract

Metal silicides continue to be an important part of the design philosophy in semiconductor technology due to their application as contacts or interconnects. Among these silicides, titanium disilicide is currently the most widely used as it possesses the lowest resistivity (14μΩ-cm) of all silicides, a low contact resistance and a good thermal stability. Titanium-silicide formation with and without capping layers, through diffusion barrier layers and on stressed Si(100) substrate was studied.

The oxidation of titanium makes accurate kinetics measurements very difficult. Capping layers, namely Al_2O_3 and MgO, and sandwich technique were used in attempting to limit the unwanted oxidation. It was found that both capping layers reduced the oxygen concentration in the unreacted Ti film by 30% compared to the uncapped samples. It was also found that the reaction was faster in the MgO capped samples and slower in the Al_2O_3 capped samples. In the sandwich technique, the oxygen concentration was found to be less by 35% and the reaction was fast at high temperatures compared to the silicide formation in the unsandwiched samples.

In attempting to control the metal concentration at the growth interface diffusion barrier layers were used. Cr and Zr were used as diffusion barrier layers. Both barrier layers were found to react with silicon to form $CrSi_2$ and $ZrSi_2$ respectively. It was found that both barrier layers moved deeper into the samples as more silicide was formed on top, which indicates that Si is the dominant diffusing species during Ti-silicide formation. Both barrier layers delayed the formation of $TiSi_2$.

Tensile and compressive stresses were induced by depositing different thicknesses of Si_3N_4 and SiO_2 on the backside of Si(100) wafers. The reflection of laser light was used to measure the radius of curvature which was related to stress using Stoney's equation. It was found that the silicide phase formation was faster in samples under tensile stress and slower in samples under compressive stress. The cube root of time gave the best fit to the data for all sample groups. Therefore the $TiSi_2$ formation kinetics was neither diffusion nor reaction limited.

Singeniso

Emasilisayidi lentiwe ngalokusansimbi asachubeka nekubamba lichaza lelikhulu ekutfutfukisweni kwetekhinoloji yemasekhethi etintfo tagezi. Kulamasilisayidi, iTiSi_2 isetjentiswa kakhulu kunawowonkhe kulesikhatsi samanje ngenca yekutsi inerezistensi lengaphasi kunawo-onkhe emasilisayidi (14μΩ-cm) kanye nestabilithi lesihle kakhulu. Lomculu umayelana nekufundvwa kwekwakheka kweTiSi_2 umakusetjentiswa emaleya lasatimbonyo nobe angakasetjentiswa nendzima ledlalwa kusebentisa iSilikhoni (Si) ledvonsekile.

IThithaniyamu (Ti) yatiwakakhulu ngekutsandza kuhlangana neoxygen, loku kwenta kutsi kubematima kakhulu kufundza ngekukhula kweTiSi_2 emva kwesikhatsi lesitsite. Kusebentisa emaleya lasatimbonyo, njenge Al_2O_3 ne MgO, kanye nekuhlanganisa emasampula lamabili ndzawonye, ngitonatindlela letisetjentisiwe ekutameni kwehlisa lizinga lekuhlangana kweTi kanye ne-oxygen lengafuneki. Kutfolakale kutsi emaleya lasetjentiswe satimbonyo ehlise linani le-oxygen ngemaphesenti layi 30. Kuphindze kwatfolakala kutsi iTiSi_2 yakheke masinyane kumasampula lambonywe ngeMgO uma achatsaniswa nalawo lambonywe nge Al_2O_3. Emasampuleni lahlanganiswe ndzawonye kutfolakale kuts linani le-oxygen lehle ngemaphesenti layi 35. Nekwakheka kwe TiSi_2 kutfolakale kutsi kwenteke masinyane emazingeni ekushisa lasesetulu uma achatsaniswa nemasampula lahamba ngawodvwa.

Ekuzameni kucondzisa linani lemetali lapho kwakheka kwenteka khona, kusetjentiswe emaleya lavumela ema-atomu kutsi ahambe emkhatsini nawo (diffusion barriers). Kusetjentiswe iCr kanye ne Zr. Womabili lamaleya atfolakale kutsi ahlangene neSi kwakheka iCrSi_2 ne ZrSi_2. Kuphindze kwatfolakala kutsi womabili lamaleya ahambele ekhatsi nemasampula uma kwakheka isilisayidi lenyenti ngetulu. Loku kusho kutsi iSi ngiyo lehambako uma kwakheka iTiSi_2. Womabili emaleya akubambele kwakheka kwe-TiSi_2.

Kudvonsekela ngaphandle (tensile stress) kanye nekudvonseleka ngekhatsi (compressive stress) kwentiwe ngekutsi kuvuvutelwe emaleya lahlukene iSi_3N_4 kanye ne SiO_2 ngasemuva kwetingcwengcwe teSi(100). Kutfolakale kutsi kwakheka kwe-silisayidi kwenteke masinyane emasampuleni ladvonsekele ngaphandle kantsi kwenteke kancane kulawo ladvonsekele ngekhatsi.

Table of Contents

1. Background and Scope of investigation **1**

1.1. Silicides in semiconductor technology 1

1.1.1. Device integration 2

1.1.2. Metal-silicon interaction 2

1.2. Titanium-silicide formation 3

1.2.1. Phase formation 4

1.2.2. Formation kinetics 4

1.3. Prediction of phase formation sequence 5

1.3.1. Introduction 5

1.3.2. Effective Heat of Formation model (EHF) 6

1.3.3. Concentration Controlled Phase Selection (CCPS) 9

1.4. Scope of Investigation 12

2. Experimental Procedure **13**

2.1. Sample Preparation 13

2.1.1. Vacuum Deposition 13

2.1.2. Vacuum Annealing 15

2.2. Sample Characterization 15

2.2.1. Rutherford Backscattering Spectrometry (RBS) 15

2.2.2. X-ray Diffraction (XRD) 20

2.2.3. Stress Measurement in thin films 21

3. Silicide formation in the Ti-Si system **23**

3.1. Introduction 23

3.2. Phase formation 25

3.2.1. RBS computer simulation 25

3.2.2. RBS measurements 27

3.2.3. XRD simulation 30
3.2.4. XRD measurements 32
3.2.5. Discussions 34
3.3. Oxidation Limiting Techniques 35
3.3.1. Capping layers (Al_2O_3 and MgO) 35
3.3.2. Sandwich technique 41
3.3.3. Discussions 46
3.4. Summary and Conclusion 47

4. Ti-silicide formation through barriers 48
4.1. Introduction 48
4.2. Cr barrier layer 49
4.2.1. Sample preparation 49
4.2.2. RBS Results 49
4.2.3. XRD Results 51
4.3. Zr barrier layer 54
4.3.1. Sample preparation 54
4.3.2. RBS Results 54
4.3.3. XRD Results 56
4.4. Summary and Conclusion 59

5. Effect of stress on Ti-silicide formation 61
5.1. Introduction 61
5.2. Sample preparation and stress measurements 62
5.3. RBS Analysis 64
5.4. XRD Analysis 67
5.5. Discussions and Summary 70

6. Summary and Conclusion 72

Appendix A 75

References 78

List of Figures

1.1	Schematic diagram of a semirecessed NMOS device	1
1.2	EHF and phase diagrams of the Cr-Si binary system	8
1.3	EHF and phase diagrams for the Co-Si binary system	10
1.4	Schematic diagram for normal and direct formation of $CoSi_2$	10
2.1	Schematic diagram of HV evaporation chamber	14
2.2	Schematic representation of an elastic backscattering	16
2.3	Schematic diagram of a sample with a thin film on the backside	22
3.1	EHF and phase diagrams of the Ti-Si binary system	24
3.2	RUMP simulation of different phases in the Ti-Si system	26
3.3	RBS spectrum of sample annealed at 550°C for 30 minutes	28
3.4	RBS spectrum of sample annealed at 550°C for 120 minutes	28
3.5	Ti-silicide thickness vs. time plots	29
3.6	RBS spectrum of sample annealed at 600°C for 60 minutes	29
3.7	Powder diffraction pattern lines of Ti_5Si_4 and TiSi	31
3.8	Powder diffraction pattern lines of C49-$TiSi_2$ and C54-$TiSi_2$	31
3.9	XRD spectra of as deposited samples and after annealing at 550°C	33
3.10	XRD spectra of samples annealed at 600°C and 650°C	33
3.11	RBS spectrum of Al_2O_3 capped sample annealed at 530°C	37
3.12	RBS spectrum of MgO capped sample annealed at 530°C	37
3.13	$TiSi_2$ thickness vs. time plots	38
3.14	XRD spectra of as deposited samples from each set	40
3.15	XRD spectra of samples from each set annealed at 530°C for 64 minutes	40
3.16	XRD spectra of samples from each set annealed at 530°C for 144 minutes	40

3.17	Schematic diagram of two sandwiched samples	41
3.18	RBS spectra of sandwiched and control samples annealed at 550°C	42
3.19	RBS spectra of sandwiched and control samples annealed at 600°C	43
3.20	RBS spectra of covered and uncovered parts annealed at 550°C	44
3.21	RBS spectra of covered and uncovered parts annealed at 600°C	45
4.1	RBS spectra of samples from each set annealed at 570°C for 30 minutes	50
4.2	RBS spectra of samples from each set annealed at 660°C	50
4.3	XRD spectra of as deposited samples from each set	52
4.4	XRD spectra of samples annealed at 570°C	52
4.5	XRD spectra of samples annealed at 630°C	53
4.6	XRD spectra of samples annealed at 700°C	53
4.7	RBS spectra of as deposited samples and annealed 570°C for 30 minutes	55
4.8	RBS spectra of both sets of samples annealed at 660°C	55
4.9	XRD spectra of as deposited samples from both sets	57
4.10	XRD spectra of samples annealed at 570°C	57
4.11	XRD spectra of samples annealed at 660°C	58
4.12	XRD spectra of samples annealed at 700°C	58
4.13	$TiSi_2$ thickness vs. temperature plots	60
5.1	Schematic diagram showing total stress	63
5.2	RBS spectra of samples from each group annealed at 530°C	65
5.3	RBS spectra of samples annealed 600°C	65
5.4	Plot of $TiSi_2$ thickness versus cube root of time	66
5.5	XRD spectra taken from as deposited samples	68
5.6	XRD spectra taken from samples annealed at 530°C for 16 minutes	68
5.7	XRD spectra taken from samples annealed at 530°C for 64 minutes	69
5.8	XRD spectra taken from samples annealed at 600°C	69
5.9	Plot of stress as a function of temperature	71

List of Tables

1.1	Comparison of resistivity values for some silicides and metals	3
3.1	Height ratios of the Ti and Si in silicide layers	26
3.2	Summary of XRD results	39
4.1	Summary of the Cr XRD results	51
4.2	Summary of the Zr XRD results	56
4.3	Summary of phase formation thickness	59
5.1	Radius of curvature and stress related values	62
5.2	Summary of XRD results	67

Chapter 1

Background and Scope of investigation

1.1. Silicides in semiconductor technology

Silicon has become the dominant semiconductor material in integrated-circuit technology because of its ability to grow a stable oxide [May-90]. Silicon dioxide forms the basis of the planar technology. In industrial practice, silicon dioxide layers are frequently formed by thermal oxidation of silicon in the temperature range 900 to 1200°C. The thermal oxidation process is one of the steps in the fabrication of silicon semiconductor devices and integrated circuits. Thermal oxides are used to mask selectively against dopant diffusion, to passivate device junctions, and for device isolation. **Fig 1.1** shows the cross section of a semirecessed oxide NMOS device (*n*-channel metal-oxide-Si field-effect transistor).

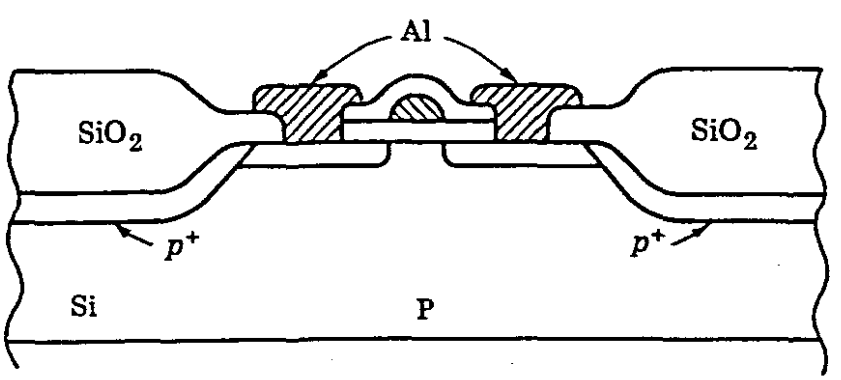

Fig. 1.1 Schematic diagram of the cross section of semirecessed oxide NMOS device [May-90]

1.1.1. Device Integration

The concept of device integration is founded on the simple observation that the computing power (or density of data storage) available on the surface of a chip increases greatly as the size of the individual device features is reduced and the devices packed very closely together [Gro-89]. The operating speed of a microelectronic circuit is improved when the lengths of the interconnecting paths between devices are shortened, and the power dissipated in devices also decreases with size. The power consumption of a complete system can thus be reduced by miniaturization of the component device. It was predicted that by the year 2000 it would be possible to pack together about 1 billion (10^9) individual devices onto the surface of a silicon chip. Many of these densely populated chips contain mostly metal-oxide-semiconductor (MOS) devices.

1.1.2. Metal-Silicon Interaction

Metal silicides are widely used as contacts and interconnects in silicon based microelectronic devices [Pre-97]. Metal silicides are usually formed by a reaction between a deposited metal layer and a silicon substrate. The interactions between metal film layers and silicon typically take place at temperatures well below the melting point of the product and the reactants. The specific phase depends on the temperature of formation. Disilicides, monosilicides and metal-rich silicide formation takes place when bonded silicon and metallic bonded metal atoms react to form compounds. The phase diagrams for binary metal-silicide-forming systems usually show several equilibrium phases [May-90]. Some of these phases are present as detectable growth phases under steady-state annealing conditions. In thin film systems, only one compound phase usually forms between two components, silicon and metal. It is believed that phase formation in thin films is dictated by kinetics rather than by thermodynamics. After the metal layer has been totally consumed in forming the first phase, a second phase, when present in the phase diagram, will form at higher and/or at longer annealing times [May-90]. For a new phase to form, it is necessary for the atoms of the metal and silicon to get together near the interface and form a nucleus of the appropriate composition and structure. In a bulk system usually most or all of the compound phases given by the phase diagram are found.

1.2. Titanium-Silicide Formation

Titanium silicide is a material of great technological importance because of its widespread use in the self-aligned silicide (salicide) process for the fabrication of field effect metal oxide-semiconductor transistors [Via-00]. $TiSi_2$ is currently the most widely used silicide for ultra large scale integrated circuits as it possesses the lowest resistivity of all silicides (see **Table 1.1**), a low contact resistance and a good thermal stability [Waa-99]. The thermal stability of a silicide is its ability to resist degradation when subjected to a prolonged heat treatment at high temperatures [Sab-00]. To be used in integrated circuits a silicide must have sufficient thermal stability to withstand the entire thermal processing that is required such as layer deposition and dielectric reflow. Thermal stability is affected by decreasing film dimensions (i.e. line width and thickness) and by substrate nature (polycrystalline silicon). Therefore the thermal stability will become more and more important in future.

Table 1.1: Comparison of resistivity values for some silicides and metals [Nic-83, Gro-89].

Material	Resistivity (μΩ-cm)
CoSi	150
Co_2Si	66
WSi_2	55
$NiSi_2$	39
Ni_2Si	24
NiSi	20
$CoSi_2$	14
$TiSi_2$	14
Al	3
Cu	2

1.2.1. Phase Formation

Many studies have been carried out regarding first phase formation during the reaction between a thin Ti film and a Si substrate [Pre-93B]. The phase formation sequence is by no means well established and varying reports can be found in the literature. For example, the $TiSi_2$ phase is reported to be the only phase found for temperatures greater than 500°C [Bey-85]. In another study $TiSi_2$ was also reported as a first phase, but titanium–rich silicides were observed to grow on top of the disilicide layer [Ben-85]. Contrary to these reports, other studies show that all the titanium is converted to TiSi prior to formation of $TiSi_2$ at temperatures between 450 and 700°C [Pic-88]. In low temperature reactivity investigations a silicide corresponding to the monosilicide was also found together with unreacted but intermixed material. The formation of TiSi at temperatures of 450 [Nem-85] and 600°C [Wei-85] has also been reported for rapid thermal annealing (RTA). However, not all RTA studies show the initial formation of TiSi, as there is evidence for the first phase formation of Ti_5Si_4 after 6s RTA at 600°C [Dex-88]. In contrast to reports of the formation of an initial crystalline phase, the formation of an amorphous Ti-Si alloy before the appearance of any silicide is reported for temperatures not exceeding 450°C. The complexity of the Ti-Si system is further reflected not only by the conflicting reports on identification of a first phase, but also by numerous reports of simultaneous phases that are found initially. A layered structure containing Ti_5Si_3, TiSi and $TiSi_2$ is reported for e-beam-deposited titanium, while Ti_5Si_3, Ti_5Si_4 and TiSi were found initially at intermediates between 400 and 600°C [Lak-89]. On the other hand the presence of Ti_5Si_3 and TiSi in sputter-deposited samples was reported [Hsu-87].

1.2.2. Formation Kinetics

Growth kinetics of a reaction is classified into diffusion-controlled or reaction-controlled kinetics. In the diffusion-controlled case the main characteristic is that the thickness of the silicide formed increases proportionally to the square root of time. The relation is given by $x^2 = k_D t$, where x is the thickness of the growing phase, t is the time and k_D is the rate constant. The limiting step is the diffusion of one or both of the components (Ti and Si in the case of Ti-silicide) across the growing layer. In the reaction-controlled case the rate of formation is the limiting factor, hence reaction-

controlled. In this case the relation is given by $x = k_R t$, where x and t are defined as above and k_R is the rate constant. The relationship between the rate at which the phase formation increases in thickness and the time is dependent on whether the diffusion or the reaction is the slowest part of the phase formation. The slower of the two processes will dominate the kinetics. The kinetics of any system can be determined by plotting x versus $t^{1/2}$ and x versus t. If the x versus $t^{1/2}$ graph gives a straight line the kinetics is diffusion-controlled or non-linear. If the kinetics is reaction-controlled x versus t will give a straight line graph (linear kinetics). Annealing thin titanium on silicon at sufficiently high temperatures and sufficiently long time always leads to the formation of $TiSi_2$ eventually [Lak-89], but the kinetics of the reaction is not so reproducible [Hun-83]. The kinetics of $TiSi_2$ formation depends upon the orientation of the substrates, with $TiSi_2$ growing linearly with time on Si(111) and parabolically with time on Si(100) [Pic-88]. When the total silicide thickness is considered, a nearly parabolic growth rate on all substrates is reported [Pic-88].

1.3. Prediction of phase formation sequence

1.3.1. Introduction

There has been considerable interest in predicting first phase compound formation and subsequent phase formation sequence in binary thin film systems [Pre-93A]. Unlike the bulk case, not all of the compound phases present in the equilibrium phase diagram are observed. In the case of silicides for instance, only one compound phase usually forms between two components, silicon and metal. For example, nickel films deposited on silicon (or vice versa) form an intermediate layer of Ni_2Si at temperatures above 200°C, with no indication of the presence of the other equilibrium phases as long as both unreacted nickel and silicon are still available. For much thicker diffusion couples, say greater than 10μm, usually most or all the compound phases given by the phase diagram are found. The latter case is referred to as the bulk case, in contrast to the thin film case, where single phase formation usually takes place. Apart from the obvious academic interest, knowledge of phase formation sequence should enable the materials scientist to control experimental parameters in such a way as to form specific phases with desirable properties. One of the first rules for predicting phase formation was that of Walser and Bené which

states: *The first compound nucleated in planar binary reaction couples is the most stable congruently melting compound adjacent to the lowest temperature eutectic on the bulk equilibrium phase diagram.*

1.3.2. Effective Heat of Formation Model (EHF)

The above-mentioned rule, however, does not make direct use of the thermodynamic data, such as heats of formation and entropy. A fundamental approach in predicting first phase formation was taken by Pretorius et al. [Pre-93] by giving an extensive description of the Effective Heat of Formation (EHF) model. In this model an effective heat of formation is defined which depends on the available concentration of the reacting atomic species at the growth interface. By choosing the effective concentration of the reaction to be that of the composition of the lowest eutectic (or liquidus minimum), the EHF model has been successfully used to predict silicide phase formation sequence and to explain how the presence of impurities can alter phase formation sequence.

The model is based in part of the fact that the driving force for a process to take place can be given by the change in the Gibbs free energy,

$$\Delta G^\circ = \Delta H^\circ - T\Delta S^\circ \qquad (1.1)$$

For solid state interaction ΔH° is a good measure of the change in free energy ΔG° because the change in entropy ΔS° is usually only of the order of 0.001 kJ deg^{-1} mol^{-1} of atoms. It should therefore be possible to use heats of formation to predict phase formation sequence when activation or nucleation barriers do not exist, as a system would always want to go to its lowest possible free energy state.

The reaction to form CrSi is favored when the available concentration matches the compound concentration. An effective heat of formation $\Delta H'$ for a compound is defined as:

$$\Delta H' = H^0 \times \frac{\text{effective concentration limiting element}}{\text{compound concentration limiting element}} \qquad (1.2)$$

Where $\Delta H'$ and ΔH^0 are expressed in kJ mol^{-1} of atoms. To illustrate the concept of an effective heat of formation ($\Delta H'$), consider for example the solid state interaction

between Cr and Si to form the compound phase CrSi (Compound concentration of 50 at. % Si and 50 at. % Cr). Suppose we originally have an ensemble of 10 atoms at the reaction zone, of which five are Si and five are Cr. In this case the available or effective concentration of atoms that can partake in the reaction is 50 at. % Si and 50 at. % Cr. When phase formation takes place, all the available Cr and Si atoms would be used up in the reaction and five CrSi molecules would be formed. Since all the available atoms are used up in this reaction, the total amount of heat released would be given by the standard heat of formation ($\Delta H°$). For this case the effective heat of formation is equal to the standard heat of formation, i.e. $\Delta H' = \Delta H°$. Next consider the case where there are only three Cr atoms in an ensemble of 10 atoms, the rest being Si atoms. In this case the available or effective concentration of atoms that will be engaged in the reaction is 30 at. % Cr and 70 at. % Si. Now clearly, when forming the compound phase CrSi, only three Cr and three Si atoms would be used, the rest of the Si atoms being in excess. For this particular case it can be seen that Cr is the limiting element in the reaction to form CrSi, while Si is in excess. For the above-mentioned case, where the relative available concentrations at the growth interface are assumed to be 30 at.% Cr and 70 at.% Si the effective heat of formation for growth of CrSi is given by:

$$\Delta H' = -30.2(0.30/0.50) = -18.1\,\mathrm{kJ(mol.at.)^{-1}} \qquad (1.3)$$

With **eqn. 1.2** *the effective heat of formation of any compound can be calculated as a* function of the concentration of the reacting species. For a relative Si concentration less than 50 at. %, Si is the limiting element, whereas for larger silicon concentration Cr becomes the limiting element. Such effective heat of formation diagrams can be calculated for all the chromium silicides phases and are given with the Cr-Si phase diagram in **Fig. 1.2**.

It can be seen that for each phase the most negative value of $\Delta H'$, and thus the largest energy released from the system for each silicide that is forming, occurs when the Cr and Si concentrations match that of a particular compound phase, e.g. CrSi. In such a case, as **eqn. 1.2** clearly demonstrates the concentration ratio is unity. Effective heats of formation diagrams are thus readily constructed by plotting the heats of formation ΔH^0, expressed in kJ(mol of atoms)$^{-1}$ of each compound in the binary system at its compositional concentration and completing the triangulation by connecting these points to the end points of the concentration axis.

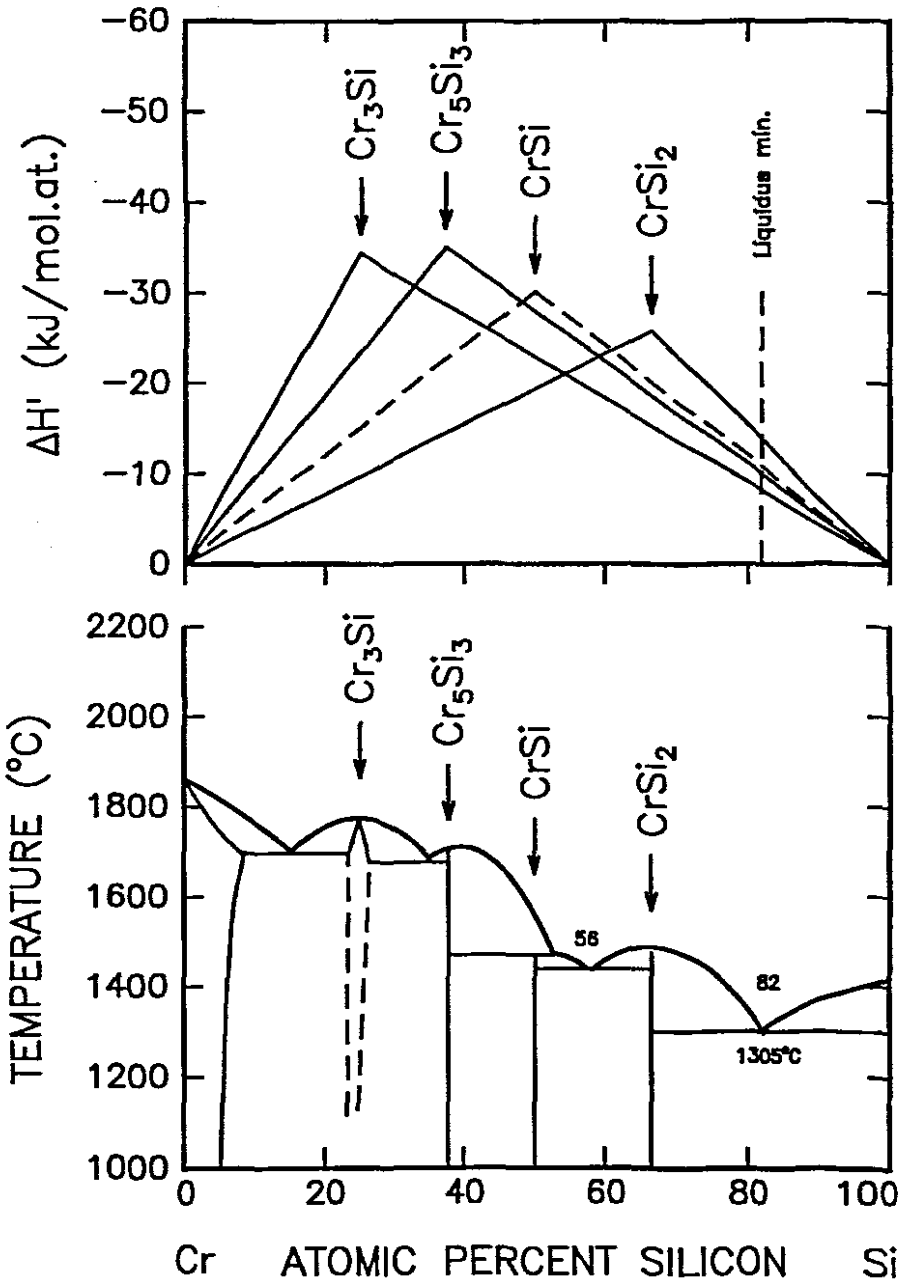

Fig. 1.2 The effective heat of formation ($\Delta H'$) and the phase diagrams of the Cr-Si binary system. Each triangle of the effective heat of formation represents the energy released per mole of available atoms at a given effective or available concentration as a function of concentration during formation of a particular chromium silicide phase.

1.3.3. Concentration Controlled Phase Selection (CCPS)

The effective heat of formation and the phase diagram for the Co-Si system is given in **Fig. 1.3**. During normal cobalt silicide formation the effective concentration at the growth interface is controlled by the liquidus minimum. At this concentration according to the EHF model, it can be seen from **Fig. 1.3** that Co_2Si has the most negative $\Delta H'$ and is expected to form first. For the case of thin Co on thick silicon all the Co will be consumed to form Co_2Si and the effective concentration moves to the left of the EHF model diagram (see **Fig. 1.3**) until an effective concentration of about 60 at. % is reached where CoSi formation should lead to the most negative $\Delta H'$. After complete transformation of Co_2Si to CoSi the effective Co concentration at the growth interface decreases further to a concentration of less the 40 at. % Co, where $CoSi_2$ formation is thermodynamically favoured.

Epitaxial growth occurs when the atoms in the silicide are aligned with the atoms in the underlying single crystal Si substrate [Waa-99]. Epitaxial silicides are found to be advantageous due to their improved electrical resistance, uniformity, low contact resistivity, and better thermal stability. $CoSi_2$ can form epitaxially on all silicon orientations as like silicon it crystallizes in the cubic system and has a close lattice match with silicon. Growth of epitaxial cobalt disilicide on single crystal silicon has been demonstrated by evaporating Co directly onto silicon in vacuum followed by subsequent annealing. During heating Co_2Si is the first phase to form followed by CoSi and subsequent $CoSi_2$ formation, the final phase forming at temperatures above 500°C.

It has been demonstrated that epitaxial $CoSi_2$ can be formed directly as the first phase through the use of a Ti interlayer (see **Fig. 1.4**). In this approach the Co diffuses through the Ti barrier layer and the process is referred to as titanium-interlayer mediated epitaxy (TIME). It is thought that the Ti interlayer plays two roles, namely, as a getterer for removing the native oxide layer on the Si surface and as a barrier preventing Co_2Si and CoSi formation. It was proposed [Pre-97] that $CoSi_2$ is formed by concentration controlled phase selection (CCPS). A general approach is also proposed whereby phase formation can be selected by controlling the

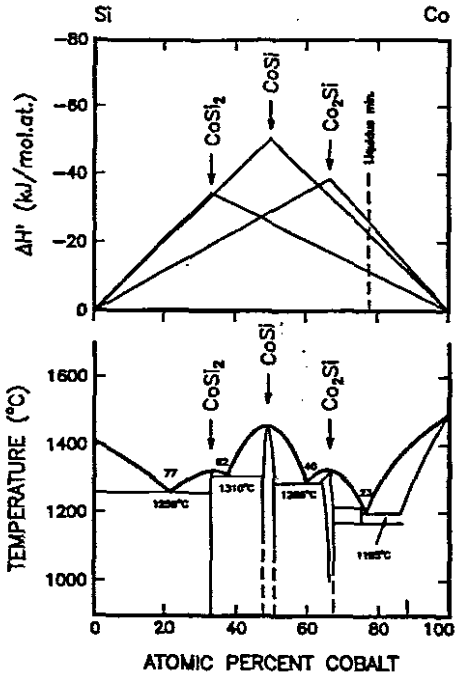

Fig. 1.3 The effective heat of formation ($\Delta H'$) diagram for compound phase formation (top) and the phase diagram (bottom) for the Co-Si system.

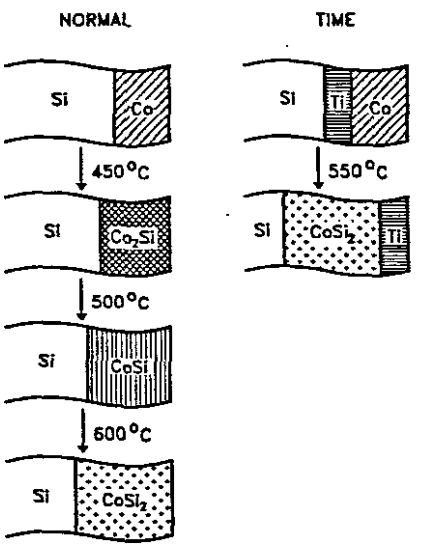

Fig 1.4 Normal $CoSi_2$ formation and direct formation of $CoSi_2$, by titanium interlayer mediated epitaxy (TIME). In the latter case the Co reacts with the silicon to form $CoSi_2$, by diffusing through the Ti barrier layer, which is then displaced to the surface.

concentration of the reactants at the growth interface. For the TIME case, the Ti interlayer serves as a diffusion barrier to the Co thereby moving the effective concentration to the region where $CoSi_2$ formation would lead to the biggest change in free energy (see **Fig. 1.3**) and therefore $CoSi_2$ is formed first.

Another example of concentration controlled phase selection (CCPS) is the formation of $NiSi_2$ at temperatures as low as 350°C in the presence of a NiZr diffusion barrier. The normal temperature for $NiSi_2$ formation with single crystal silicon is above 750°C and it is therefore interesting that $NiSi_2$ can form at temperatures as low as 350°C in the presence of a NiZr diffusion barrier. This anomalous behavior can be explained thermodynamically. In the case of normal $NiSi_2$ formation, NiSi reacts with single crystal silicon to form $NiSi_2$, whereas in Si<>/NiZr/Ni structures, $NiSi_2$ forms directly as the first phase. The heats of reaction ΔH_R^0 for these two cases can be calculated from the ΔH^0 values as follows:

(i) *Normal $NiSi_2$ formation (Si/Ni):*

NiSi	+	Si	=	$NiSi_2$
2(-42.4)		1(0)		3(-29.3)

$\Delta H_R^0 = (-3.1)/3 = -1.0 \pm 4.4$ kJ (mol. at.)$^{-1}$

(ii) $NiSi_2$ formation with barrier (Si/NiZr/Ni):

Ni	+	2Si	=	$NiSi_2$
1(0)		1(0)		3(-29.3)

$\Delta H_R^0 = (-87.9)/3 = -29.3 \pm 2.9$ kJ (mol. at.)$^{-1}$

The heat of reaction for $NiSi_2$ formation from the preceding NiSi phase, without diffusion barrier is for all practical purpose zero and it is only at higher temperatures that the entropy term in equation $\Delta G = \Delta H^0 - T\Delta S^0$, makes the free energy negative. In the case of $NiSi_2$, first phase formation in Si<>/NiZr/Ni structures, the heat of reaction is very negative, as there is direct interaction between Ni and Si and a high temperature is therefore not needed to make the reaction thermodynamically possible.

1.4. Scope of investigation

Titanium disilicide is currently the most widely used silicide for ultra large scale integrated circuits, as it possesses the lowest resistivity of all silicides. The purpose of this work was to understand better the phase formation by solid state interaction between thin Ti films and Si substrate. Various thicknesses of titanium thin films were deposited on to silicon substrates using a vacuum deposition chamber. Reaction was induced by annealing samples in a vacuum furnace. Rutherford Backscattering Spectrometry (RBS) and X-ray Diffraction (XRD) were used to identify the composition and the crystallographic phases of the thin films. These experimental techniques are discussed in **Chapter 2**. Titanium is known to be a getterer of oxygen during titanium-silicide formation. In **Chapter 3** the solid state reaction between Ti thin film and Si substrate with and without capping layers is discussed. Al_2O_3 and MgO capping layers and a sandwich technique were used in attempting to limit the unwanted oxidation in the Ti-silicide formation. **Chapter 4** deals with Ti-silicide formation through diffusion barriers. Cr and Zr were used as barrier layers. It was found that both barrier layers delayed the formation of the $TiSi_2$ phase. The effect of stress on Ti-silicide formation is discussed in **Chapter 5**. A metallic film (Si_3N_4) and an insulator (SiO_2) were used to induce stress on the backside of the silicon substrate. Si_3N_4 causes tensile stress on the front side of the silicon substrate whereas SiO_2 causes compressive stress. Summary and conclusion of this investigation is presented in **Chapter 6**.

Chapter 2

Experimental Procedure

2.1. Sample Preparation

Single crystal silicon wafers were used in this work. Samples were cut from 625μm thick wafers to squares of 9 x 9 mm^2 sizes. *Si(100)* wafers were used throughout this study. The samples were first cleaned in an ultrasonic bath with organic solvents. The cleaning was done in the following procedure: methanol, acetone, trichloroethylene, acetone, methanol and finally distilled water. The samples were then etched in a 20% solution of HF to remove the native oxide layer. After cleaning, the samples were mounted on sample holders which were fitted into a high vacuum evaporation chamber.

2.1.1. Vacuum Deposition

The evaporation chamber consisted of two areas, separated by a baffle valve (see **Fig. 2.1**). The top area consisted of three crucibles onto which materials to be evaporated were loaded, an electron gun, a quartz thickness monitor and a sample changer. The quartz thickness monitor was used to determine the rate at which the depositions were done as well as the thickness of the evaporated layers. The sample changer can hold up to six sample holders. Each sample holder can hold up to ten samples. The three crucibles were initially cleaned with fine emery paper before loading the metals to be evaporated. The bottom area of the chamber consisted of six ion pumps, a Ti-sublimation pump and a cryopanel. This part of the evaporator

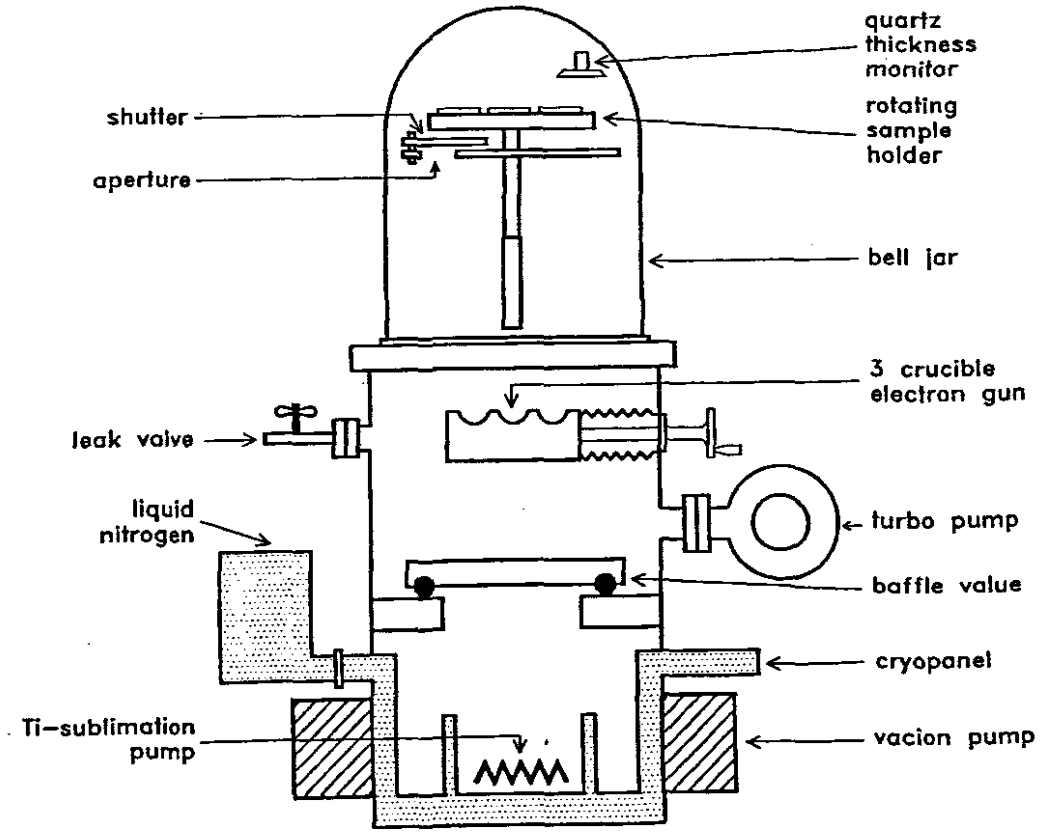

Fig. 2.1 A Schematic representation of the vacuum deposition chamber used to prepare thin film structures.

was kept under vacuum during the cleaning of the crucibles and the loading of the samples. This was done by keeping the baffle valve closed and keeping the ion pumps switched on. The turbo and rotary pumps were used to reduce the pressure of the top area to about 3×10^{-6} kPa. At this point the baffle valve was opened to allow the ion pumps to reduce the pressure to 2×10^{-7} kPa. Liquid nitrogen was poured in the cryopanel to make the pressure better than 3×10^{-8} kPa. The metal to be deposited was first preheated to release adsorbants before the actual deposition was carried out. After deposition the samples were allowed to cool down for an hour in vacuum before being transferred to a vacuum furnace.

2.1.2. Vacuum Annealing

After deposition the samples were loaded in a vacuum furnace. The furnace consisted of a carousel, which can accommodate up to eight boats. Each boat, which can load six samples, was first preannealed to release any adsorbed gases. The boats were able to slide in and out of the tube furnace without breaking the vacuum. A programmable Eurotherm unit was used to control the temperature of the furnace. All anneals were done in vacuum at a pressure better than $3x10^{-8}$ kPa. This pressure was obtained by using a turbo pump and a liquid nitrogen cryopanel. Samples were left to cool down for an hour before letting nitrogen gas in to break the vacuum.

2.2. Sample Characterization

2.2.1. Rutherford Backscattering Spectrometry

Rutherford backscattering spectrometry (RBS) is a simple, fast and direct method for obtaining elemental depth profiles in solids [Chu-78]. During analysis by RBS, a beam of monoenergetic and collimated alpha particles (^{4}He nuclei) impinges on a target and particles scattered backward by angles more than 90° from the incident direction are detected. The backscattered particles are detected by a solid state detector. There are three basic concepts, which are of importance in RBS, each responsible for an analytic capability of the method:

(i) the kinematic factor k (mass analysis)

(ii) the differential scattering cross-section (quantitative analysis)

(iii) the energy loss (depth analysis)

Kinematic factor k

When a particle of mass m, moving with constant velocity, collides elastically with a stationary particle of mass M, energy will be transferred from the moving to the stationary particle. The energy of the backscattered particle is determined by its own mass, the mass of the target atom and the scattering angle, measured in laboratory coordinates. The typical geometry for backscattering is shown in **Fig. 2.2.** The kinematic energy is defined as the ratio of the projectile energies after (E_1) and before (E_o) collision [Chu-78]. Making use of conservation of energy and momentum it can be shown that:

$$k = \frac{E_1}{E_0} = \left[\frac{m\cos\theta + (M^2 - m^2\sin^2\theta)^{1/2}}{m+M} \right]^2 \qquad (2.1)$$

This equation indicates the dependence of the energy of the backscattered particle on the target mass. If the energy of the backscattered particle is measured at a known angle θ then the mass M of the atom from which it is scattered can be calculated.

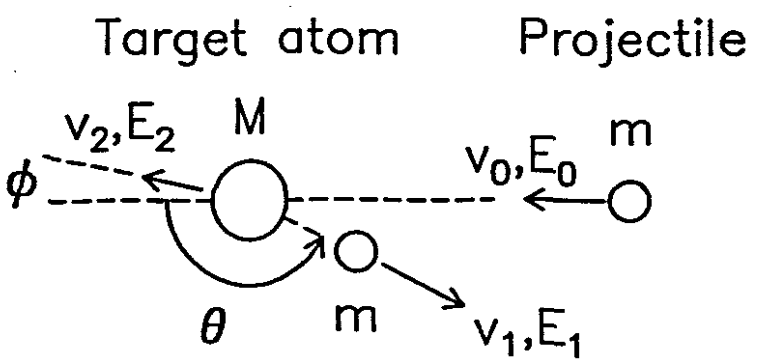

Fig. 2.2 A schematic representation showing an elastic backscattering of a light alpha particle from a heavier atom.

Differential scattering cross-section

The differential scattering cross-section is given by the following expression, in laboratory coordinates [Chu-78]:

$$\frac{d\sigma}{d\Omega} = \left[\frac{zZe^2}{4E_0}\right]^2 \frac{4}{\sin^4\theta} \frac{\left\{\cos\theta + \left[1 - \left(\frac{m}{M}\sin\theta\right)^2\right]^{1/2}\right\}^2}{\left[1 - \left(\frac{m}{M}\sin\theta\right)^2\right]^{1/2}} \qquad (2.2)$$

where *z and Z are the atomic numbers of the projectile and target atoms* respectively, E_0 is the energy of the projectile immediately before scattering and Ω is the finite solid angle spanned by the detector. The following significant functional dependences can be derived from the above equation:

(i) $d\sigma/d\Omega$ is proportional to z^2. Higher backscattering yields are possible with heavier particle beams.

(ii) $d\sigma/d\Omega$ is proportional to Z^2. Backscattering spectrometry is much more sensitive to heavy elements than to light ones.

(iii) $d\sigma/d\Omega$ is inversely proportional to the square of the projectile energy ($\propto E^{-2}$). The yield of scattered particles rises rapidly with decreasing bombarding energy.

(iv) $d\sigma/d\Omega$ is axially symmetrical with respect to the axis of the incident beam and therefore is a function of θ only.

(v) $d\sigma/d\Omega$ is approximately inversely proportional to $\sin^4\theta$ when $m << M$. This gives a rapidly increasing yield as the scattering angle θ is reduced.

Energy loss dE/dx

When a projectile penetrates a target, it loses its energy throughout its trajectory to the electrons of the target atoms by ionization and excitation as well by nuclear collisions. When the projectile undergoes an elastic collision it can change its trajectory into an outward direction with respect to the target surface. During its outward path it again loses energy to the target atoms until it emerges from the target. By measuring the energy loss of the projectile as it moves into the sample and is backscattered onto the detector it is possible to determine the depth to which the particle has penetrated. The energy loss per unit length is expressed as stopping power, $\frac{dE}{dx}$. The stopping cross section is given as $\varepsilon = \frac{1}{N}\frac{dE}{dx}$, where N is the atomic density of the target. Both stopping power and cross section are dependent on the target composition and incoming beam energy. In general though for small variations in energy the stopping power $\left(\frac{dE}{dx}\right)$ does not change much and the relationship between energy loss (ΔE) and depth (t) can be expressed as $\Delta E = [S]t$, where $[S]$ is called backscattering energy loss factor. In the so called surface approximation, where the target films is very thin, it can be assumed that $\left(\frac{dE}{dx}\right)$ of the projectile does not change and can be evaluated at the energy E_0 for its incoming path and $E_1 = KE_0$ for its outgoing path. Thus, the energy lost by a projectile (mass m) which was backscattered by an atom (mass M) at depth t, can be approximated as

$$\Delta E = [S]t = \left(\frac{K}{\cos\theta_1}\frac{dE}{dx}\bigg|_{E_0} + \frac{1}{\cos\theta_2}\frac{dE}{dx}\bigg|_{KE_0} \right) t \qquad (2.3)$$

where θ_1 and θ_2 are the angles of the incoming and outgoing particle with respect to the normal. In a compound there will be more than one element say A and B in the sample. The alpha particle scatters off only one atom and therefore only one of the

elements in target. The energy loss of the alpha particle backscattered off element A at depth t in a compound A_mB_n using the surface energy is given by:

$$\Delta E_A = [S]^{A_mB_n} t = \left(\frac{K_A}{\cos\theta_1} \frac{dE}{dx}\bigg|_{E_0} + \frac{1}{\cos\theta_2} \frac{dE}{dx}\bigg|_{KE_0} \right) t \qquad (2.4)$$

where K_A is the backscattering kinematic factor of element A. Bragg's rule states that $\varepsilon^{A_mB_n} = m\varepsilon^A + n\varepsilon^B$ where ε^A and ε^B are the stopping cross section of atoms A and B respectively. The total energy loss of the charged particle in the compound A_mB_n can thus be given as

$$\Delta E = [S]^{A_mB_n} t = \frac{m}{m+n}[S]_A^{A_mB_n} t + \frac{n}{m+n}[S]_B^{A_mB_n} t \qquad (2.5)$$

The height of the spectrum H gives the number of backscattered particles with energy in a certain energy enterval δE between E and $(E+\delta E)$ and is given by[Che-78]

$$H = n_0 \Omega \left(\frac{d\sigma}{d\Omega}\right) N \frac{\delta\sigma}{[S]\cos\theta_1} \qquad (2.6)$$

Where n_0 is the number of incident particles, Ω the solid angle of the detecting system and N the atomic density, while $\left(\frac{d\sigma}{d\Omega}\right)$ and $[S]$ are given by **eqns. 2.2** and **2.3** respectively. The height of the spectrum H_A for element A in compound A_mB_n can be given in the same way as equation.

$$H_A = n_0 \Omega \left(\frac{d\sigma}{d\Omega}\right)_A N_A \frac{\delta E}{[S]\cos\theta_1} \qquad (2.7)$$

Where N_A refers to the density of atoms of element A in compound A_mB_n. A similar equation holds for H_B the height of the spectrum peak for element B. It is obvious that N_A and N_B are proportional to m and n, thus

$$\frac{H_A}{H_B} = \frac{\sigma_A}{\sigma_B}\frac{m}{n}\frac{[S]_B^{A_mB_n}}{[S]_A^{A_mB_n}} \qquad (2.8)$$

Where σ_A is the average differential scattering cross section given by

$$\sigma_A = \frac{1}{\Omega}\int\left(\frac{d\sigma}{d\Omega}\right)_A d\Omega \qquad (2.9)$$

2.2.2. X-ray diffraction

X-ray diffraction (XRD) is a quick and efficient technique for phase identification in thin films. X-ray diffraction is most suited to films thicker than a few tenths of nanometers (nm). To limit the penetration of the beam and enhance the diffraction pattern of the film with respect to the substrate, glancing angle geometries are used. Individual crystalline phases were identified by the characteristic diffraction patterns. Such X-ray patterns also reveal information on the orientation and size distribution of crystallites. X-ray techniques provide superior angular resolution and more accurate structural data than available from electron diffraction but over a large volume area of the sample.

The basis of X-ray diffraction is the well-known Bragg equation which describes the conditions for constructive interference for X-rays scattering from atomic planes of a crystal. The condition for constructive interference is

$$2d\sin\theta = n\lambda \qquad (2.10)$$

with d the interplanar spacing, n the order of the reflection, λ the wavelength of the incident radiation and θ the incident angle. The Bragg law requires that θ and λ be matched for diffraction. By varying θ and recording where constructive interference occurs the d spacing of the crystal planes can be measured. Diffraction occurs from crystallites which happen to be oriented at the angle to satisfy the Bragg condition.

2.2.3. Stress measurement in thin films

Thin films deposited onto a substrate can bend the substrate as a result of thermal stress. *Thermal stress is generated when a film-substrate system experiences a* change in temperature. By measuring the change in wafer curvature and assuming that the stress in the thin film (which must be much thinner than the wafer) is isotropic the stress can be calculated using Stoney's equation

$$\sigma_{film} = \left(\frac{E_{Sub}}{1-\upsilon_{Sub}}\right)\left(\frac{d_{Sub}^2}{d_{film}}\right)\left(\frac{1}{R}-\frac{1}{R_0}\right) \qquad (2.11)$$

where σ_{film} is the stress in the thin film (negative = compressive and positive = tensile), E_{sub} is Young's modulus and ν_{Sub} is Poisson's ratio for the substrate, d_{sub} and d_{film} *are the substrate and film thickness,* R_0 *is the initial radius of curvature before* film deposition and R is the measured radius of curvature after deposition. The following assumptions are made when using Stoney's equation to calculate the stress in the film from the radius of curvature of the sample.

- *This is only true if* $d_{film} << d_{Sub}$
- The stress in the thin film is uniformly distributed throughout its thickness.
- There is zero stress in the center of the substrate when it is deformed. The stress therefore changes sign from the front to the backside.
- The wafer deformation must be small in comparison to the substrate thickness. The bow(b) of the sample (see **Fig. 2.3**) should be less than the substrate thickness.

If the stress in the thin film is not isotropic then it will be biaxial with both components in the plane of the film. There cannot be a stress component normal to the film surface. If the stress is not isotropic the curvature must be measured as a function of position and from there the stress field can be calculated. The substrate curvature is

measured by scanning a laser across a line on the surface of the sample. During the scan the position of the reflected light is measured with a position sensitive light detector at a fixed distance from the sample. The scanning is done by a rotating mirror and lens setup in such a way that for a flat sample the position of the reflected light moves proportionally to the position of the laser spot on the sample. The curvature of the sample can be deduced from the gradient of the reflected light position versus laser spot position curve.

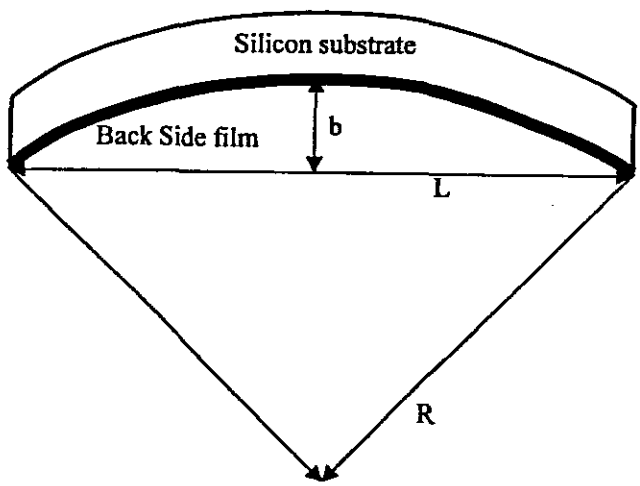

Fig 2.3 A Schematic representation of a curved sample with a thin film deposited on the Back Side (BS) where b=bow, L=sample size and R=radius of curvature. A positive radius of curvature means that the deposited film is under tensile stress and a negative radius would mean that the film is under compressive stress. In this case the radius of curvature is positive.

Chapter 3

Silicide formation in the Ti-Si system

3.1. Introduction

Many studies have been carried out regarding first phase formation during the reaction between thin Ti films and Si substrates [Pre-93B]. Different groups have reported $TiSi_2$, Ti_5Si_3, Ti_5Si_4 and TiSi being formed as first phase [Bey-85, Lak-89, Dex-88, Nem-85]. The only phase given in the Ti-Si equilibrium phase diagram that has not been reported to form initially is Ti_3Si. When applying the effective heat of formation model to the Ti-Si system, the most important variable is the effective concentration at the reaction interface. The effective heat of formation (EHF) and phase diagrams of the Ti-Si binary system are shown in **Fig. 3.1**. It can be seen that there are two liquidus minima (or eutectics) with the same temperature of 1330°C. A titanium-rich eutectic exist at 14 at. % Si and a silicon-rich eutectic is found at 84 at. % Si. If the effective concentration at the reaction interface is 84 at. % Si then the formation of the silicon-rich $TiSi_2$ is favored while an effective concentration of 14 at. % Si favors the more titanium-rich silicides. The true effective concentration could be anywhere between these two values and application of the EHF model therefore suggests that a whole range of phases could be formed, as is found experimentally. The native oxide layer usually found on silicon surface and the Ti affinity for oxygen further affect the effective concentration at the reaction interface.

$TiSi_2$ is a polymorphic material [Man-95] and may exist in two crystalline phases, namely the high resistivity (60 μΩ-cm) orthorhombic base-centered C49 phase and the low resistivity (14 μΩ-cm) orthorhombic face-centered C54 phase. The high

resistivity C49 phase forms at temperatures ranging between 550 and 700°C and then transforms into the low resistivity C54 phase at temperatures greater than ~750°C [Man-95]. The C54-$TiSi_2$ phase is currently the most widely used silicide for ultra large scale integrated circuits, as it possesses the lowest resistivity of all silicides, a low contact resistance, good thermal properties and is compatible with the self aligned silicide process. A previous study done by Mann *et. al.* [Man-95] showed that the low resistivity C54-$TiSi_2$ phase formation temperature could be lowered by 100-150°C by ion implanting a small dose of Mo into Si substrate before the deposition of a Ti thin film.

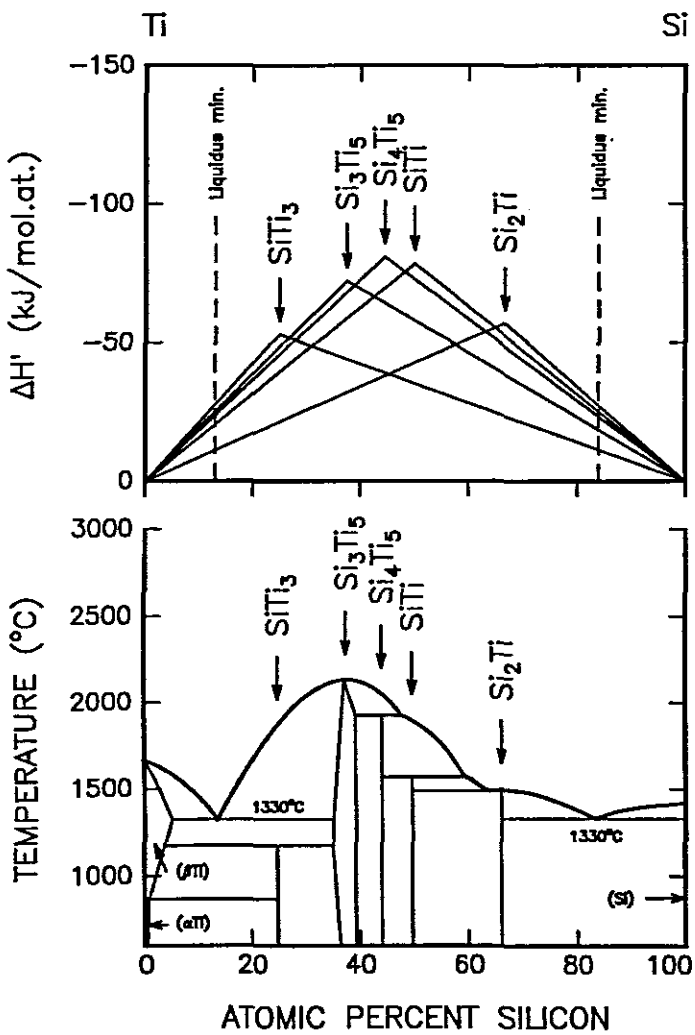

Fig. 3.1 The effective heat of formation and phase diagram for the Ti-Si binary system. This system has two liquidus (eutectics) minima at a temperature of 1330°C. A titanium-rich eutectic exist at 14 at. % Si and a silicon-rich eutectic is found at 84 at. % Si.

3.2. Phase Formation

3.2.1. RBS Computer Simulation

RBS data is analyzed using a specifically designed data manipulation package called RUMP [Doo-85]. Spectral simulation is an extremely powerful tool for understanding complex RBS spectra involving overlap of numerous elements or compounds. After defining a theoretical sample structure consisting of numerous layers of varying thickness, a simulation package will construct the theoretical spectrum used in an interactive manner to arrive at a best set of parameters in the sample structure which fit a given sample spectrum. RUMP includes a very fast and powerful simulation package referred to as SIM. Used properly, SIM can provide reliable estimates for layer thickness and compositions on extremely complex samples. The simulator in RUMP is both accurate and relatively fast, allowing complex simulations to be calculated in a few seconds. The accuracy of a simulation is limited primarily by uncertainties in the stopping cross sections, non-Rutherford scattering cross sections at low and high energies, and failure of Bragg's law for compounds. The RUMP simulator can compute the spectrum for any laterally uniform sample consisting of as many as 100 layers of 20 elements each. Non-uniform interfaces can be roughly simulated by summing several simulations together, each with slightly varying thickness. Impurities and diffusion profiles are simulated by generating relatively fine layers with a slowly varying composition in each layer.

The RUMP simulation spectra of the different phases in the Ti-Si binary system are shown in **Fig. 3.2**. The first spectrum shows a simulation of a titanium layer, 1200 Å thick, on a silicon substrate. If the titanium layer (1200 Å thick) is assumed to completely react with the silicon to form a titanium-rich silicide, a thickness of 1600 Å Ti_3Si will be formed whereas if the silicon-rich silicide is assumed to be formed a thickness of 3600 Å $TiSi_2$ is expected. It can be seen that after reaction the Ti signal has spread, this is due to the presence of the Si atoms. The Si signal exhibits a step corresponding to Si in the silicide layer. As the Si composition increases, so the Ti height decreases. The ratio of the heights of Ti (H_{Ti}) and Si (H_{Si}) in the silicide layer gives the composition of the layer and can be calculated using equation 3.1.

$$\frac{H_{Ti}}{H_{Si}} \cong \frac{N_{Ti}}{N_{Si}} \frac{\sigma_{Ti}}{\sigma_{Si}} \qquad (3.1)$$

where N_{Ti} , N_{Si} are the atomic densities of Ti and Si respectively and σ_{Ti} , σ_{Si} are scattering cross sections of Ti and Si respectively. **Table 3.1** shows the height ratios

of Ti and Si in the Ti-silicide layers and their corresponding phases. These ratios were taken for incident alpha energy of 2 MeV.

Table 3.1 Height ratios of the Ti and Si in the silicide layers if the incident energy of the alpha particles is assumed to be 2 MeV. This ratios gives the composition of the layer.

Compound Phase	Heights ratios of Ti (H_{Ti}) and Si (H_{Si})
Ti_3Si	7.26
Ti_5Si_3	4.01
Ti_5Si_4	3.04
TiSi	2.47
$TiSi_2$	1.24

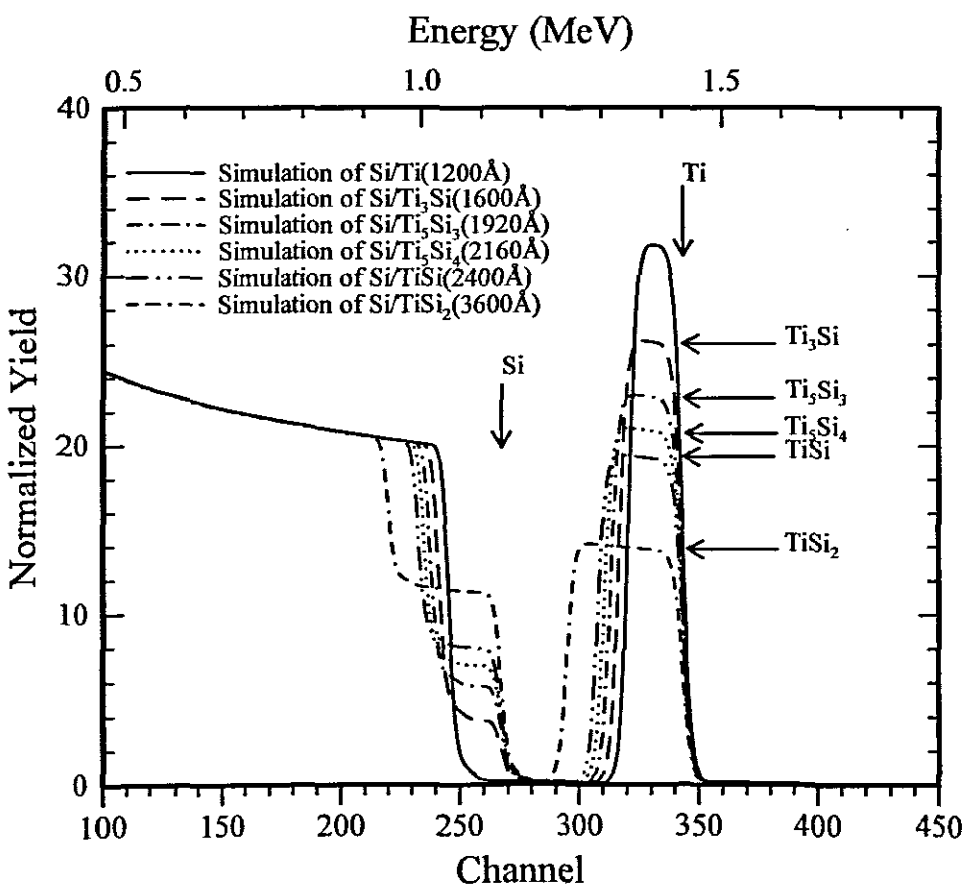

Fig. 3.2 RUMP simulation spectra of different phases in the Ti-Si binary system. From the Ti and Si height ratios the phase composition can be calculated.

3.2.2. RBS measurements

Samples were prepared in a high vacuum electron beam chamber at a pressure better than 3 x 10^{-8} kPa. They were made by depositing 1200 Å of titanium thin film on a Si(100) substrate. The reaction between the Ti thin film and Si was induced by annealing the samples in a furnace at temperatures between 550 and 650°C for different times. The annealing was also done in vacuum at a pressure better than 3 x 10^{-8} kPa.

The RUMP simulation showed that the unannealed sample had 1200 Å Ti thin film. **Fig 3.3** shows the RBS and simulation spectra of the sample annealed at 550°C for 30 minutes. The simulation revealed that the Si reacted with the Ti film to form 750 Å of Ti_5Si_4 and 550 Å of $TiSi_2$ with 800 Å of Ti film still unreacted. It was not clear which of these two phases was formed first. The unreacted Ti film showed the presence of 20 at. % oxygen. Ti in particular has a very high affinity for oxygen. Oxygen can enter the system either during the evaporation of the Ti film or during the annealing stage. **Fig. 3.4** shows RBS spectrum and an overlaid RUMP simulation of the sample annealed at 550°C for 120 minutes. The simulation showed that 1200 Å of Ti_5Si_4 and 750 Å of $TiSi_2$ were formed before all the Ti had been consumed. The 600 Å unreacted Ti had 35 at. % of oxygen. **Fig. 3.5** shows the non-linear growth of the silicides as a function of time for samples annealed at 550°C. From the plots it can be concluded that the thickness of the two phases increased simultaneously as the annealing times was increased. The oxygen concentration in the unreacted Ti also showed an increase.

Fig. 3.6 show RBS spectra and overlaid simulation of the sample annealed at 600°C for 60 minutes. The sample formed 570 Å of Ti_5Si_4 and 2250 Å of $TiSi_2$ with 500 Å of Ti + O still unreacted. The overlaid simulation had the following structure: Si<100>/ 2250 Å $TiSi_2$ / 570 Å Ti_5Si_4 / 500 Å Ti + O. The simulation also showed that there was 50 at. % oxygen in the unreacted titanium. The amount of Ti_5Si_4 formed at 600°C for 60 minutes (570 Å) is less than what was formed at 550°C for 30 minutes. Therefore, **Fig. 3.6** shows that at 600°C some of the Ti-rich Ti_5Si_4 phase transformed to the Si-rich $TiSi_2$ before the unreacted Ti was consumed. All annealed samples showed the presence of oxygen in the unreacted Ti. The oxygen concentration was found to increase throughout the Ti thin film as the annealing time was increased. The total amount of oxygen in the unreacted Ti thin layer was found to be higher in the samples annealed for longer times.

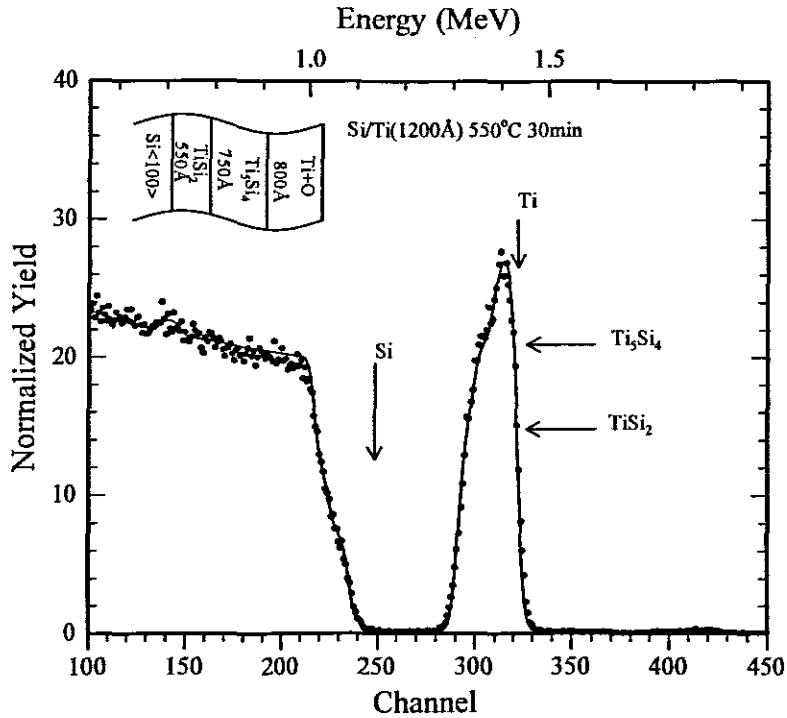

Fig. 3.3 RBS and an overlaid RUMP simulation spectra of the sample annealed at 550°C for 30 minutes. The simulation revealed that 750 Å of Ti_5Si_4 and 550 Å of $TiSi_2$ were formed. The 800 Å unreacted Ti film showed the presence of 20 at. % oxygen.

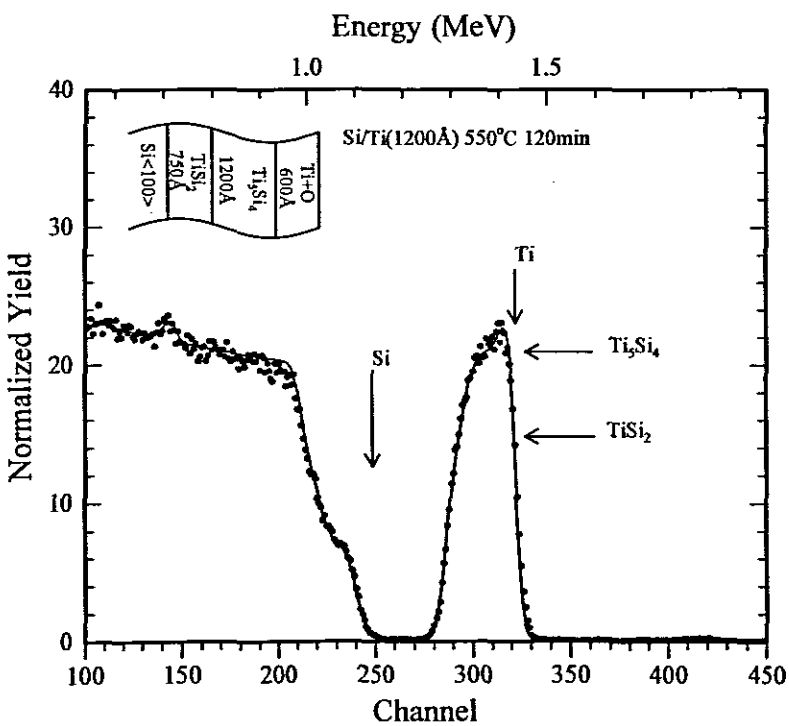

Fig. 3.4 RBS spectrum and RUMP simulation of sample annealed at 550°C for 120 minutes. More Ti_5Si_4 and $TiSi_2$ phases were formed simultaneously. The oxygen concentration in the unreacted Ti film increased to 35 at. %.

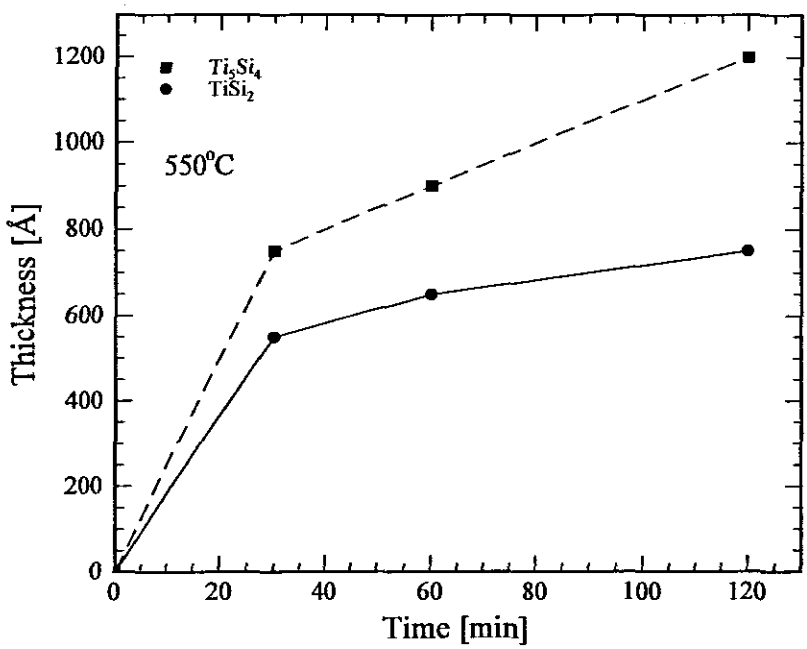

Fig. 3.5 Ti-silicide thickness versus time plots of samples annealed at 550°C showing non-linear kinetics. Ti_5Si_4 and $TiSi_2$ were the two phases formed and continued to grow simultaneously as the annealing times was increased.

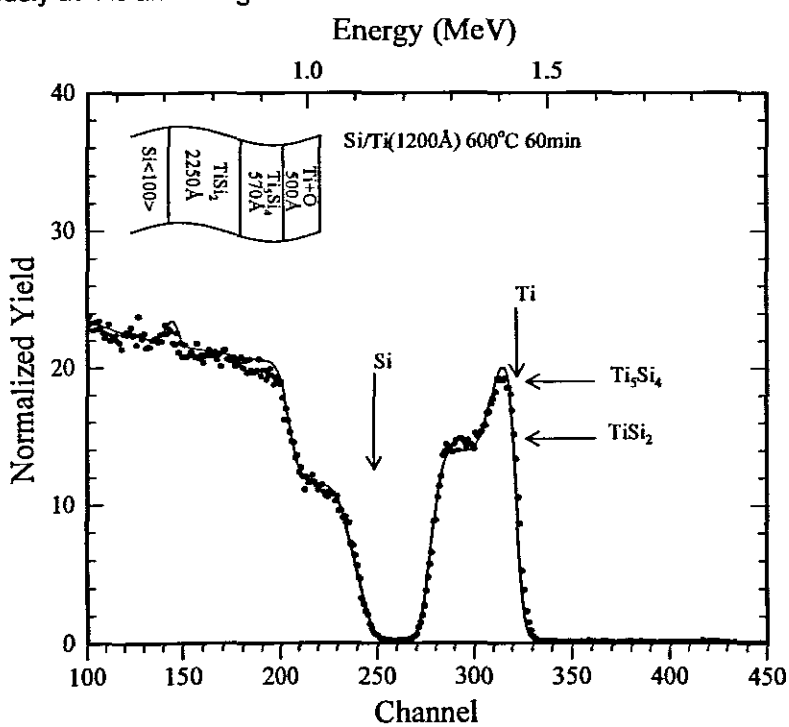

Fig. 3.6 RBS and RUMP simulation spectra of samples annealed at 600°C for 60 minutes. The simulation showed that 570 Å of Ti_5Si_4 and 2250 Å of $TiSi_2$ were formed. The unreacted Ti film showed the presence of 50 at. % oxygen. Some of the Ti-rich Ti_5Si_4 phase formed at low temperature converted to the Si-rich $TiSi_2$ phase before the Ti thin layer is consumed.

3.2.3. XRD simulation

Phase identification of an unknown phase in a thin film environment can be simplified if the expected diffraction patterns of all the possible phases are known by using X-ray Diffraction (XRD). The identity of the phases present can be determined by a comparison between known data and an observed poly-crystalline diffraction pattern. Powder diffraction patterns are used to do the phase identification [Cul-78]. The powder patterns is a characteristic of that substance and forms a sort of a fingerprint by which the substance may be identified. Any powder pattern is characterized by a set of line positions 2Θ and a set of relative line intensities I. The angular position of the lines depends on the wavelength used, and a more fundamental quantity is the spacing d of the lattice planes forming each line. Each pattern is therefore described by listing the d and I values of its diffraction lines. Since more than one substance can have the same, or nearly the same, d value for its strongest line and its second strongest line, each substance can be better characterized by using the d values of its three strongest peaks [Cul-78].

Fig. 3.7 shows powder diffraction patterns of the titanium-rich Ti_5Si_4 phase and the monosilicide TiSi phase calculated using *CCMiller* [Chu-95] program. *CCMiller* uses crystallographic parameters of metal silicide phases given in *Pearson's Handbook of Crystallographic Data for Inter-metallic Phases* [Vil-85] to display calculated diffraction patterns of poly-crystalline specimen for X-ray diffraction. Poly-crystalline standard specimen is prepared in such a way as to preclude any preferred orientation. **Fig. 3.7(a)** and **(b)** shows that the Ti_5Si_4 and the TiSi phases have the strongest peak at 38.67° and 46.15° respectively. Therefore these two phases have different 2Θ values of the strongest peaks.

$TiSi_2$ exists in two crystal phases. The metastable low temperature C49 phase and the stable high temperature C54 phase. The high temperature C54 phase has a low resistivity (14μΩcm) whereas the low temperature C49 phase has a high resistivity (60μΩcm). **Fig. 3.8(a)** and **(b)** shows the powder diffraction patterns of the C49 and the C54-$TiSi_2$ phases respectively. The C49 show a strongest peak at 40.40° while the C54 has a strong peak at 39.18°. Therefore the two crystallographic phases of $TiSi_2$ can be characterized by the 2Θ values of the strongest peak.

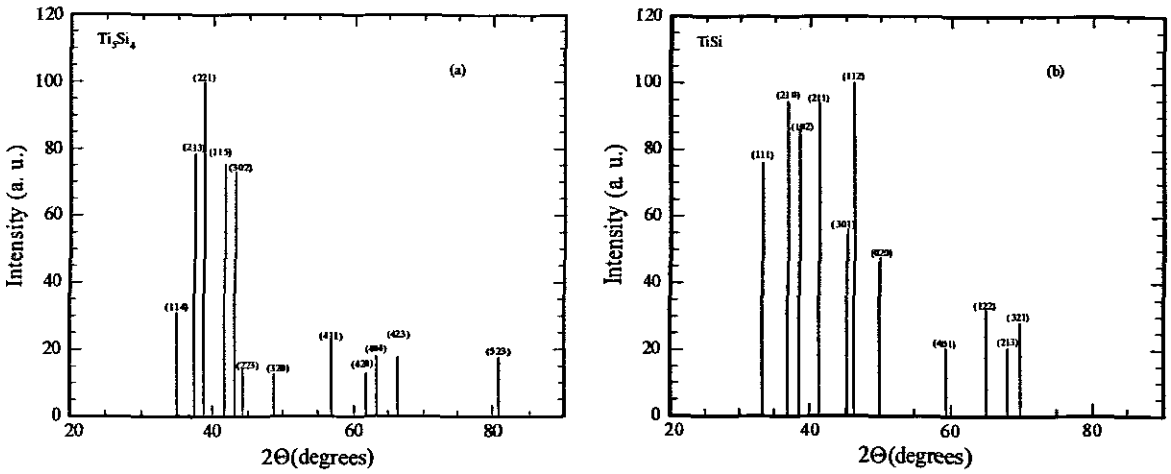

Fig. 3.7 The powder diffraction pattern lines of *(a)* the titanium-rich Ti_5Si_4 phase and *(b)* the monosilicide TiSi phase. It can be seen that the two phases has different 2Θ for the strongest peaks.

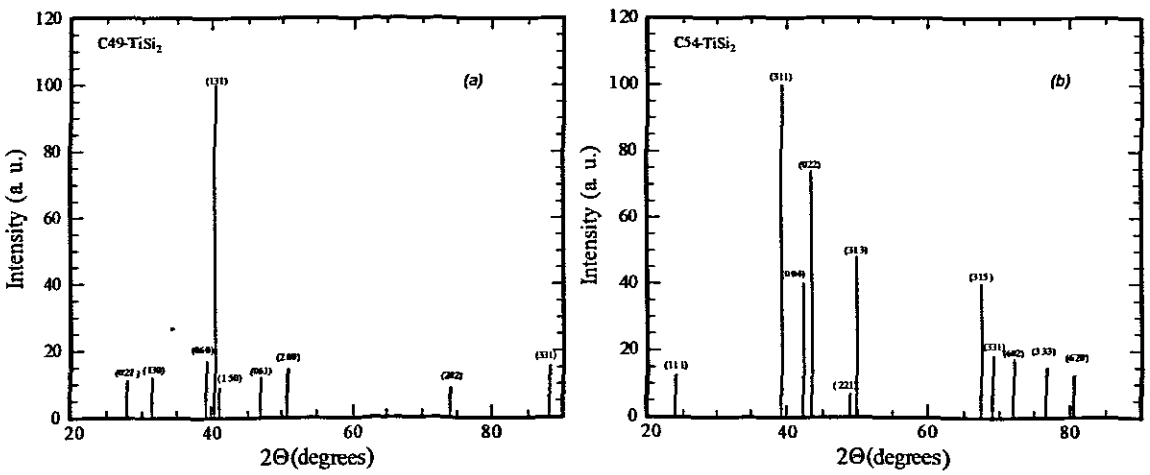

Fig. 3.8 The powder diffraction pattern lines of the two crystal phases of $TiSi_2$, namely *(a)* the C49 phase and *(b)* the C54 phase. The two phases can be characterized by the 2Θ values of the strongest peaks.

3.2.4. XRD Measurements

Samples were also analyzed using X-ray diffraction (XRD) to determine the crystalline phases formed during reaction. XRD can easily separate the two crystallographic phases of $TiSi_2$ (C49 and C54). In thin films most of the diffraction pattern lines are not shown. This is because the crystal planes in thin films are not randomly oriented as in powder specimens.

Fig. 3.9(a) shows XRD spectrum of the as deposited sample. Only a reflection from the Ti film was observed. No reflection from the Si substrate was seen because of the Ti layer being too thick for the X-rays to penetrate to the substrate. **Fig. 3.9*(b)*)** shows XRD spectrum of the sample annealed at 550°C for 30 minutes. The XRD results show that at this temperature a Ti-rich silicide, viz Ti_5Si_4 and a Si-rich silicide, $TiSi_2$, had formed. This was shown by the strong Ti_5Si_4 and the weak $TiSi_2$ peaks. The $TiSi_2$ phase formed was the high resistivity C49 phase.

More C49-$TiSi_2$ was formed after samples were annealed at 600°C for 30 minutes. This was shown by the strong C49 reflection in **Fig. 3.10*(a)***. No Ti_5Si_4 phase was detected at this temperature. Therefore the Ti_5Si_4 phase that forms when samples are annealed at 550°C for 30 minutes, transforms to the $TiSi_2$ phase if the sample is annealed at higher temperature, 650°C for 30 minutes. **Fig. 3.10*(b)*** shows XRD spectrum of sample annealed at 650°C for 30 minutes. Only reflections from the high temperature C54-$TiSi_2$ phase were seen. This means the high resistivity C49-$TiSi_2$ phase has transformed to the low resistivity C54 phase. Although RBS show the presence of oxygen in the unreacted Ti film of the annealed samples, no reflections from titanium oxide compounds were detected with XRD.

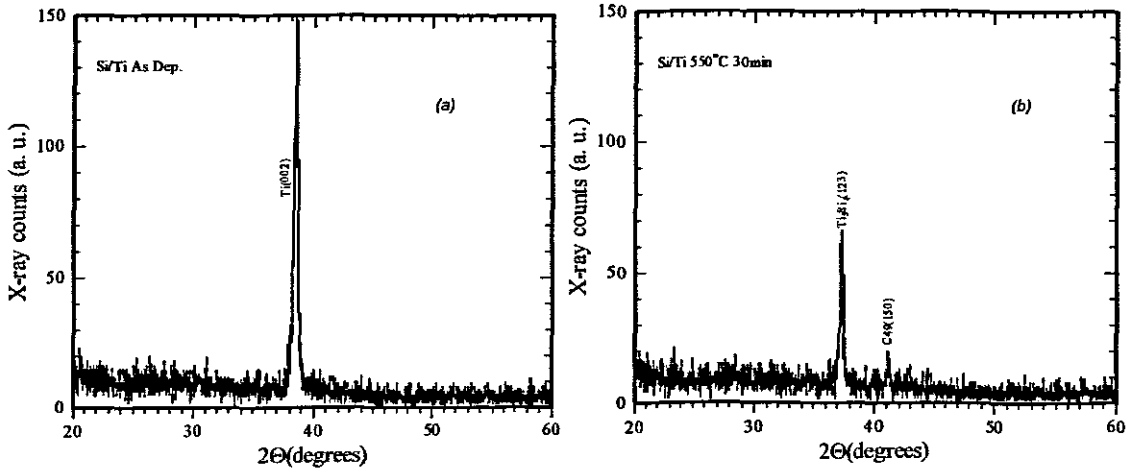

Fig. 3.9 shows XRD spectra *(a)* of the unannealed sample. Only the reflection from the Ti thin layer was detected. *(b)* of the sample annealed at 550°C for 30 minutes. It shows that Ti_5Si_4 and C49-$TiSi_2$ phases have formed.

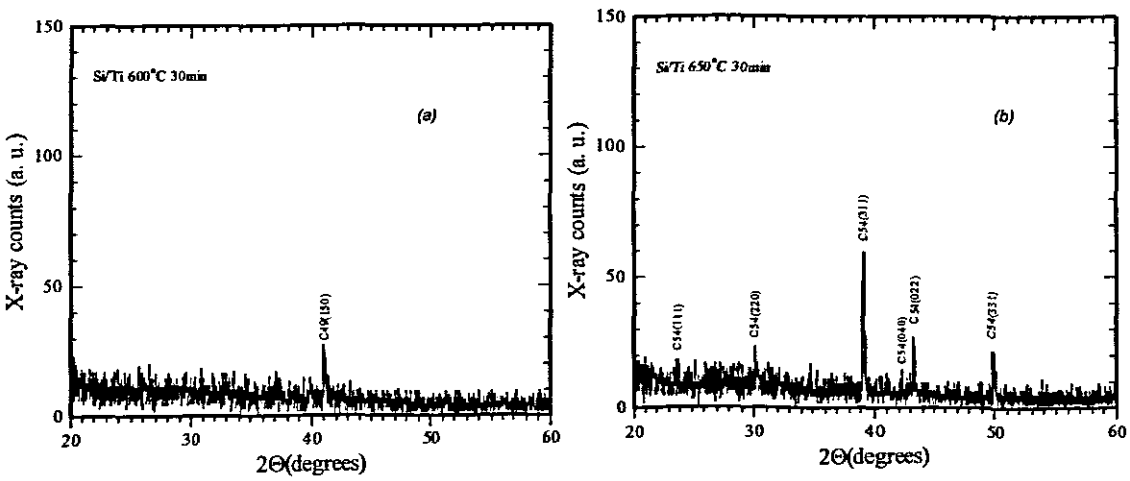

Fig. 3.10*(a)* shows XRD spectrum of the sample annealed at 600°C for 30 minutes. More C49-$TiSi_2$ has formed and no Ti_5Si_4 was detected. Fig. 3.10*(b)* shows the spectrum of the sample annealed at 650°C for 30 minutes. The C49-$TiSi_2$ phase has transformed to the low resistance C54-$TiSi_2$ phase.

3.2.5. Discussions

Several first phase formation have been reported for titanium thin-film reactions with silicon [Pre-93B]. As mentioned before $TiSi_2$, Ti_5Si_3, Ti_5Si_4 and TiSi have been found to form as first phase in the Ti-Si binary system. It is interesting to form Ti_5Si_4 and TiSi as a first phase as non-congruent melting phases are usually not formed in thin film silicide system. In this work, the RBS results showed that Ti_5Si_4 and $TiSi_2$ were formed at low temperature and continue to grow simultaneously as the annealing time was increased (see **Figs. 3.3** and **3.4**). At high annealing temperatures the Ti_5Si_4 phase converted to the silicon-rich $TiSi_2$ phase. Previous work has shown that silicon is the dominant diffusion species during Ti-silicide formation [Bot-92, Chu-75]. The growth of the silicide, as has been reported in the literature may be either diffusion limited, in which case the silicide thickness grows non-linearly with time [Hun-83] or reaction limited in which case the thickness grows linearly with time [Pic-88]. A possible cause of this inconsistency is the oxidation of the Ti-film. Titanium has a very high affinity for oxygen. Initially the two reactions (Ti-oxide and Ti-silicide formation) do not affect each other but as the reaction progresses the consumption of Ti by the oxidation process on the surface of the sample results in the slowing down of the silicide growth. In this work the RUMP simulation of annealed samples showed the presence of oxygen in the unreacted Ti film. The oxygen concentration increased as the annealing time was increased.

The XRD results revealed that Ti_5Si_4 and $TiSi_2$ were formed at low temperatures (see **Fig.3.9(b)**). The $TiSi_2$ that was formed is the high resistance C49 phase. The C49-$TiSi_2$ phase transformed to the low resistance C54-$TiSi_2$ phase after annealing samples at 650°C (see **Fig. 3.10(b)**). Therefore, the XRD results agree with RBS results that Ti_5Si_4 and $TiSi_2$ phases were formed at low temperatures. No reflection from titanium oxide was shown by XRD.

3.3. Oxidation Limiting Techniques

Titanium is known to oxidize very easily during titanium-silicide formation. The oxidation of the titanium during the silicide formation makes accurate kinetic measurement difficult. Oxygen can enter the system in two stages. The first stage is during the evaporation of the titanium thin film and the second is during the annealing stage. A previous work in attempting to limit this unwanted oxidation of the Ti film was done by De Waal *et. al.* [Waa-99] by using titanium oxide (labeled as Ti-O) as a capping layer in the Ti-silicide formation. The Ti-O deposition was done by bleeding oxygen into the chamber while the Ti was deposited. It was found that the samples capped with Ti-O reacted faster to form the C49-$TiSi_2$ phase than the uncapped samples. De Waal argued that the Ti-O cap seemed to form a gettering site which seemed to cleaned up the Ti film of oxygen acquired during the deposition process an also forms a barrier for atmospheric oxygen in the furnace. In this work two methods were used in attempting to limit the oxidation of the Ti thin film. In the first method thin layers of Al_2O_3 and MgO were used as capping layers. In the second method a sandwich technique was used whereby two samples were annealed together in the furnace with one sample on top of another with front sides facing each other.

3.3.1. Capping Layers

Three sets of samples were prepared by depositing 1200 Å of Ti onto a Si(100) substrate using an electron beam vacuum deposition system with a base pressure of 3×10^{-8}kPa. Two sets of samples were then capped with 250 Å of Al_2O_3 and MgO respectively. The third set was used as a control (no capping layer). To induce reaction, samples were annealed at 530°C for times ranging between 16 and 256 minutes in a vacuum furnace at a pressure better than 3×10^{-8}kPa. Samples from each set were annealed in the same boat.

RBS Results

The RUMP simulation showed that the as deposited samples from each set had 1200 Å of Ti thin film. The RBS results of the samples from each set annealed at 530°C for 16 minutes revealed that Ti_5Si_4 was the phase to form. **Fig. 3.11** shows the RBS and RUMP simulation spectra of the sample capped with Al_2O_3 after annealing at 530°C for 256 minutes. The RUMP simulation revealed that 700 Å of Ti_5Si_4 and 600 Å of $TiSi_2$ were formed with 700 Å of Ti + O still unreacted. The unreacted Ti film showed a presence of 35 at. % oxygen. The uncapped sample annealed at this temperature for the same time formed 750 Å of Ti_5Si_4 and 800 Å of $TiSi_2$. The 600 Å unreacted Ti had 50 at. % oxygen.

Fig. 3.12 shows the RBS and RUMP simulation spectra of the sample capped with MgO at 530°C for 256 minutes. The simulation showed that 750 Å of Ti_5Si_4 and 1200 Å of $TiSi_2$ were formed with about 300 Å of Ti + O still left unreacted. The simulation also showed that 35 at. % oxygen present in the unreacted Ti thin film. Therefore, it can be said that the Ti-silicide formation was faster in the sample capped with MgO and slower in the sample capped with Al_2O_3. All annealed samples from each set showed the presence of oxygen in the unreacted Ti film. Both Al_2O_3 and MgO capped samples annealed the same time and at the same temperature showed the same oxygen concentration in the unreacted Ti film. The total amount of oxygen in MgO samples was less than in the Al_2O_3 capped samples. It was found that the oxygen concentration in the capped samples was less by 30% compared to the uncapped samples.

Fig. 3.13 shows the $TiSi_2$ thickness versus time plots of samples from each set annealed at 530°C for varying times. From the plots it can be seen that the control samples formed $TiSi_2$ at 64 minutes whereas in the capped samples it only began to form after annealing samples for 144 minutes. Therefore both caps delayed the formation of the $TiSi_2$ phase.

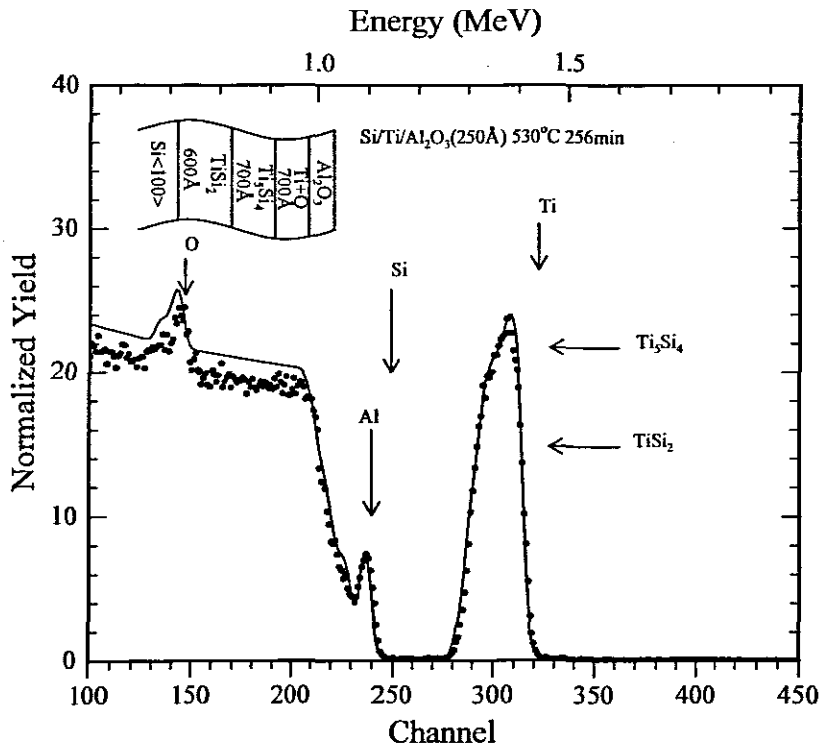

Fig. 3.11 RBS and RUMP simulation spectra of the sample capped with 250 Å of Al_2O_3 annealed at 530°C for 256 minutes. The simulation revealed that 600 Å of $TiSi_2$ and 700 Å of Ti_5Si_4 with 700 Å of Ti + O still unreacted.

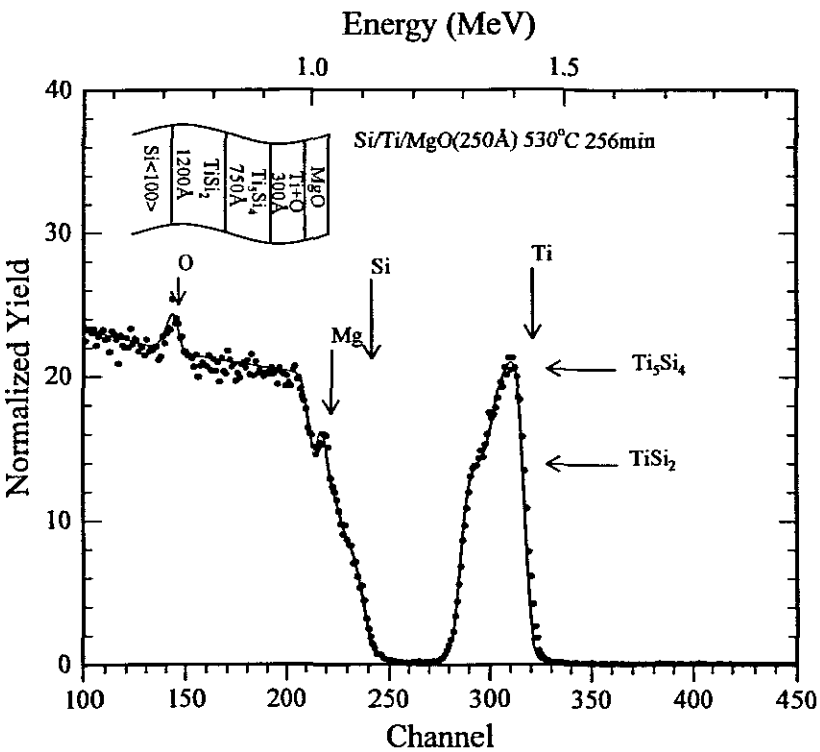

Fig. 3.12 RBS and RUMP simulation spectra of sample capped with 250 Å MgO annealed at 530°C for 256 minutes. The simulation revealed that 1200 Å of $TiSi_2$ and 750 Å of Ti_5Si_4 were formed with 300 Å of Ti + O still unreacted.

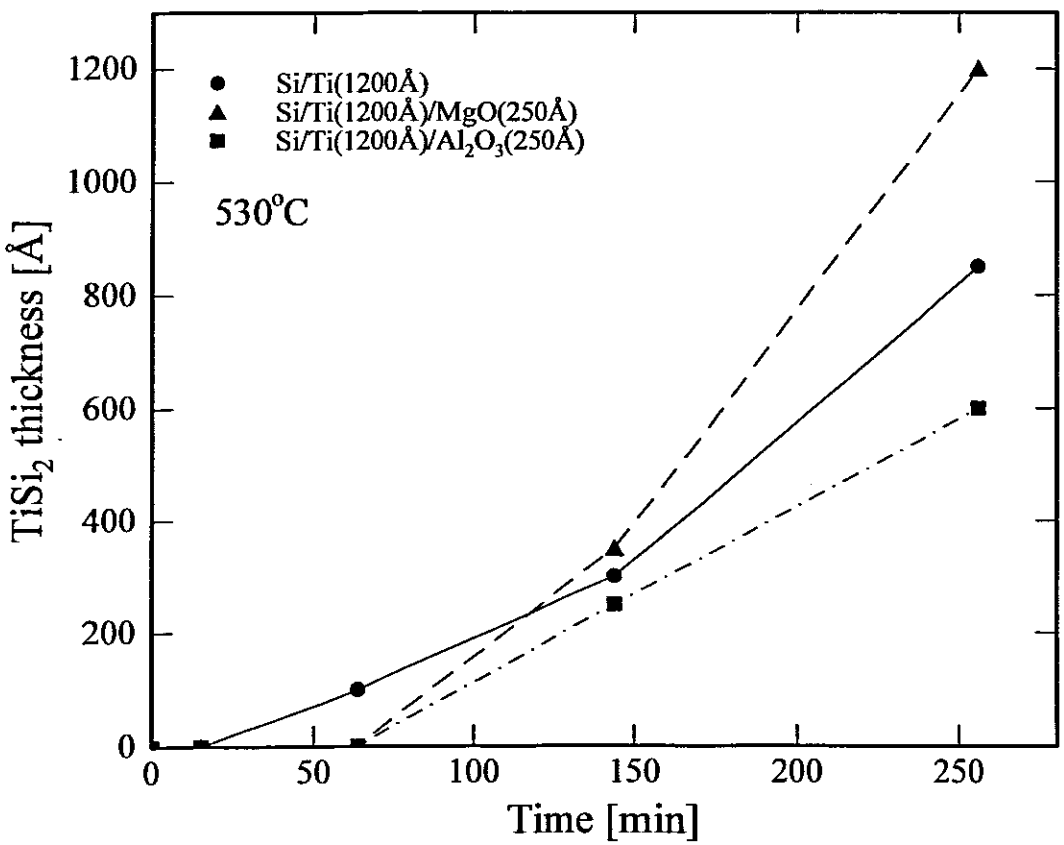

Fig. 3.13 $TiSi_2$ thickness versus time plots of samples from each set after annealing at 530°C showing non-linear kinetics. Both capping layers delayed the $TiSi_2$ phase formation and the reaction was found to be faster on the MgO capped samples.

XRD Result

Fig. 3.14 to **Fig. 3.16** shows the XRD spectra of a set of uncapped, MgO capped and Al_2O_3 capped samples that have been annealed at 530°C for 64 and 144 minutes (see summary in **Table 3.2**). The XRD results did not show silicide in the as deposited sample. Samples annealed at 530°C for 64 minutes show the presence of the Ti_5Si_4 phase in the uncapped and the MgO capped samples. This agrees with the RBS results that Ti_5Si_4 was the first phase formed. Not enough silicide was formed in the Al_2O_3 capped sample to be detected by XRD. Samples annealed at 530°C for 144 minutes show reflections from the Ti_5Si_4 and the $TiSi_2$ phases in the uncapped and the MgO capped samples whereas the sample capped with Al_2O_3 shows only the Ti_5Si_4 phase (as shown in **Fig. 3.16**). The XRD, therefore, agree with the RBS that the reaction was slow in the sample capped Al_2O_3 and faster in the samples capped with MgO. In both samples that formed $TiSi_2$, only the C49 phase was present. All samples annealed above 530°C for 16 minutes showed the presence of titanium oxide, tentatively labeled Ti_2O. No Ti_2O reflections were seen on the previous XRD measurements (see **Figs. 3.9** and **3.10**). One difference being that the XRD analysis was done immediately after annealing while in these samples it was done after a week. The samples were exposed to air for long time which might have resulted in oxidation.

Table 3.2 XRD results showing which compound phases were formed in the sample with different capping layers after annealed at 530°C for varying times.

Temp and Time	Uncapped Samples	MgO capped samples	Al_2O_3 capped samples
530°C 16 minutes	Ti_5Si_4	Ti_5Si_4	-
530°C 64 minutes	Ti_5Si_4, Ti_2O	Ti_5Si_4, Ti_2O	Ti_2O
530°C 144 minutes	Ti_5Si_4, Ti_2O, C49-$TiSi_2$	Ti_5Si_4, Ti_2O, C49-$TiSi_2$	Ti_5Si_4, Ti_2O

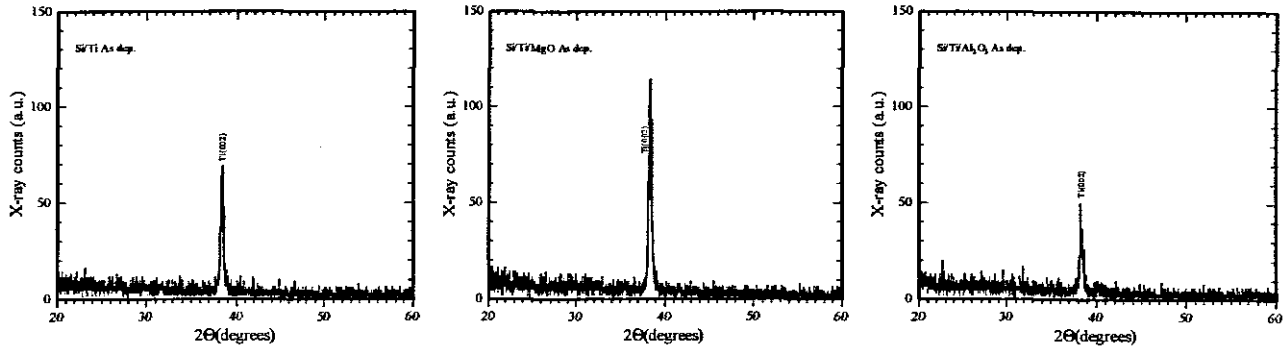

Fig. 3.14 XRD spectra of the as deposited samples from each set. Only reflections from the Ti thin film are present.

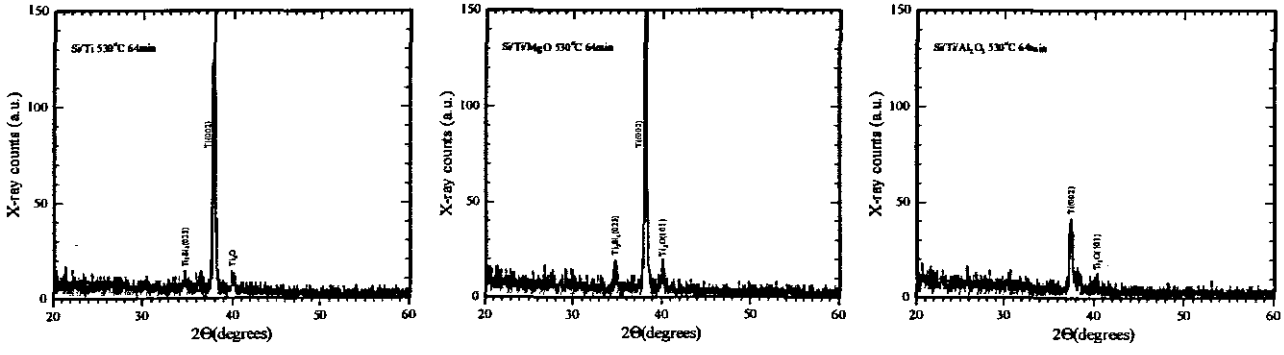

Fig. 3.15 XRD spectra of three samples from each set annealed 530°C for 64 minutes. Not enough silicide was formed in the Al_2O_3 capped sample to be detected while the uncapped and the MgO capped sample show reflection from the Ti_5Si_4 phase.

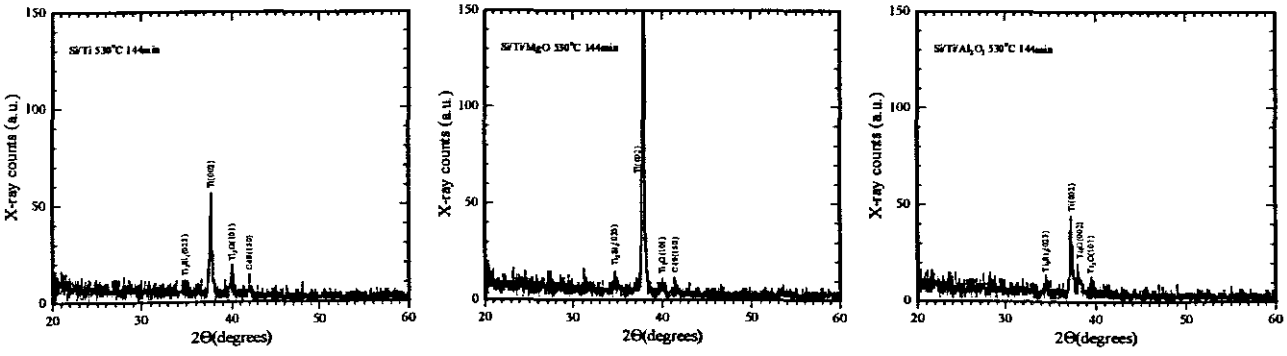

Fig. 3.16 XRD spectra of the samples annealed at 530°C for 144 minutes. The uncapped and the MgO capped samples show reflections from the Ti_5Si_4 and the C49-$TiSi_2$ phases while only the Ti_5Si_4 phase was formed in the Al_2O_3 capped samples. Ti_2O was present in all samples.

3.3.2. Sandwich Technique

Samples were prepared using an e-beam vacuum deposition system by depositing 1200 Å of Ti thin film onto silicon substrates. Pairs of similar samples were sandwiched together by putting one sample on top of the other sample with the front sides facing each other (see **Fig. 3.17**). Sandwich and control (unsandwiched) samples were subsequently annealed at 550, 600 and 650°C for varying times. One pair of sandwich samples and one control sample were annealed in the same boat.

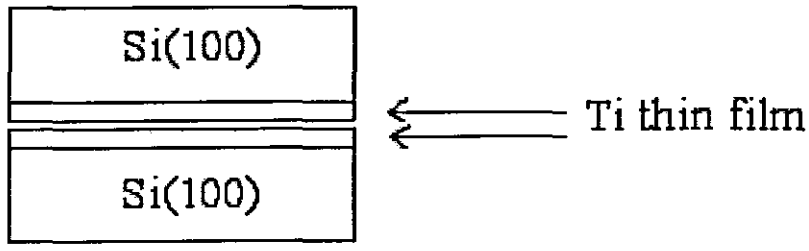

Fig. 3.17 A schematic diagram showing how two samples were sandwiched together before being loaded into a boat for annealing.

Fig 3.18 shows RBS and RUMP simulation of the sandwich and control samples annealed at 550°C for 30 minutes. The RUMP simulation revealed that the sandwich sample formed 550 Å of the Ti_5Si_4 phase with 1000 Å of Ti + O still unreacted. The control sample formed 750 Å of Ti_5Si_4 phase and 550 Å of $TiSi_2$ with 750 Å of Ti + O still unreacted. It was found that the sandwich sample had 10 at. % oxygen in the unreacted Ti whereas the control sample had 20 at. % oxygen. Although the oxygen concentration in the unreacted Ti was found to increase in both sets of samples at longer annealing times, it was less in the sandwich samples by ~35%. **Fig 3.19** shows RBS spectra of the sandwich and the control samples annealed at 600°C for 60 minutes. The simulation revealed that all the Ti film in sandwich sample reacted to form 3800 Å of $TiSi_2$ whereas the control sample formed 570 Å of Ti_5Si_4 and 2250 Å of $TiSi_2$ with 500 Å of Ti + O still unreacted. The later sample had 50 at. % oxygen in the unreacted Ti. Therefore at high temperatures the reaction in the sandwich samples is faster than in the control samples.

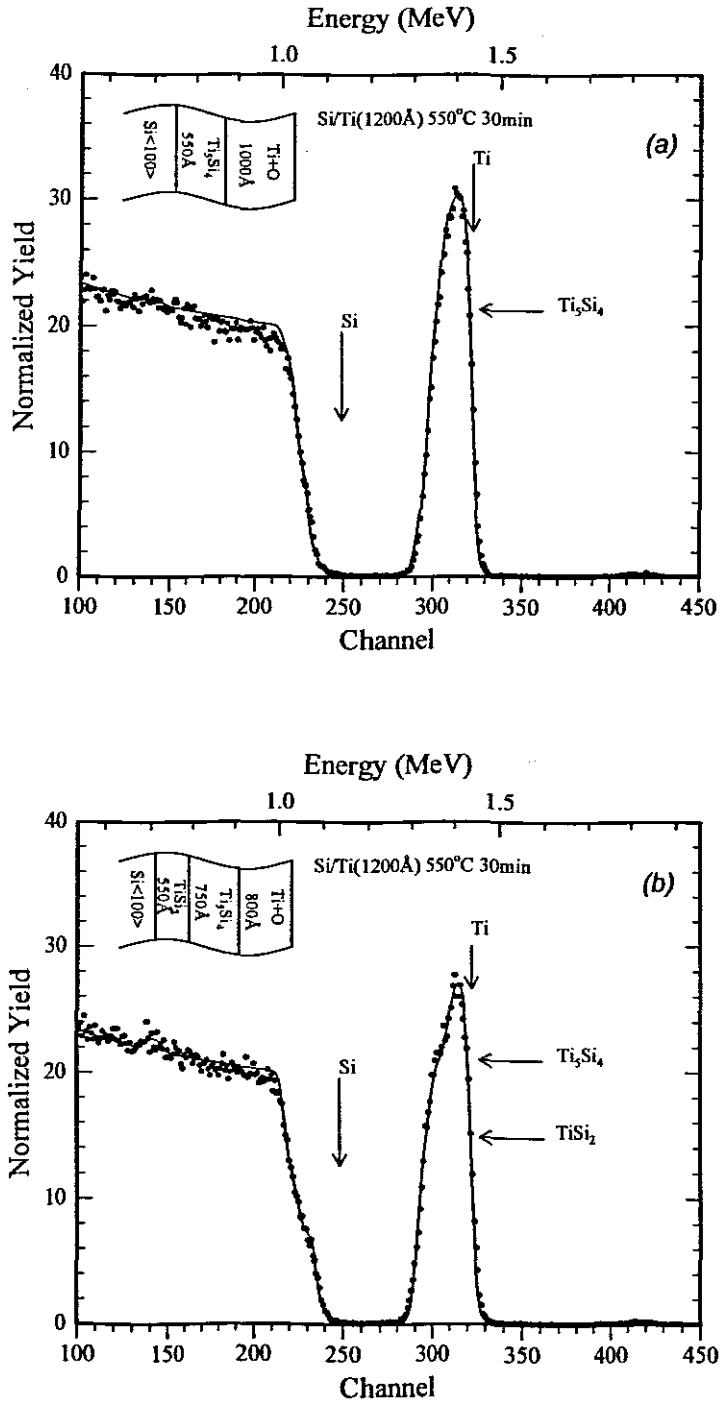

Fig. 3.18 RBS and RUMP simulation spectra of *(a)* the sandwich and *(b)* control samples annealed at 550°C for 30 minutes. Only 550 Å of the Ti_5Si_4 phase was formed in the sandwich sample while the control sample formed 750 Å of Ti_5Si_4 and 550 Å of the $TiSi_2$ phase. The sandwich sample showed 10 at. % oxygen in the unreacted Ti whereas the control showed 20 at. % oxygen.

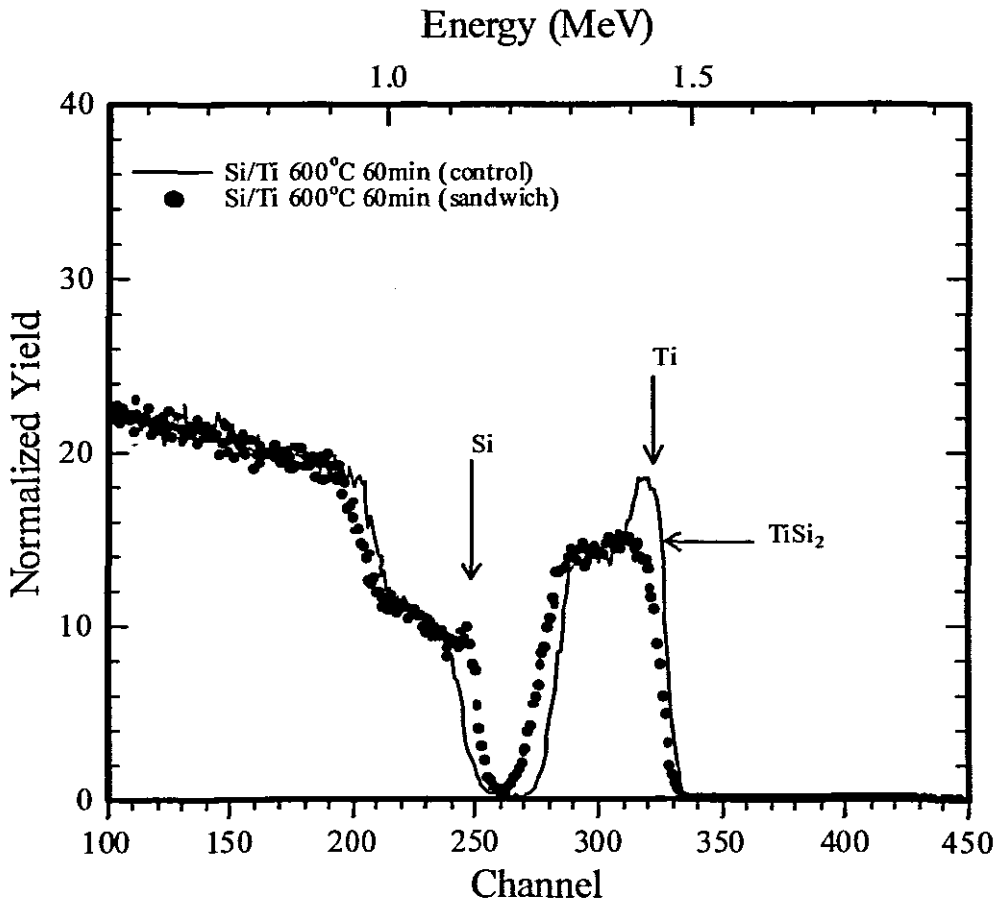

Fig 3.19 RBS spectra of a sandwich and a control samples annealed at 600°C for 60 minutes. All the titanium in the sandwich sample reacted to form the $TiSi_2$ phase. The control sample formed Ti_5Si_4 and $TiSi_2$ phases with 500 Å of Ti + O still left unreacted. Therefore, at high temperatures the reaction in the sandwich sample is faster than in the control sample.

Some of the sandwich sample had a small portion that was not covered by the other sample. RBS analysis was done on both the covered and the uncovered part of the same sample. **Fig. 3.20** shows the RBS spectra taken from the covered and the uncovered parts of a sample annealed at 550°C for 120 minutes. It can be seen that both parts of the sample formed equal silicide thickness. **Fig. 3.21** shows the RBS spectra taken from the covered and the uncovered parts of a sample annealed at 600°C for 60 minutes. It was found that all the Ti in the covered portion of the sample has reacted to form $TiSi_2$ whereas in the uncovered portion there was unreacted Ti film left. Therefore, at low temperatures the reaction in both portions of the sample is the same. At high temperatures the reaction is faster in the covered part of the sample and slow in the uncovered part.

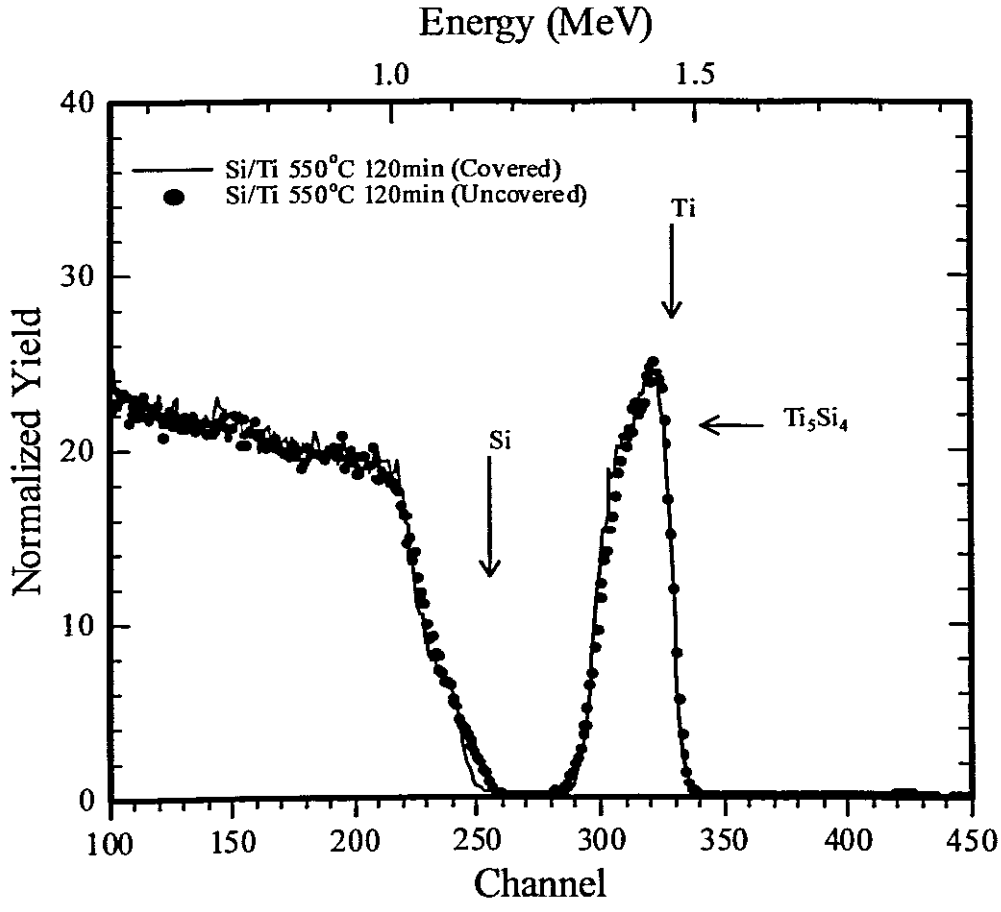

Fig 3.20 RBS spectra taken from the uncovered and covered parts of a sample annealed at 550°C for 120 minutes. It can be seen that both parts of the sample formed the same silicide thickness.

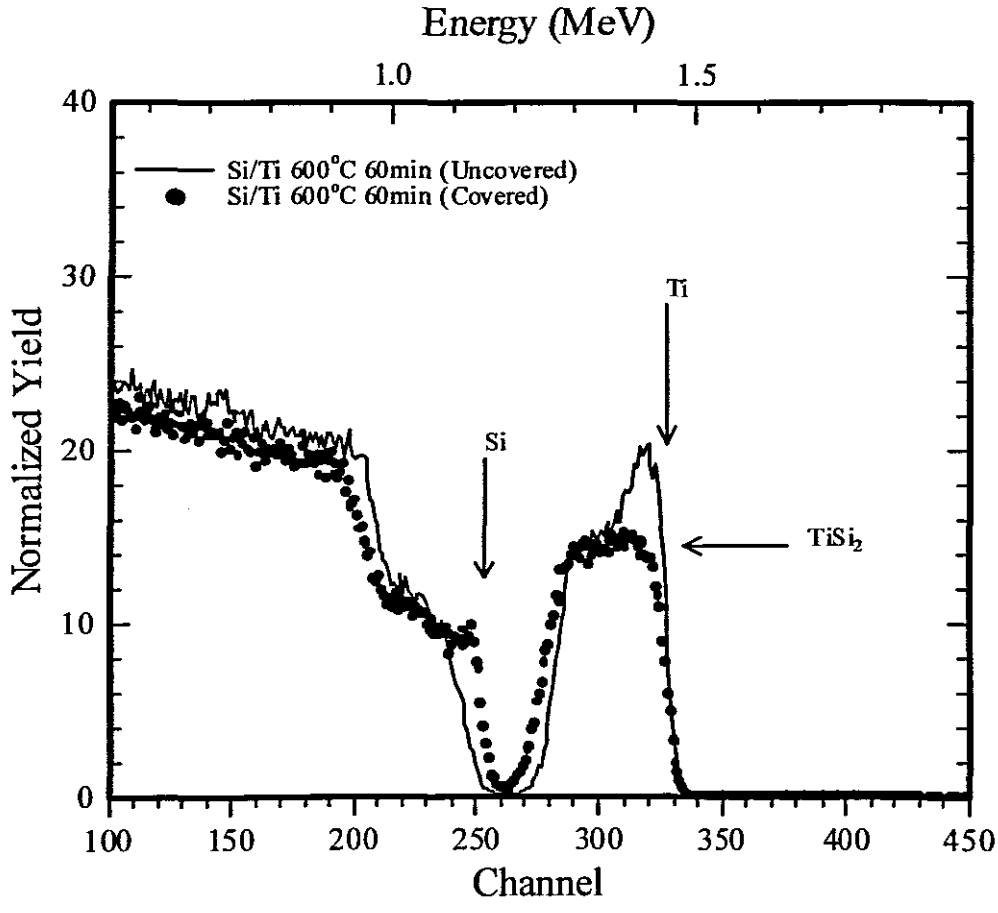

Fig. 3.21 RBS spectra taken from uncovered and covered parts of a sample annealed at 600°C for 60 minutes. All the Ti film in the covered part of the sample has reacted to form the $TiSi_2$ while there's unreacted Ti film left in the uncovered part. Therefore, at high temperature the reaction was faster in the covered part of the sample and slow in the uncovered part.

3.3.3. Discussions

The RBS analysis showed that samples capped with MgO and Al_2O_3 formed Ti_5Si_4 as a first phase. The $TiSi_2$ phase was formed after annealing samples for longer times. The silicide thickness was larger in the samples capped with MgO than those capped with Al_2O_3 for samples annealed at the same temperature and same time (see **Figs. 3.11** to **3.13**). Therefore, the RBS analyses reveal that the reaction was faster in the samples capped with MgO and slower in the samples capped with Al_2O_3. Although it seems that the capping layers did limit the effect of oxidation, RBS showed the presence of oxygen in all the annealed samples.

The XRD analysis showed that the Ti_5Si_4 was the first phase to form in the sample capped with MgO and it continue to grow (see summary in **Table 3.2**). Although samples capped with Al_2O_3 also formed Ti_5Si_4 as a first phase it was detected on samples annealed for longer times. The C49-$TiSi_2$ and the Ti_5Si_4 phases were formed after longer annealing times in the samples capped with MgO while samples capped with Al_2O_3 formed only the Ti_5Si_4 phase as shown in **Fig. 3.16**. All annealed samples from each set showed the presence of Ti_2O. The XRD analysis, therefore, agree with the RBS analysis that Ti_5Si_4 was formed first in both MgO and Al_2O_3 capped samples. The two analyses also agree that the reaction was faster in the samples capped with MgO and slow in the samples capped with Al_2O_3. Therefore, MgO seems the better capping layer of the two.

In the case of the sandwich technique, RBS results showed that the titanium-rich Ti_5Si_4 phase was formed (see **Fig. 3.18(a)**). Samples annealed at low temperature showed that both the sandwich and the control samples formed the same silicide thickness as shown in **Fig. 3.20**. At high temperatures it was found that the silicide formation was faster in the sandwich samples and slower in the control samples. Although the sandwich technique did not stop the unreacted Ti film from oxidizing, the RBS results showed that the oxygen concentration was less in the sandwich sample.

3.4. Summary and Conclusion

The purpose of the study was to investigate the solid-state reaction in the Ti-Si binary system and the effect of oxygen limiting techniques in $TiSi_2$ formation. Samples were prepared in a high vacuum deposition chamber with a base pressure of 3×10^{-8} kPa. A thin layer Ti film was deposited onto a Si(100) substrate. Reaction was induced by annealing samples at varying temperatures in a vacuum furnace. Both XRD and RBS results showed that Ti_5Si_4 and C49-$TiSi_2$ were formed at low temperatures. The high resistance C49-$TiSi_2$ phase was then transformed to the low resistance C54-$TiSi_2$ phase at 650°C. Oxygen was present in the unreacted Ti film of the annealed samples.

Two methods were used in attempting to limit the unwanted oxidation during Ti-silicide formation. Capping layers, namely Al_2O_3 and MgO, and the sandwich technique were used. Both capping layers were found to limit the oxygen concentration in the unreacted Ti film by 30%. It was revealed that the MgO cap enhanced the silicide formation while the Al_2O_3 delayed the reaction. In the case of the sandwich technique, it was found that at high temperatures the reaction was faster in the sandwich samples than in the control samples. The sandwich samples showed 35% less oxygen compared to the control samples.

Chapter 4

Ti-silicide formation through barriers

4.1. Introduction

Previous studies have shown that Si is the dominant diffusing species during solid state reaction between titanium thin films and silicon [Bot-92, Chu-75]. During silicide formation this interlayer (marker) moves towards the surface [Bot-82] of the sample if the metal is the diffusing species to form a silicon-rich phase. A movement of the interlayer (marker) deeper into the sample indicates that silicon is the dominant diffusing species and a titanium-rich phase will be formed. In some of the studies a radioactive ^{31}Si (half-life, 2.62h) was used as a marker [Bot-92]. This was achieved by first depositing a few hundred angstroms of radioactive silicon onto a single-crystal silicon substrate, followed by the deposition of a few angstroms of Ti film. It was found that during the reaction the Si marker moved deeper into the sample and that the Si diffusion takes place by substitutional (vacancy) diffusion mechanism.

During normal silicide formation between titanium thin film and silicon the effective concentration at the growth interface is controlled by the liquidus minimum [Pre-93A]. Most of the titanium silicide phases found in the Ti-Si binary phase diagram have been reported to form as a first phase [Pre-93B] because of the existence of two liquidus minima in the Ti-Si binary system (see **Fig. 3.1**). If an interlayer (marker) is introduced between the titanium layer and the silicon substrate acting as a barrier layer, it will decrease [Pre-97] the titanium or silicon concentration at the growth interface depending on which material diffuses through the interlayer. The aim of this work was to attempt to change the Ti-Si phase formation sequence by using such diffusion barriers.

4.2. Cr barrier layer

4.2.1. Sample Preparations

Two sets of samples were prepared in an e-beam high vacuum deposition chamber at a pressure better than 2 x 10^{-8} kPa. This was done by first depositing 10 Å of chromium (Cr) on one set of Si(100) substrates. This was then followed by the deposition of 1200 Å of titanium film onto both sets of samples. The Cr layer in the first set was used as an interlayer that acts as a barrier layer between the Ti film and the Si substrate. The second set, without Cr layer, was used as control. Reaction was induced by annealing samples in a vacuum furnace at temperatures between 570 and 800°C for 30 minutes. RBS and X-ray diffraction were used to analyze the samples.

4.2.2. RBS Results

RUMP simulations of the as deposited samples from each set showed that 1200 Å of titanium thin layer was deposited. **Fig. 4.1** shows RBS spectra taken from each set of samples annealed at 570°C for 30 minutes. The RUMP simulation revealed that 450Å of titanium-rich Ti_5Si_4 phase was formed. The simulation also revealed that 800 Å of Ti_5Si_4 and 1000 Å of $TiSi_2$ were formed in the control sample. Therefore, the silicide formation was faster in the control sample than on the sample with Cr barrier layer **Fig. 4.2** shows RBS spectra from each set of samples annealed at 660°C for 30 minutes. It can be clearly seen that all the Ti film in the control sample reacted to form a silicon-rich $TiSi_2$ phase. In the sample with a Cr interlayer, it was found that Ti_5Si_4 and a thin layer of $TiSi_2$ were formed. The RUMP simulation showed that the Cr interlayer reacted to form a $CrSi_2$ phase. It also showed that the barrier layer moved deeper into the sample as more Ti-silicide was formed. This indicates that Si is the diffusing species during Ti-silicide formation.

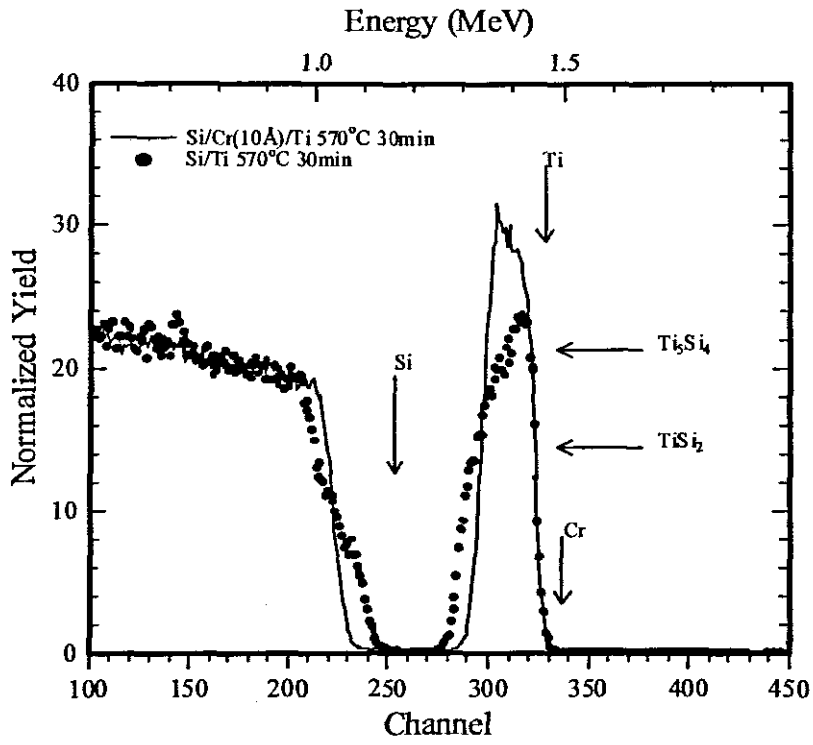

Fig. 4.1 RBS spectra taken from each set of samples after they had been annealing at 570°C for 30 minutes. A very thin layer of Ti_5Si_4 was formed in the sample with Cr barrier layer whereas Ti_5Si_4 and $TiSi_2$ were formed in the control sample. It can be seen that the reaction was faster in the control sample and slower in the sample with Cr barrier layer.

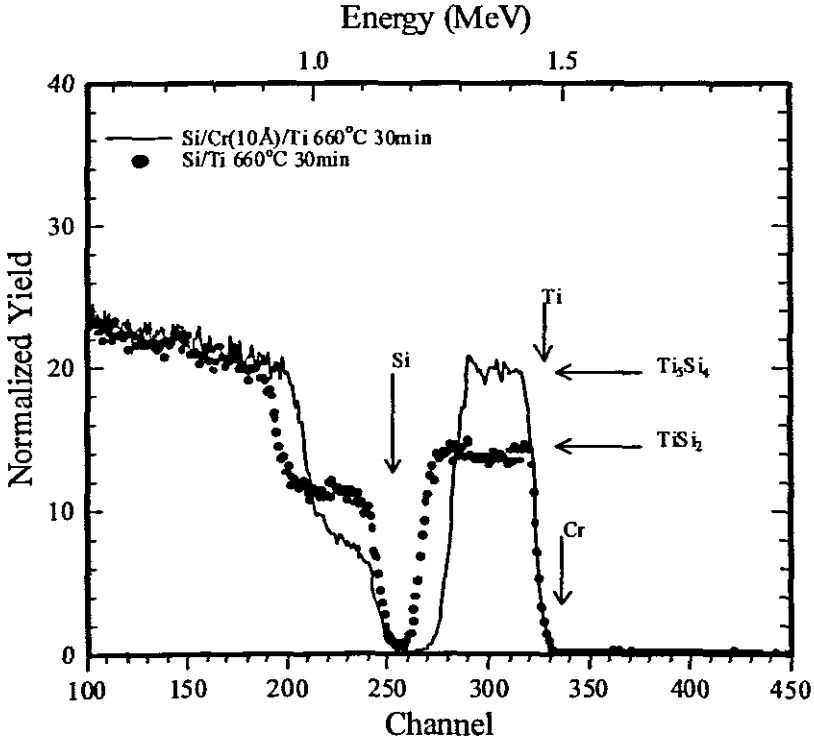

Fig 4.2 RBS spectra of samples from both sets of samples annealed at 660°C for 30 minutes. *All the Ti film in the control sample* has reacted to form $TiSi_2$ while samples with Cr barrier layer had formed Ti_5Si_4 and a very thin layer of $TiSi_2$.

4.2.3. XRD Results

Fig 4.3 to **Fig. 4.6** shows a series of XRD spectra taken in θ-2θ geometry from each set of samples in the as deposited condition as well as after annealing at 570, 630 and 700°C for 30 minutes (as summarized in **Table 4.1**). Both as deposited samples from each set showed strong peaks corresponding to Ti(002) (see **Fig. 4.3**). After annealing samples at 570°C for 30 minutes, Ti_5Si_4 and $TiSi_2$ were formed in the control sample. This is manifested by the well-defined Ti_5Si_4 and the weak C49-$TiSi_2$ reflections (as shown in **Fig. 4.4**). Therefore XRD result agrees with the RBS result that Ti_5Si_4 and $TiSi_2$ were formed in the control samples after annealed at 570°C for 30 minutes. The sample with Cr interlayer formed Ti_5Si_4 and the monosilicide TiSi phase. This was shown by the weak reflections from Ti_5Si_4(023) and TiSi(020). A reflection from unreacted Ti film was also present. More C49-$TiSi_2$ was formed in the control sample after annealing samples at 600°C for 30 minutes (see **Fig. 4.5**). This was shown by the increase in intensity of the C49-$TiSi_2$ peak. No reflection from the Ti_5Si_4 phase was detected. This means the Ti_5Si_4 phase converted to the silicon-rich $TiSi_2$ phase. Sample with Cr barrier layer showed reflections from Ti_5Si_4(203) and Ti(002). Therefore not enough $TiSi_2$ was formed to be detected by XRD. After annealing samples from each set at 700°C for 30 minutes, the low resistance C54-$TiSi_2$ phase was formed as shown in **Fig. 4.6**. This was shown by the well-defined C54-$TiSi_2$ reflections from the control sample and weak reflections from the sample with Cr barrier layer. Therefore the high resistivity C49-$TiSi_2$ phase was transformed to the low resistivity C54-$TiSi_2$ phase.

Table 4.1: Summary of XRD results taken from samples with Cr barrier layer and control samples after annealed at different temperatures.

Temperature & Time	Control Samples	Samples with Cr barrier layer
570°C 30 minutes	Ti_5Si_4, C49-$TiSi_2$	Ti_5Si_4, TiSi
600°C 30 minutes	C49-$TiSi_2$	Ti_5Si_4, TiSi
630°C 30 minutes	C49-$TiSi_2$	Ti_5Si_4
660°C 30 minutes	C54-$TiSi_2$	Ti_5Si_4, C49-$TiSi_2$
700°C 30 minutes	C54-$TiSi_2$	C54-$TiSi_2$

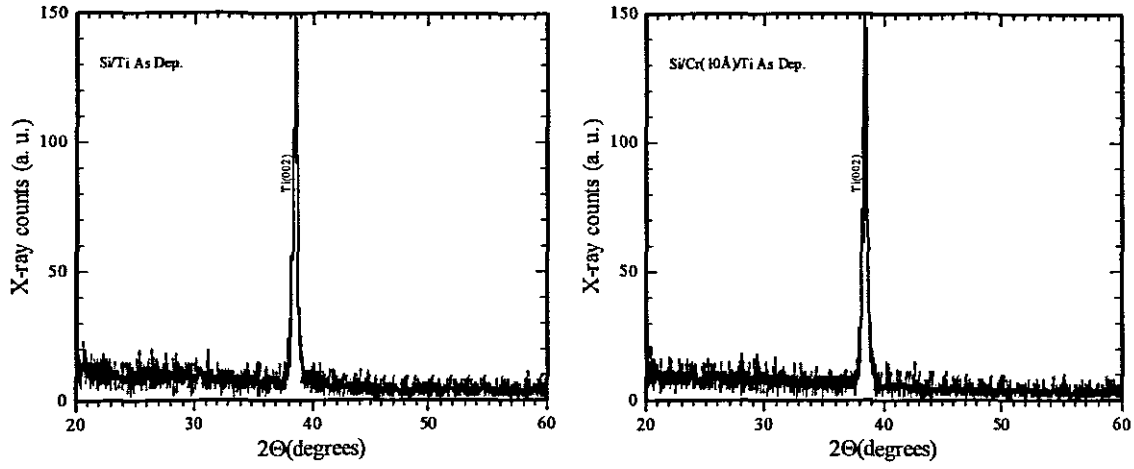

Fig. 4.3 XRD spectra taken from the as deposited samples of each set. Both samples showed well-defined reflections at 38.4° corresponding to Ti(002).

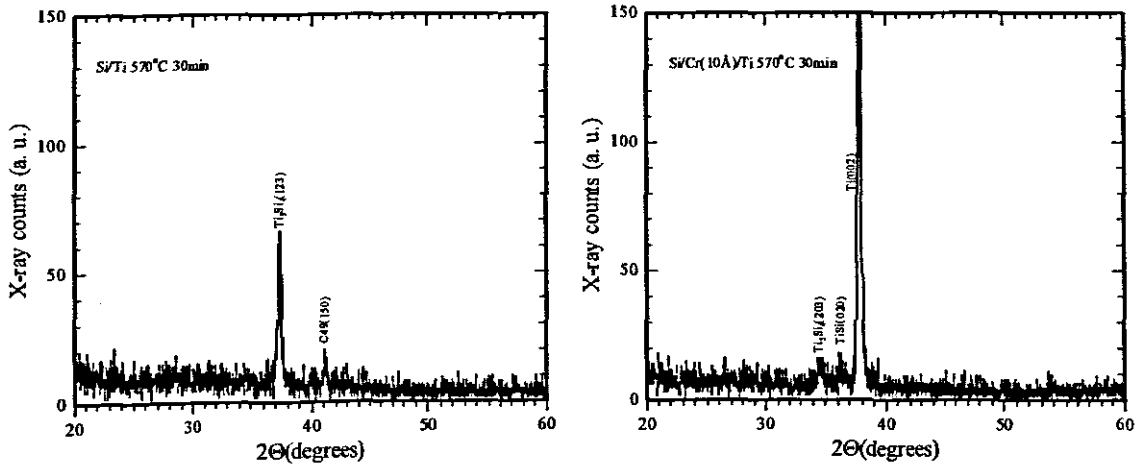

Fig. 4.4 XRD spectra taken from both sets of samples annealed at 570°C for 30 minutes. C49-$TiSi_2$ and Ti_5Si_4 were formed in the control sample while Ti_5Si_4 and TiSi were formed in the sample with Cr barrier layer. A reflection from Ti was also present.

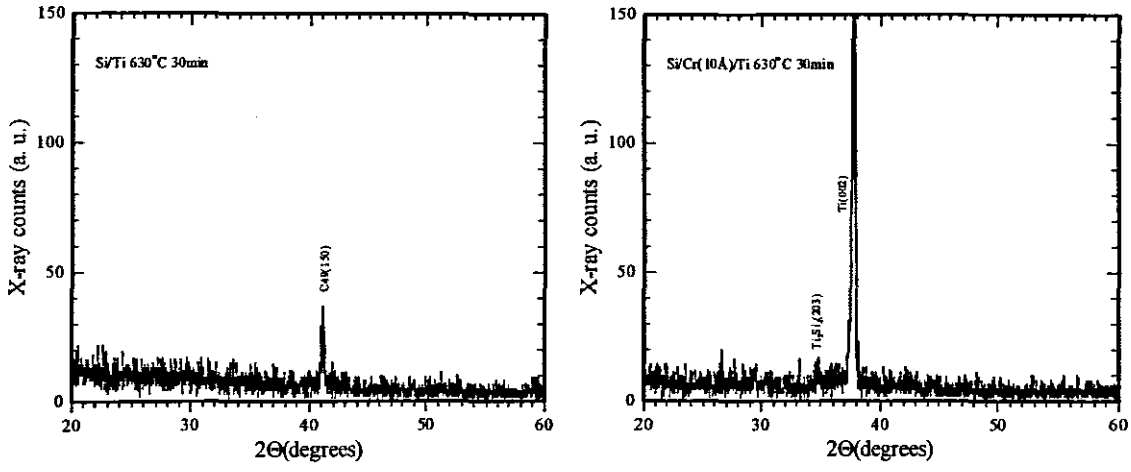

Fig. 4.5 XRD spectra taken from both sets of samples annealed at 630°C for 30 minutes. More C49-$TiSi_2$ phase was formed in the control sample whereas not enough $TiSi_2$ was formed in the sample capped with Cr barrier layer to be detected by XRD.

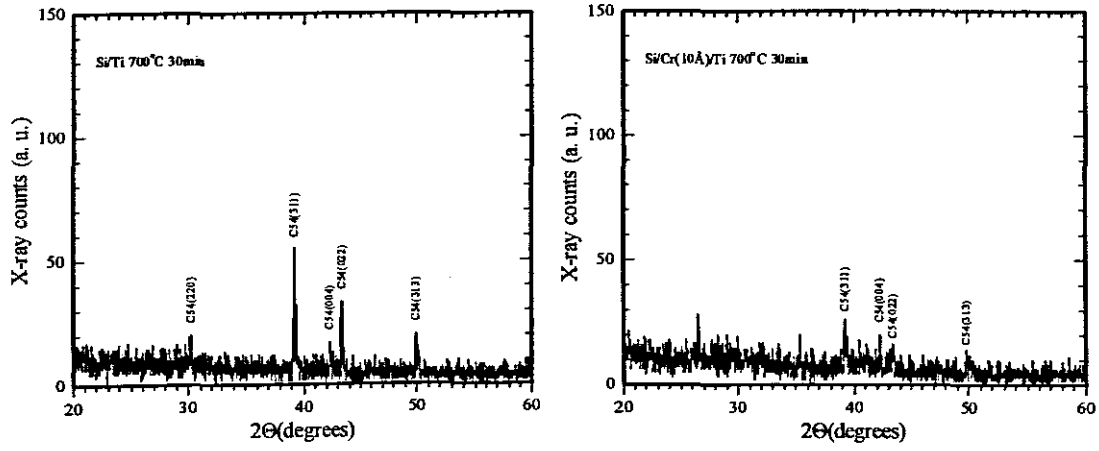

Fig. 4.6 XRD spectra taken from both sets of samples annealed at 700°C for 30 minutes. All samples formed the low resistivity C54-$TiSi_2$ phase. This was manifested by the well-defined C54-$TiSi_2$ reflections in the control samples and the weak reflections in the sample capped with Cr interlayer.

4.3. Zr barrier Layer

4.3.1. Sample Preparation

Two sets of samples were prepared. In the first step 10Å of zirconium (Zr) was deposited onto one set of Si(100) substrates. This was then followed by the deposition of 1200 Å of Ti thin film onto both sets of samples. The Zr layer in the first set was used as a barrier layer. Samples were subsequently annealed in a vacuum furnace with pressure better than 3×10^{-8} kPa at temperatures ranging between 570 and 800°C for 30 minutes. Sample analysis was done using RBS and XRD techniques.

4.3.2. RBS Analysis

Fig. 4.7 shows RBS spectra in the as deposited condition as well as after annealing at 570°C for 30 minutes. The RUMP simulation revealed that the as deposited samples from both sets had 1200Å of Ti thin layer. It also revealed that in the reacted samples 500 Å of Ti_5Si_4 was formed in the sample with Zr barrier layer whereas 800 Å Ti_5Si_4 and 1000 Å $TiSi_2$ were formed in the control sample. This shows that the interlayer delayed the formation of the silicon-rich $TiSi_2$ phase. It can be seen from the figure that the Zr interlayer moved to lower energies after annealing. This means the interlayer moved deeper into the sample as more Ti-silicide was formed on top of the interlayer. **Fig. 4.8** shows RBS spectra of samples from each set annealed at 660°C for 30 minutes. The simulation showed that the Zr layer reacted with silicon to form $ZrSi_2$. It also showed that $TiSi_2$ and 800 Å Ti_5Si_4 were formed with 100 Å Ti + O still unreacted. All the Ti film in the control samples reacted to form $TiSi_2$ phase. Therefore, these results agree with the results of the samples annealed at 570°C that the Zr layer delays the $TiSi_2$ formation. Since the interlayer was found to move deeper into the sample during silicide formation, it follows that Si is the dominant diffusing species during Ti-silicide formation.

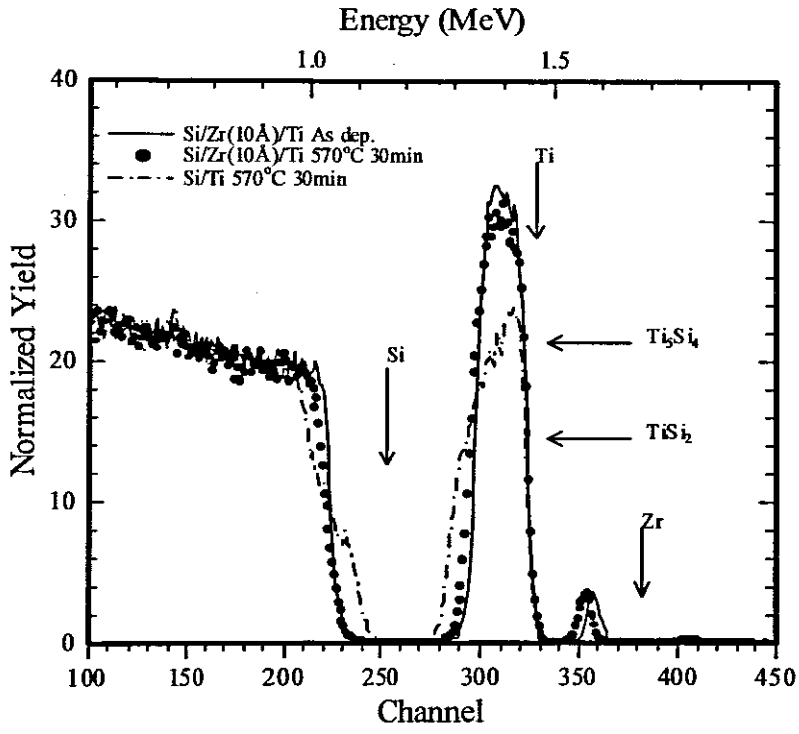

Fig. 4.7 RBS spectra taken from samples in the as deposited condition as well as samples annealed 570°C for 30 minutes. Only a very thin layer of Ti_5Si_4 was formed in the sample with Zr barrier layer whereas Ti_5Si_4 and $TiSi_2$ were formed in the control samples. The Zr interlayer moved to lower energies after annealing.

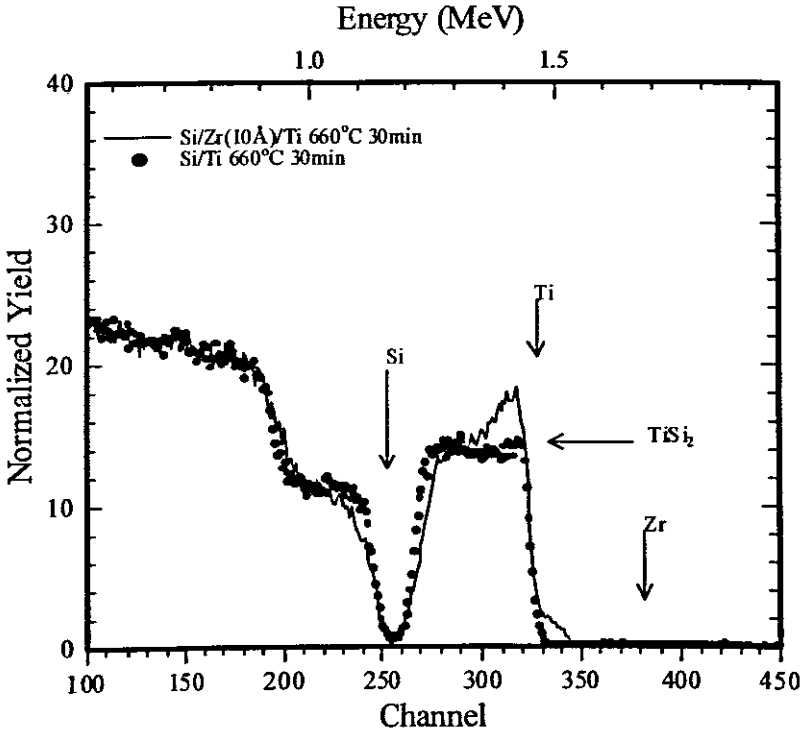

Fig. 4.8 RBS spectra taken from both set of samples annealed at 660°C for 30 minutes. All Ti film in the control sample reacted to form $TiSi_2$ whereas sample with Zr interlayer formed Ti_5Si_4 and $TiSi_2$ with 100 Å of Ti + O still unreacted. The barrier layer moved deeper into the sample.

4.3.3. XRD Analysis

Fig. 4.9 to **Fig. 4.12** shows a series of XRD spectra taken in θ-2θ geometry from both sets of samples in the as deposited condition as well as after annealed between 570 and 700°C for 30 minutes. In the as deposited samples from each set there was evidence of hexagonal Ti. This was manifested by an intense peak at 38.4° corresponding to Ti-hexagonal(002) as shown in **Fig. 4.9**. In the reacted samples, it was found that Ti_5Si_4 and $TiSi_2$ were formed in the control sample whereas Ti_5Si_4 and monosilicide TiSi were formed in the sample with Zr barrier layer (see **Fig. 4.10**). This was shown by the strong Ti_5Si_4 reflections and the weak C49-$TiSi_2$ and TiSi reflections. No reflections from $TiSi_2$ were observed in the sample with Zr barrier layer. Therefore, the XRD results agree with RBS that no $TiSi_2$ was formed in the sample Zr barrier layer annealed at 570°C for 30 minutes. The control sample annealed at 660°C for 30 minutes showed that the C49-$TiSi_2$ phase was transformed to the high temperature C54-$TiSi_2$ phase (see **Fig 4.11**). In the sample with Zr barrier layer, it was found a C49-$TiSi_2$ phase begun to form. The titanium-rich Ti_5Si_4 and Ti_5Si_3 were also found to be present. **Fig. 4.12** shows XRD spectra taken from both sets of samples annealed at 700°C for 30 minutes. Samples from both sets showed the presence of the low resistivity C54-$TiSi_2$ phase. This was shown by the well-defined C54-$TiSi_2$ peaks. The summary of all the XRD results taken from samples with Zr barrier layer and control samples after annealed at different temperatures is shown **Table 4.2**.

Table 4.2: Summary of XRD results taken from samples with Zr barrier layer and control samples after annealed at different temperatures.

Temperature and Time	Control Samples	Samples with Zr barrier layer
570°C 30 minutes	Ti_5Si_4, C49-$TiSi_2$	Ti_5Si_4, TiSi
600°C 30 minutes	C49-$TiSi_2$	Ti_5Si_4, TiSi
630°C 30 minutes	C49-$TiSi_2$	Ti_5Si_4, Ti_5Si_3, TiSi
660°C 30 minutes	C54-$TiSi_2$	Ti_5Si_4, C49-$TiSi_2$, Ti_5Si_3
700°C 30 minutes	C54-$TiSi_2$	C54-$TiSi_2$

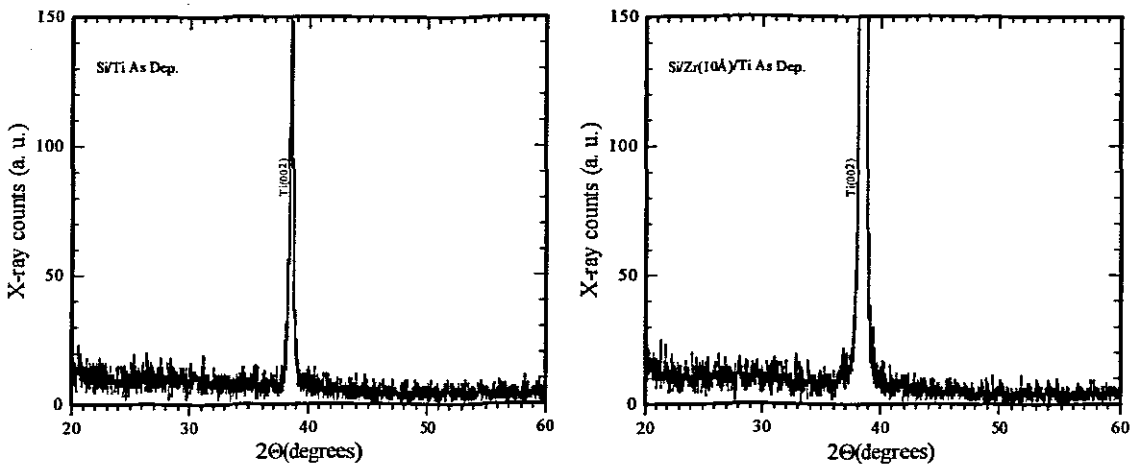

Fig. 4.9 XRD spectra taken from the as deposited sample from both sets. Only reflection from Ti(002) were present in both samples. No silicide reflections were present.

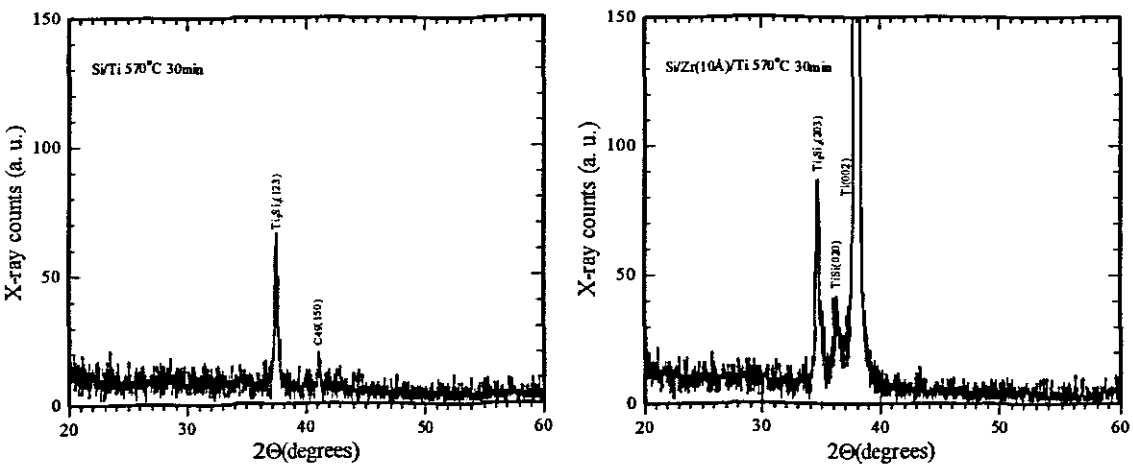

Fig. 4.10 XRD spectra taken from each set of samples annealed at 570°C for 30 minutes. The control sample formed Ti_5Si_4 and C49-$TiSi_2$ whereas Ti_5Si_4 and the monosilicide TiSi were formed in the samples with Zr barrier layer. No $TiSi_2$ was formed in the sample with Zr barrier layer.

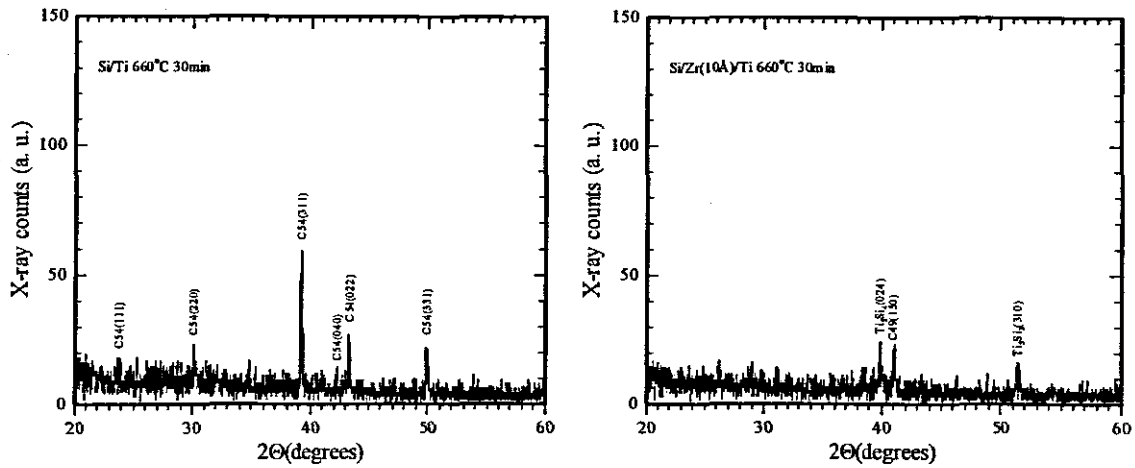

Fig. 4.11 XRD spectra taken from both sets of samples annealed at 660°C for 30 minutes. The C49-$TiSi_2$ formed in the control sample was transformed to the C54-$TiSi_2$ phase. A C49-$TiSi_2$ begun to form in the sample with Zr barrier layer. Other phases present were Ti_5Si_4 and Ti_5Si_3.

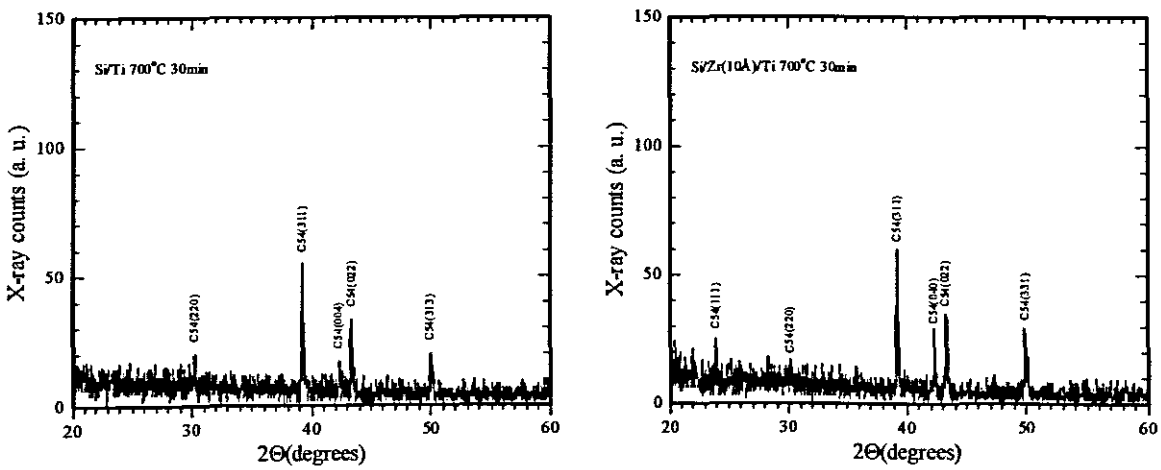

Fig. 4.12 XRD spectra taken from samples annealed at 700°C for 30 minutes. Both samples from each set formed the low resistivity C54-$TiSi_2$ phase.

4.4. Summary and Conclusion

The RBS results taken from samples with barrier layers showed that at low temperature the Ti_5Si_4 was formed whereas in the control samples two phases, namely, Ti_5Si_4 and $TiSi_2$ were formed. A summary of the Ti_5Si_4 and $TiSi_2$ thickness formed in the three different groups of samples after annealing at different temperatures is shown in **Table 4.3**. **Fig. 4.13** shows $TiSi_2$ thickness versus temperature plots of samples from each set after annealing between 570 and 800°C for 30 minutes. It was not clear which of the two ($TiSi_2$ and Ti_5Si_4) phases formed in the control samples nucleated first. In the reacted samples it was found that both barrier layers reacted with silicon to form $CrSi_2$ and $ZrSi_2$ respectively. The rump simulation revealed that both barrier layers moved to lower energies as the reaction progresses. Therefore, the barrier layers moved deeper into the samples as more silicide was formed which indicated that Si was diffusing through the barrier layer to form silicide at the barrier-titanium interface. This results, therefore, agree with previous work done by Botha *et. al.* [Bot-82] and Chu *et. al.* [Chu-75] that Si is the diffusing species during Ti-silicide formation. It was found that the reaction in the samples with barrier layers was slow compared to the reaction in the control samples. Therefore the barrier layers slowed the silicide formation.

Table 4.3: A summary of phase formation measured in all groups of samples after annealing at different temperatures.

Temperature & Time	Phases Formed	Control Samples	Samples with Cr Barrier	Samples with Zr Barrier
570°C 30min	Ti_5Si_4 $TiSi_2$	800 Å 1000 Å	450 Å 0 Å	500 Å 0 Å
600°C 30min	Ti_5Si_4 $TiSi_2$	1150 Å 1600 Å	600 Å 0 Å	750 Å 0 Å
630°C 30min	Ti_5Si_4 $TiSi_2$	850 Å 2200 Å	1050 Å 300 Å	1700 Å 450 Å
660°C 30min	Ti_5Si_4 $TiSi_2$	0 Å 4200 Å	2100Å 600Å	800 Å 2800 Å
700°C 30min	Ti_5Si_4 $TiSi_2$	0 Å 4300 Å	0 Å 3900 Å	0 Å 4200 Å
750°C 30min	Ti_5Si_4 $TiSi_2$	0 Å 4400 Å	0Å 4200Å	0 Å 4300 Å
800°C 30min	Ti_5Si_4 $TiSi_2$	0 Å 4500 Å	0 Å 4500 Å	0 Å 4500 Å

XRD results showed that no silicide was formed in the as deposited samples. In the reacted samples, XRD revealed that at low temperature Ti_5Si_4 and the monosilicide TiSi were formed in the samples with barrier layers whereas Ti_5Si_4 and C49-$TiSi_2$ were formed in the control samples. Therefore the XRD results agree with RBS that the barrier layers delayed the formation of $TiSi_2$ phase. The $TiSi_2$ phase was formed at higher temperature although there was still the presence of the titanium-rich phases. All samples formed the low resistance C54-$TiSi_2$ above 660°C.

Therefore it can be concluded that the Cr and Zr barrier layers delayed the $TiSi_2$ formation. Silicon was found to be the dominant diffusing species during Ti-silicide formation as reported before.

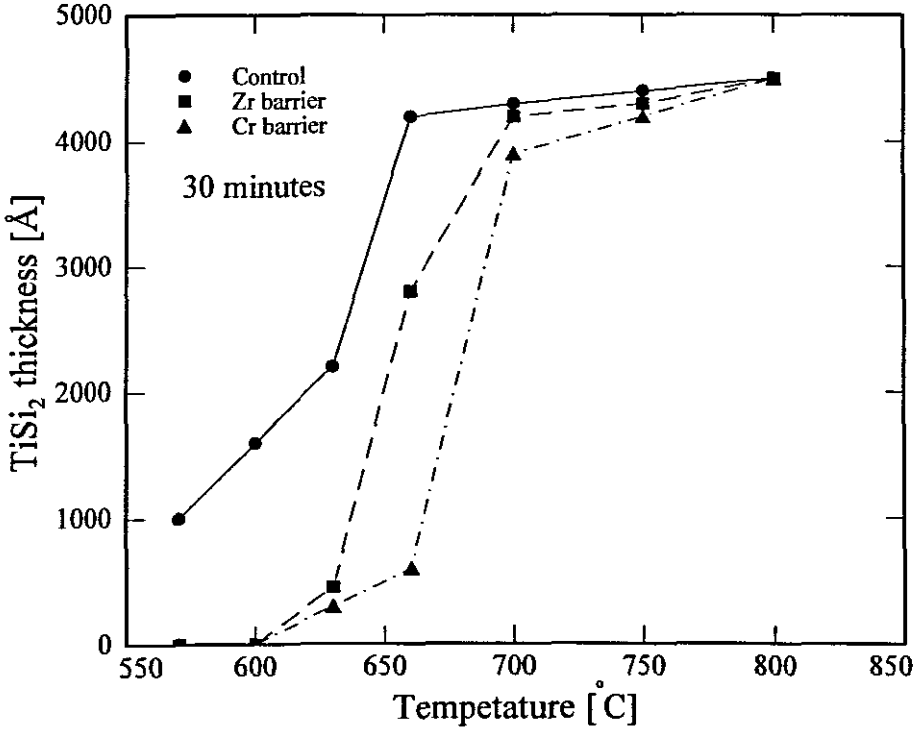

Fig. 4.13 $TiSi_2$ thickness versus temperature plots of samples from each set after annealing at different temperatures. It can be seen that at 600°C already a $TiSi_2$ phase was formed in the control sample whereas no $TiSi_2$ was formed in both samples with barrier layers. Therefore, both barrier layers delayed the formation of $TiSi_2$.

Chapter 5

Effect of stress on Ti-silicide formation

5.1. Introduction

As the device dimensions scale down to the deep submicron regime with a multilayer structure, issues related to stress become troublesome in semiconductor device fabrication [Che-99]. Stress can degrade gate oxides in metal-oxide-semiconductor field effect transistors and cause cracks in interconnect lines [Che-00]. A recent finite-element calculation showed that the substrate regions at the oxide edge are compressively stressed to a significant extent [She-96]. The stress level near the silicon substrate surface inside the oxide openings is, therefore, of major concern to the formation of silicides. Diffusion in thin films is known to be retarded under compressive stress [Che-99].

Stress in uniform thin film structures can be classified as either coherency, thermal or intrinsic (or growth) stress [Cam-99]. Coherency stress results when a thin film is lattice matched to a substrate that has an equilibrium in plane lattice parameter different from that of the film [Cam-99]. Thermal stress is generated when a film-substrate system experiences a change in temperature. If the film and substrate have different thermal expansion coefficients, a temperature change will result in a difference in thermal expansion between the film and the substrate. Stress generated during film growths that are not as a result of coherency or thermal effects are called intrinsic.

Thermal stress can be used to engineer stress in a thin film system by depositing a film with a different thermal expansion to that of the substrate. In this work different

thicknesses of Si_3N_4 and SiO_2 films were deposited onto the backside (BS) of silicon wafers to induce different stress situations in the front side (FS) of the substrates. The reaction between the differently stressed silicon wafers and a front side film of Ti was then studied.

5.2. Sample preparation and stress measurements

Samples were prepared in two steps. The first step was to introduce stress by either growing SiO_2 or depositing Si_3N_4 films of varying thickness onto the backside of a Si(100) wafer. The second step was to deposit 500 Å of titanium onto the front side of the same wafer. Three groups of samples were made. One set had 400nm SiO_2 on the backside and two sets had 200nm and 400nm Si_3N_4, respectively. The reflection of laser light was used to measure the radius of curvature of the samples. Measurements were done before the first deposition and again after the first and second depositions. Using Stoney's equation (**eqn. 2.11**) the stress in the deposited thin films was calculated from these measurements. The stress measured in the backside and front side films at room temperature is shown in **Table 5.1**.

Table 5.1: The radius of curvature and related stress values in thin films for different samples after the backside and front side deposition respectively [Waa-99].

BS film	Si Radius Undeposited (m)	R_{eff} (BS-Si) (m)	R_{eff} (FS-Si) (m)	Stress (BS-film) (MPa)	Stress (FS-film) (MPa)
400nm Si_3N_4	121	24.79	1080	1459	33.2
200nm Si_3N_4	406	53.75	733	1345	97.9
400nm SiO_2	165	-93.82	-4381	-385	-8.2

During the deposition process, samples are heated and when they return to room temperature different thermal expansion coefficients causes different contraction in the film. Insulators have a smaller thermal coefficient than Si while a metallic film usually has a larger thermal expansion coefficient. **Fig. 5.1** shows the contribution of both the front side and the back deposition to the total stress in the sample. In the case of thermally grown oxides the samples are heated to above 1000°C. SiO_2 being an insulator tends to shrink less than silicon when cooled to room temperature. Therefore, the silicon substrate experiences a compressive stress. A metallic film tends to shrink more than the silicon substrate when cooled down to room temperature. This means that the silicon substrate will experience a tensile stress. The stress caused by Si_3N_4 is positive (tensile). Therefore it has a large thermal expansion coefficient than the silicon substrate and acts as a metallic film.

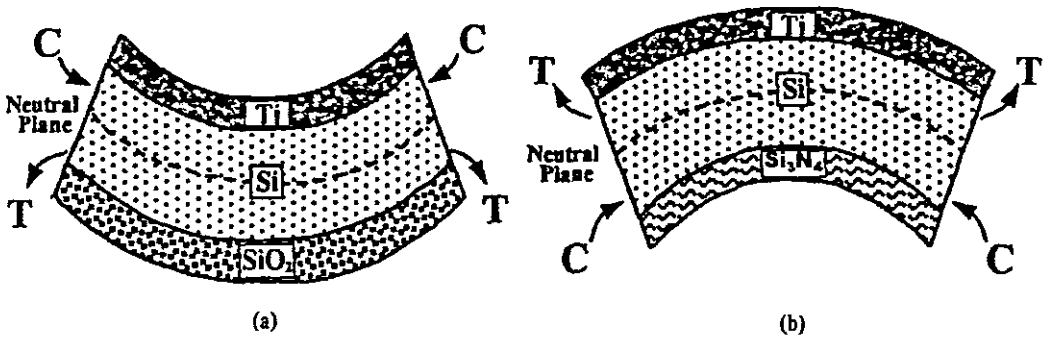

Fig. 5.1 A schematic diagram showing how thin films with different thermal expansion coefficients deposited on a Si(100) wafer can cause stress on the silicon substrate. C and T denote compressive and tensile stress, respectively.

5.3. RBS Analysis

Samples from all three groups were annealed at 530, 600 and 650°C for varying times in a vacuum furnace to induce reaction. Samples from each group were annealed together in the furnace. **Fig. 5.2** shows RBS spectra taken from each sample group annealed at 530°C for 64 minutes. A 1 MeV beam was used to improve the depth resolution. The RUMP simulation showed that the unreacted sample had 500 Å of titanium. The simulation also showed that in the reacted samples, 1050 Å of $TiSi_2$ was formed in both samples with Si_3N_4 deposited on the backside. It also revealed that 50 at. % oxygen was prominent in the unreacted Ti thin layer. The samples with SiO_2 on the backside formed only 450 Å of $TiSi_2$ and 390 Å of Ti_5Si_3 phase. The unreacted Ti layer also showed the presence of oxygen. **Fig. 5.3** shows RBS spectra taken from each samples group annealed at 600°C for 10 minutes. The simulation showed that both samples with Si_3N_4 on the backside formed 1600 Å of $TiSi_2$ phase whereas the sample with 400nm SiO_2 formed 1200 Å of $TiSi_2$ phase.

As mentioned in **Chapter 3**, the $TiSi_2$ phase has been reported to grow with linear [Pic-88] and diffusion limited kinetics [Hun-83]. In this work the cube root of time gave the best fit to the data and **Fig. 5.4** shows a plot of $TiSi_2$ thickness versus the cube root of time for the samples with 200nm Si_3N_4, 400nm Si_3N_4 and 200nm SiO_2 deposited on the backside after being annealed at 530°C. A similar growth kinetics for $TiSi_2$ grown on Pd_2Si was reported in the literature by Finstad *et. al.* [Fid-80]. He found that the time dependence of $TiSi_2$ formation between a thin layer of Ti on Si(111) substrate was found to be anomalous and close to the cube root of time. This growth kinetic can be explained by a model proposed by Barg *et. al.* [Bar-92] which say that this kind of growth can be achieved if the morphological silicide growth is an Island not a planar growth. If the Island grows in width and depth (thickness) simultaneously then its growth is proportional to the cube root of time.

From the RBS data it is clear that the amount of silicide formation depends upon the backside film. It can be seen that the Ti film reacted faster with Si on the sample with Si_3N_4 on the backside (tensile stressed) than in the sample with the SiO_2 backside film (compressive stressed). All samples showed presence of oxygen in the unreacted titanium films. The oxygen concentration seems to increase in the unreacted Ti as the annealing time is increased.

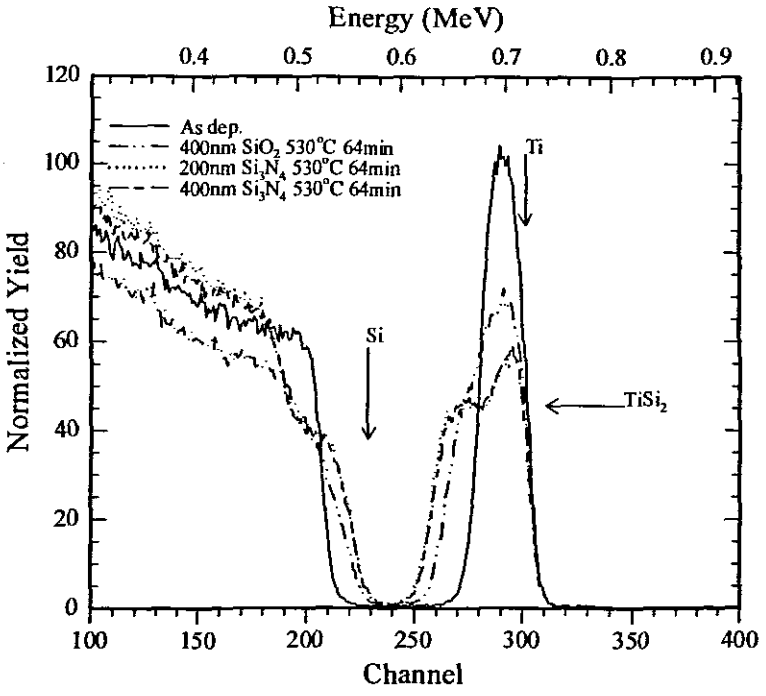

Fig.5.2 RBS spectra showing different $TiSi_2$ thickness from each sample group after being annealed at 530°C for 64 minutes. The unannealed sample had 500 Å of Ti. A 1 MeV beam was used to improve depth resolution.

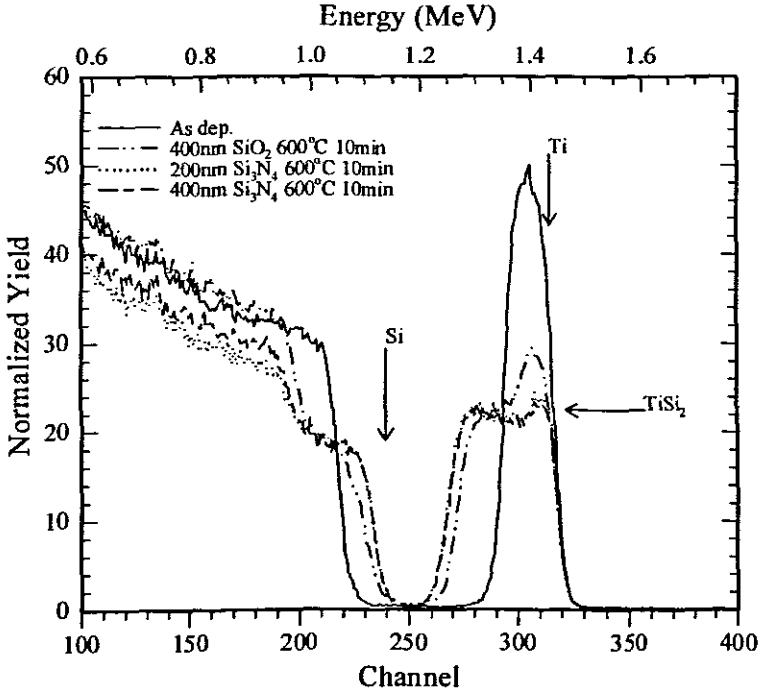

Fig. 5.3 RBS spectra taken from each samples group annealing at 600°C for 10 minutes. The simulation showed that both samples with Si_3N_4 on the backside formed 1600 Å of $TiSi_2$ phase whereas the sample with 400nm SiO_2 formed 1200 Å of $TiSi_2$ phase. A 2 MeV beam was used in this case.

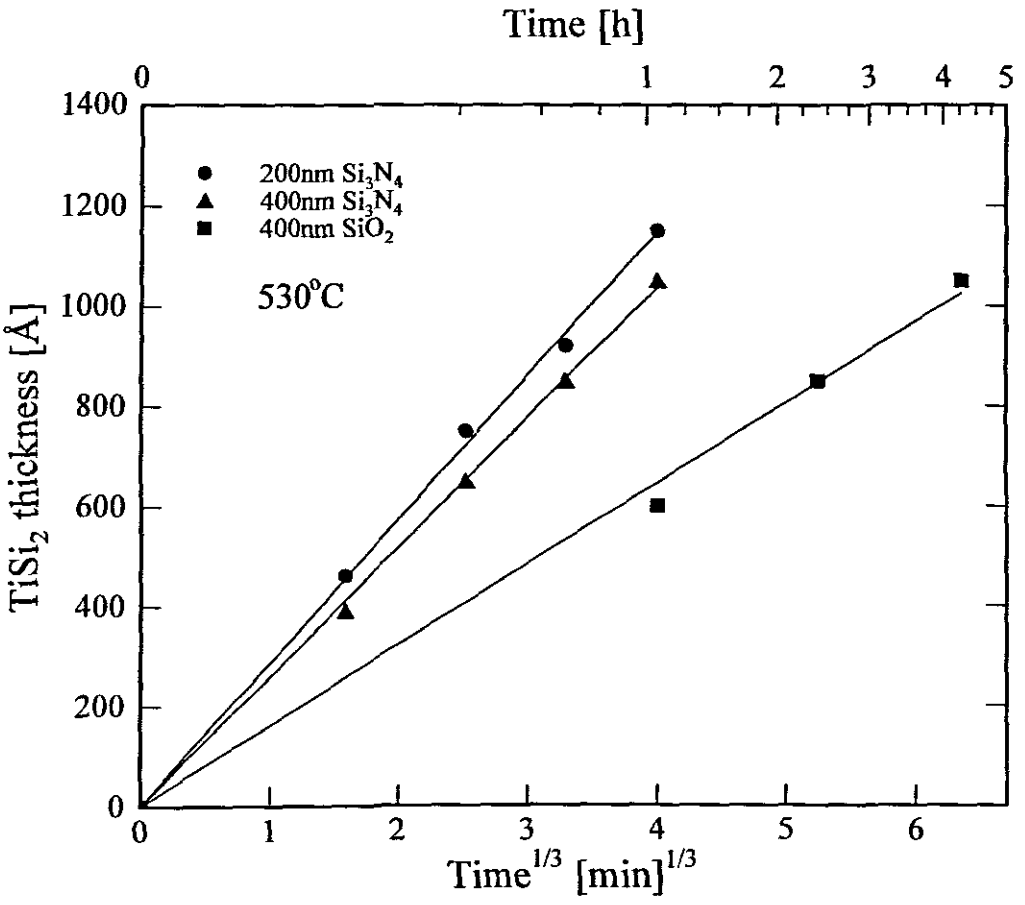

Fig. 5.4 A plot of $TiSi_2$ thickness versus the cube root of time for samples with 200nm Si_3N_4, 400nm Si_3N_4 (tensile stress) and 200nm SiO_2 (compressive stress) deposited on the backside after being annealed at 530°C. It can be seen that the cube root of time gave the best fit to the data.

5.4. XRD Analysis

Fig 5.5 to **Fig. 5.8** show XRD spectra taken from two groups of samples with 400nm Si_3N_4 and 400nm SiO_2 deposited on the back side annealed at 530 and 600°C for varying times taken in 2θ-θ geometry (see summary in **Table 5.2**). Both unannealed samples showed strong peaks at 33.04° and 38.4° corresponding to body-centered cubic Si and hexagonal Ti respectively (see **Fig. 5.5**). No silicide was detected in the unannealed samples. In the samples annealed at 530°C for 16 minutes, it was found that Ti_5Si_3 and $TiSi_2$ were formed in the tensile stressed (400nm Si_3N_4) sample whereas only Ti_5Si_3 was formed in the compressed stressed (400nm SiO_2) sample. This was manifested by the well-defined Ti_5Si_3 reflections and the weak C49-$TiSi_2$ reflection (as shown in **Fig. 5.6**). The $TiSi_2$ formed in the sample with 400nm Si_3N_4 was the high resistance C49 phase. Both samples formed the low temperature C49-$TiSi_2$ after annealed at 530°C for 64 minutes and 600°C for 10 minutes as shown in **Figs. 5.7** and **5.8** respectively. Therefore, the XRD results agree with RBS that the silicide formation was faster in the tensile stressed sample and slower in the compressive stressed samples. Although RBS showed the presence of oxygen in the unreacted Ti film, no reflection corresponding to titanium oxide was seen.

Table 5.2: XRD results showing which phases were formed in the samples from each group annealed at 530°C, 600°C and 650°C for varying times.

Temperature and Time	200nm Si_3N_4	400nm Si_3N_4	400nm SiO_2
530°C 16 minutes	Ti_5Si_3, C49-$TiSi_2$	Ti_5Si_3, C49-$TiSi_2$	Ti_5Si_3
530°C 64 minutes	C49-$TiSi_2$	C49-$TiSi_2$	C49-$TiSi_2$
600°C 10 minutes	C49-$TiSi_2$	C49-$TiSi_2$	C49-$TiSi_2$
650°C 30 minutes	C54-$TiSi_2$	C54-$TiSi_2$	C54-$TiSi_2$

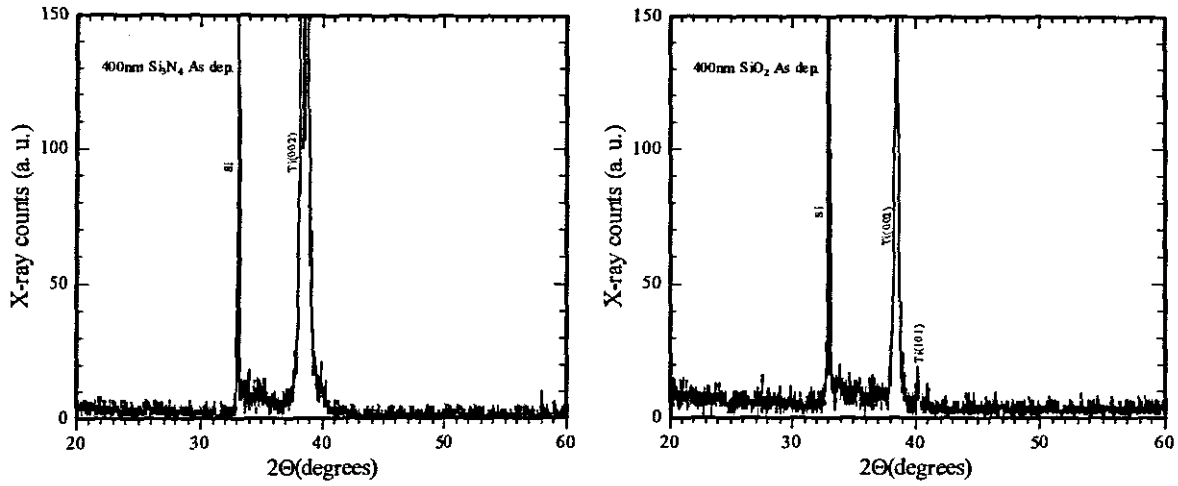

Fig 5.5 XRD spectra taken from as deposited samples with 400nm Si_3N_4 and 400nm SiO_2 films on the backside. Strong peaks at 33.04° and 38.4° corresponding to body-centered Si and hexagonal Ti were present. No silicide was formed at this stage.

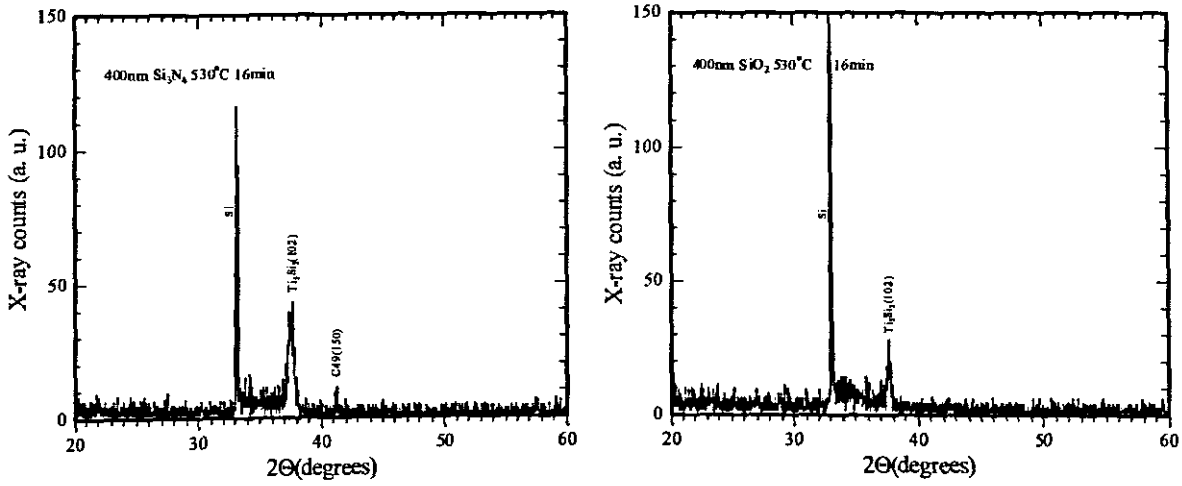

Fig. 5.6 XRD spectra taken from samples with 400nm Si_3N_4 and 400nm SiO_2 films on the backside annealed at 530°C for 16 minutes. Samples with 400nm Si_3N_4 formed Ti_5Si_3 and C49-$TiSi_2$ phases whereas only the Ti_5Si_3 was formed on the sample with 400nm SiO_2 on the backside.

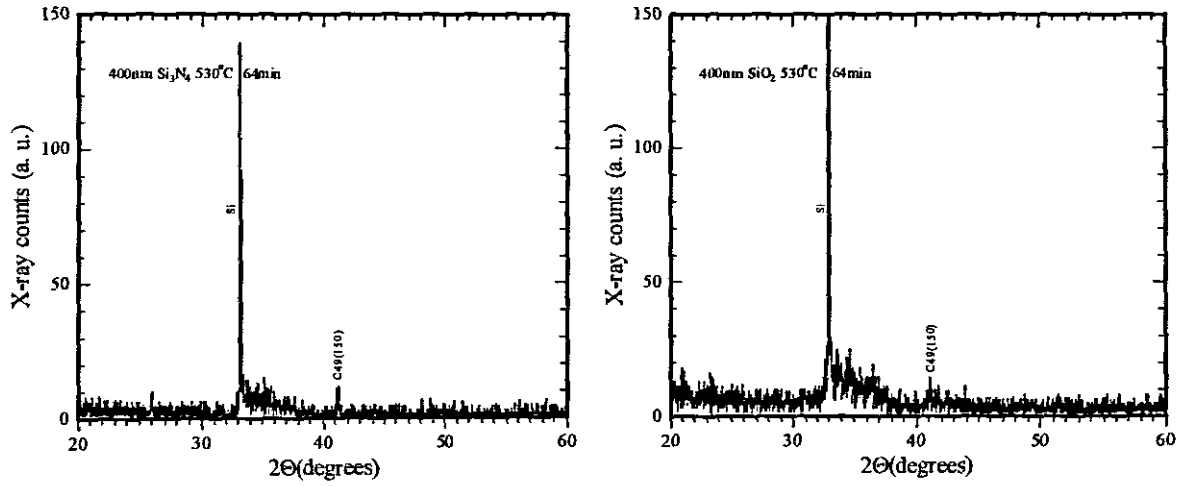

Fig. 5.7 XRD spectra taken from samples with 400nm Si_3N_4 and 400nm SiO_2 films on the backside annealed at 530°C for 64 minutes. Both samples formed the high resistance C49-$TiSi_2$ phase.

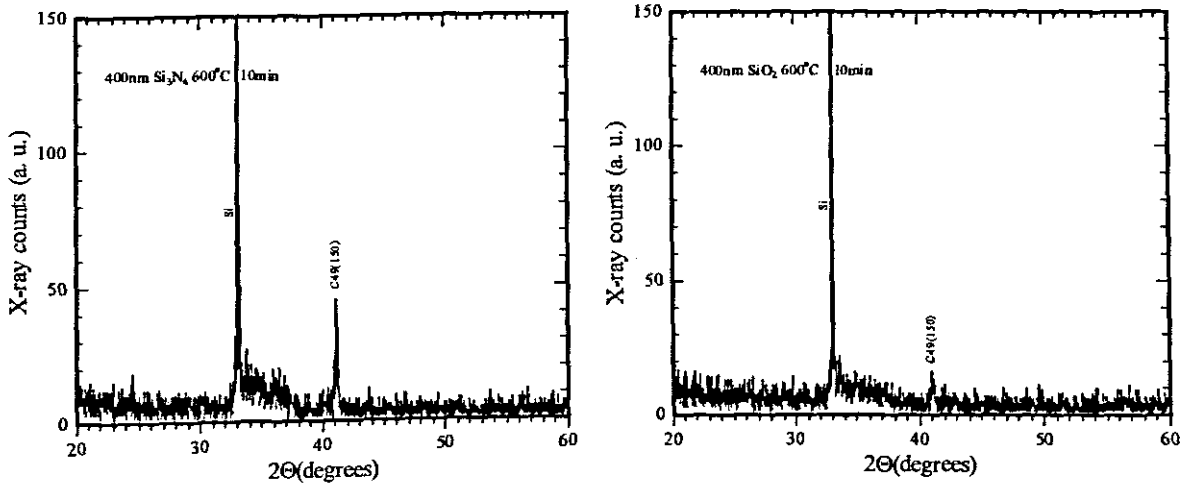

Fig. 5.8 XRD spectra taken from samples with 400nm Si_3N_4 and 400nm SiO_2 films on the backside annealed at 600°C for 10 minutes. More low temperature C49-$TiSi_2$ phase was formed in both sample groups.

5.5. Discussions and Summary

The RBS results showed that samples with Si_3N_4 on the backside formed only the $TiSi_2$ phase at low temperature whereas Ti_5Si_3 and $TiSi_2$ were formed in the samples with SiO_2 on the backside. This was also confirmed by the XRD results which showed the C49-$TiSi_2$ reflection on the samples with Si_3N_4 while reflections from the C49-$TiSi_2$ and Ti_5Si_3 were seen on the samples with SiO_2 on the backside. A similar work was done by Cheng [Che-99] in which SiO_2 and $CoSi_2$ films were grown on the backside of a single-crystal silicon wafer to induce compressive and tensile stress respectively. It was found that the contribution of stresses on the films from the samples diminished with increasing temperature (see **Fig. 5.9**).

RBS results revealed that at high temperature all stressed samples formed the silicon-rich $TiSi_2$ phase. It was found that the tensile stressed samples formed the same $TiSi_2$ thickness while the $TiSi_2$ thickness in the compressively stressed sample was found to be 25% less. XRD also confirmed the formation of the high resistivity C49-$TiSi_2$ phase in all samples annealed at 600°C for 10 minutes (see **Fig. 5.8** and **Table 5.2**). Therefore the reaction in the tensile stressed samples was faster than the reaction in the compressively stressed samples. Cheng [Che-99] argued that an increase in compressive stress on the surface of the Si wafer would lead to a loss in vacancies as the system would try to accommodate the increase in pressure and an increase in tensile stress would lead to an increase in vacancies. He further argued that the compressive stress hinders the migration of Si through the Ti/Si interface so that the formation of the $TiSi_2$ film is retarded and tensile stress promotes the Si diffusion to facilitate the growth of $TiSi_2$ thin films.

In summary, the effect of stress on the formation of $TiSi_2$ thin film was investigated. SiO_2 and Si_3N_4 deposited on the backside of a silicon wafer causes compressive and tensile stresses on the front side of the substrate respectively. Tensile stress was found to enhance the growth of $TiSi_2$ whereas compressive stress was found to retard the $TiSi_2$ growth.

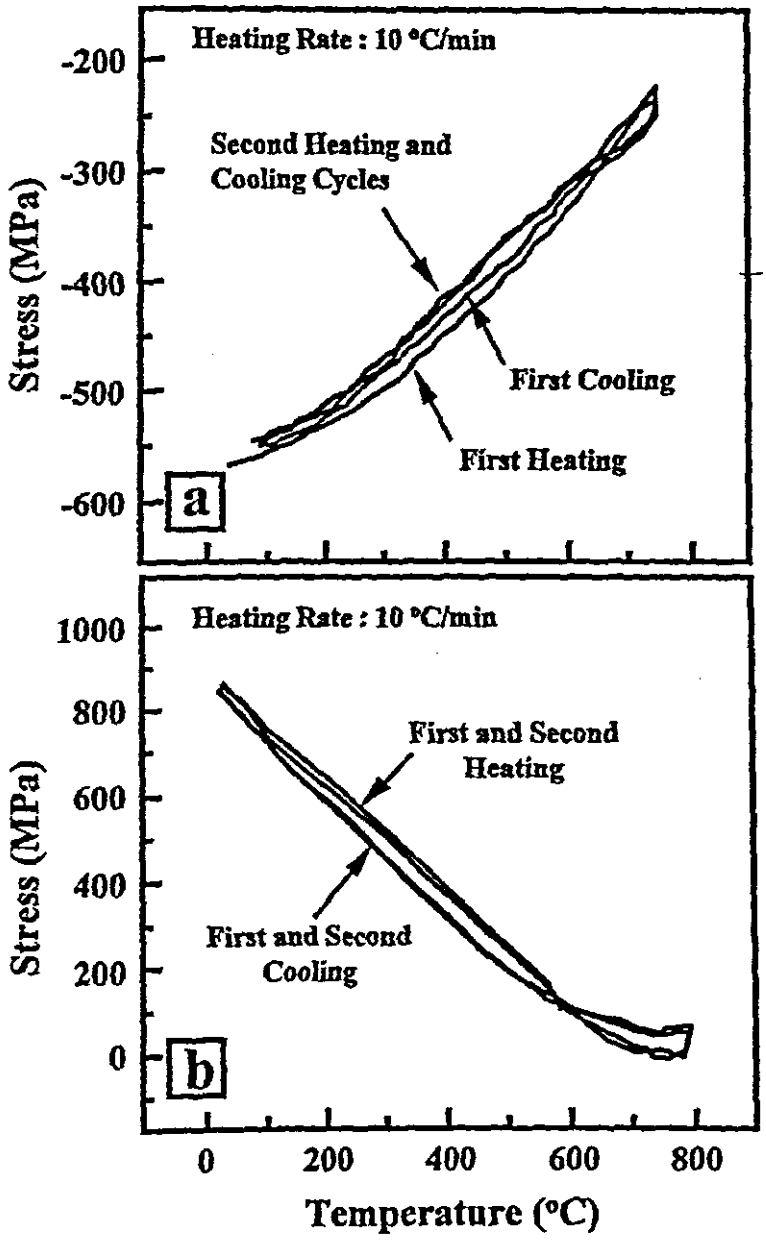

Fig. 5.9 Stress as a function of temperature (*in situ* measurements) during two heating and cooling cycles of (a) thermally grown SiO_2 and (b) $CoSi_2$ film [Che-99].

Chapter 6

Summary and Conclusion

Metal silicides continue to be an important part of the design philosophy in semiconductor technology due to their application as contacts or interconnects. Metal silicides are usually formed by a reaction between a deposited thin metal film and a silicon substrate (single crystal or polycrystalline) followed by a heat treatment at an appropriate temperature. Among these silicides, titanium disilicide is currently the most widely used as it possesses the lowest resistivity (14 μΩ-cm) of all silicides, a low contact resistance and a good thermal stability. To be used in integrated circuits a silicide must have a sufficient thermal stability to withstand the entire thermal processing that is required such as layer deposition and dielectric flow. In this investigation the titanium-silicide with and without capping layers (**Chapter 3**), Ti-silicide formation through diffusion barrier layers (**Chapter 4**) and Ti-silicide formation on stressed Si(100) substrate (**Chapter 5**) was studied.

In **Chapter 3** the normal solid state reaction between a thin layer of Ti on silicon substrate was investigated. A thin Ti layer was deposited on Si(100) substrate in a high vacuum evaporation chamber before annealing at different temperatures to induce reaction. The phase formation and depth analysis was studied using XRD and RBS. It was found that at 550°C the titanium layer reacted with silicon to form titanium-rich Ti_5Si_4 and a silicon-rich $TiSi_2$ phase. The $TiSi_2$ phase that was formed was the high resistivity C49 phase. It was not clear which of the two phases was formed first. The two phases were found to grow simultaneously as the annealing time was increased. At 600°C some of the titanium-rich Ti_5Si_4 phase was converted to the silicon-rich C49-$TiSi_2$ phase. The high resistivity C49-$TiSi_2$ was then transformed to the low resistivity C54-$TiSi_2$ phase at 650°C. Previous studies regarding first phase formation during the reaction between Ti films and silicon

substrate have shown that $TiSi_2$, Ti_5Si_4, Ti_5Si_3 and TiSi [Pre-93B] were formed as first phase. The only phase given in the Ti-Si equilibrium phase diagram (see **Fig. 3.1**) not reported to form initially is Ti_3Si.

All annealed samples showed the presence of oxygen in the unreated Ti film. The oxygen concentration was found to increase throughout the Ti film as the annealing time was increased. Oxidation of titanium during Ti-silicide formation makes accurate kinetics measurements difficult. Oxygen can enter the system either during the evaporation of the Ti film or during the annealing stage. Capping layers and a sandwich technique were used in attempting to limit the unwanted oxidation. Al_2O_3 and MgO were used as capping layers. It was found that both capping layers reduced the oxygen concentration in the unreacted Ti layer by 30%. The total amount of oxygen in the MgO capped samples was less than in the Al_2O_3 capped samples. It was also found that the reaction was faster in the MgO capped samples and slower in Al_2O_3 samples. In the sandwich technique, samples were prepared by putting one sample on top of another similar sample with the front sides facing each other before annealing in a vacuum furnace. It was found that the sandwich technique reduced the oxygen concentration by 35% compared to the control samples. At high temperatures the reaction was faster in the sandwiched samples. A similar work done by de Waal *et. al.* [Waa-99] showed that using titanium oxide (labeled as Ti-O) as a capping layer can speed up the C49-$TiSi_2$ phase formation. He argued that the Ti-O cap seemed to form a gettering site which cleaned up the Ti film oxygen in the furnace.

In **Chapter 4** the effect of diffusion barrier layers on Ti-silicide formation is reported. Cr and Zr were used as diffusion barrier layers. The results showed that Ti_5Si_4 was the first phase to form. Both barrier layers reacted with silicon to form $CrSi_2$ and $ZrSi_2$ respectively. It was found that both barrier layers moved to the lower energies as the reaction progresses. Therefore, the barrier layers moved deeper into the samples as more silicide was formed which indicates that Si was diffusing through the barrier layer. Both barrier layers delayed the $TiSi_2$ formation. In agreement, previous studies have shown that Si is the dominant diffusing species during solid state reaction between titanium thin film and silicon [Bot-92, Chu-75].

The effect of stress on Ti-silicide formation is reported in **Chapter 5**. Stress was induced in the silicon substrate by either depositing Si_3N_4 or growing SiO_2 onto the backside of the substrate. The backside film deforms the sample due to differences

in thermal expansion coefficients which leads to stress throughout the substrate. Si_3N_4 has a large thermal expansion coefficient than silicon and therefore caused tensile stress on the front side of the substrate. SiO_2 being an insulator has a smaller expansion coefficient than silicon and therefore caused compressive stress on the front side of the substrate.

The reflection of laser light was used to measure the radius of curvature of the samples. Measurements were done before the first deposition and again after the first and second depositions. Stoney's equation was used to calculate stress in the deposited thin films from these measurements. Samples were prepared by depositing 200nm and 400nm Si_3N_4 (tensile stress) and 400 SiO_2 (compressive stress) on the backside of the silicon substrate prior to the deposition of the Ti thin layer. These samples were subsequently annealed at different temperatures for varying times to induce Ti-silicide formation.

It was found that samples with Si_3N_4 on the backside formed the C49-$TiSi_2$ phase and the Ti_5Si_3 phase at low temperature whereas only the Ti_5Si_3 phase was formed in the samples with SiO_2 deposited on the backside. All samples formed the low resistivity C54-$TiSi_2$ phase at 650°C. In this work the cube root of time gave the best fit to the data in all the three sample groups. Therefore the C49-$TiSi_2$ formation kinetics was neither diffusion nor reaction limited. There was no marked difference in the C49-$TiSi_2$ kinetics in the samples with Si_3N_4 on the backside. The reaction rate of $TiSi_2$ formed in the samples with SiO_2 was found to be less than that of the samples with Si_3N_4 on the backside. Therefore, the compressive stress in the substrate causes slower silicide formation. This results were in agreement with a previous work done by Cheng *et. al.* [Che-99] which also showed that tensile stress speeded up the $TiSi_2$ growth.

Appendix A

X-ray diffraction and Crystallographic data of Ti-silicide phases

Table 1: Crystal parameters of different titanium-silicide and oxide phases.

Phase	Crystal system	Name of Structure	Space group	Lattice Constants (Å)		
				a	b	c
α-Ti	Hexagonal	Mg	$P6_3/mmc$	2.95	2.95	4.68
Si	Body-centered cubic	C	La3	6.64	6.64	6.64
Ti_5Si_3	Hexagonal	Mn_5Si_3	$P6_3/mcm$	7.44	7.44	5.14
Ti_5Si_4	Tetragonal	Zr_5Si_4	$P4_12_12$	6.71	6.71	12.19
TiSi	Orthorhombic	FeB	Pnma	6.54	3.64	4.997
C49-$TiSi_2$	Base-centered orthorhombic	$ZrSi_2$	Cmcm	3.62	13.76	3.60
C54-$TiSi_2$	Face-centered orthorhombic	$TiSi_2$	Fddd	8.27	4.80	8.55
Ti_2O	Hexagonal		$P_{-3}ml$	2.96	2.96	4.85

Table 2: Characteristic lines used for the hexagonal Ti_5Si_3 identification.

2θ in degrees	{h k l} values	Intensity
12.27	110	100%
21.32	111	5.8%
27.64	310	19.6%
36.29	321	4.2%
37.38	330	7.2%
39.48	420	11.8%
43.42	421	12.5%
45.29	510	4.6%
48.87	511	6.3%

Table 3: Characteristic lines used for the tetragonal Ti_5Si_4 identification.

2θ in degrees	{ h k l } values	Intensity
38.67	2 2 1	100%
37.25	2 1 3	78.60%
41.66	1 1 5	75.30%
43.08	3 0 2	73.10%
34.99	1 1 4	31.10%
56.93	4 1 1	22.60%
63.29	4 0 4	17.90%
80.83	5 2 3	17.60%
66.43	4 2 3	17.50%
44.22	2 2 3	14%
61.68	4 2 0	12.90%
48.77	3 2 0	12.80%
45.25	3 1 2	12.40%

Table 4: Characteristic lines used for the monosilicide TiSi identification.

2θ in degrees	{ h k l } values	Intensity
46.15	1 1 2	100%
36.9	2 1 0	94.50%
41.22	2 1 1	94.10%
38.52	1 0 2	85.60%
33.36	1 1 1	75.90%
45.31	3 0 1	55.70%
50.09	0 2 0	47.30%
64.94	1 2 2	31.90%
69.82	3 2 1	27.80%
32.68	2 0 1	22.00%
68.15	2 1 3	20.50%
59.37	4 0 1	20.40%

Table 5: Characteristic lines used to identify the high resistivity C49-$TiSi_2$ phase.

2θ in degrees	**{ h k l } values**	**Intensity**
40.4	1 3 1	100%
39.23	0 6 0	17%
87.93	3 3 1	15.20%
50.35	2 0 0	14.60%
50.66	0 0 2	14.40%
31.45	1 3 0	12%
46.92	0 6 1	11.70%
27.95	0 2 1	10.80%
88.3	3 5 0	10.40%
41.15	1 5 0	8.90%
74.22	2 0 2	8.60%
87.32	2 6 2	6.10%

Table 6: Characteristic lines used to identify the low resistivity C54-$TiSi_2$ phase.

2θ in degrees	**{ h k l } values**	**Intensity**
39.18	3 1 1	100%
43.31	0 2 2	73.70%
49.82	3 1 3	47.70%
42.28	0 0 4	39.70%
67.36	3 1 5	18.40%
68.87	3 3 1	17.10%
72.05	6 0 2	14.90%
76.68	3 3 3	12.40%
23.87	1 1 1	12.20%
80.46	6 2 0	10.90%
78.03	0 2 6	11.80%

References

[Bar-92] A. I. Barg, B. S. Bokstein and L. M. Klinger, Kinetics of diffusion growth of silicides in silicon-thin-metal-film systems, J. Appl. Phys., 72 (1992) 1356.

[Ben-85] G. G. Bentini, R. Nipoti, A Armigliato, M. Berti, A. V. Drigo and C. Cohen, Growth and structure of titanium silicide phase formed by thin films on Si crystals, J. Appl. Phys., 57 (1985) 270.

[Bey-85] R. Beyers and R. Sinclair, Metastable phase formation in titanium-silicon thin films, J. Appl. Phys., 57 (1985) 5240.

[Bot-92] A. P. Botha and R. Pretorius, $CoSi_2$, $ZrSi_2$ and $TiSi_2$ formation studied by a radioactive ^{31}Si maker technique, Thin Solid Films, 93 (1982) 127.

[Cab-97] C. Cabral, Jr., L. A. Clevenger, J. M. E. Harper, F. M. D'Heurle, R. A. Roy, K. L. Saenger, G. L. Miles and R. W. Mann, Lowering the formation temperature of the C54-$TiSi_2$ phase using a metallic interfacial layer, J Mater. Res., 12 (1997) 304.

[Cam-99] R. C. Cammarata, J. C. Bilello, A. L. Greer, K. Sieradzki and S. M. Yalisove, Stresses in Multilayered Thin Films, MRS Bulletin, 24 No. 2 (1999) 34.

[Che-99] S. L. Cheng, H. Y. Huang, Y. C. Peng, L. J. Chen, B. Y. Tsui, C. J. Tsai and S. S. Guo, Effects of stress on the growth of $TiSi_2$ thin films on (001)Si, Appl. Phys. Lett., 74(1999) 1406.

[Che-00] L. J. Chen, Solid State amorphization in metal/Si system, Materials Science and Engineering, R29 (2000) 115.

[Chu-75] W. K. Chu, S. S. Lau, J. W. Mayer,H. Müller and K. N. Tu, Implanted noble gas atoms as diffusion markers in silicide formation, Thin Solid Films, 25 (1975) 393.

[Chu-78] W. K. Chu, J. W. Mayer and M. Nicolet, Backscattering Spectromety, (Academic Press, New York), (1978).

[Chu-95] C. L. Churms, Facilitating the identification of solid state phases and concentration in micro-volumes, PhD thesis, University of Stellenbosch (1995), The program may be retrieved by anonymous ftp from ftp://nacdh4.nac.ac.za/churms/ccminstl.exe

[Cul-78] B. D. Cullity, Elements of X-ray diffraction, 2nd Edition, Addison-Wesley Publishing Company, Inc., 1978,398.

[Dex-88] C. X. Dexin, H. B. Harrison and G. K. Reeves, Titanium silicide formed by rapid thermal vacuum processing, J. Appl. Phys., 63 (1988) 2171.

[Doo-85] L. R. Doolittle, Algorithms for the rapid simulation of Rutherford backscattering spectra, Nucl. Instr. And Meth., B9 (1985) 344.

[Fin-80] T. G. Finstad and M. –A. Nicolet, Interaction of evaporated palladium and titanium films with single-crystal silicon, Thin Solid Films, 68 (1980) 393.

[Gro-89] C. R. M. Grovenor, Microelectronic Materials (Adam Hilger, Bristol and Philadelphia, 1989) p. 68.

[Hsu-87] C. C. Hsu, Y. X. Wang, S. D. Yin, B. Q. Li, M. R. Ji and J. X. Wu, Formation of silicides in the Ti, $Ti(O_x)/Si(111)$, and $Ti/SiO_2/Si(111)$ systems, J. Vac. Sci. Technol. A, 5 (1987) 1402

[Hun-83] L. S. Hung, J. Gyulai, J. W. Mayer, S. S. Lau and M-A. Nicolet, Kinetics of $TiSi_2$ formation by thin Ti films on Si, J. Appl. Phys., 54 (1983) 5076.

[Lak-89] S. T. Lakshmikumar and A. C. Rastogi, The growth of titanium silicides in thin film Ti/Si structures, J. Vac. Sci. Technol. B, 7 (1989) 604.

[Man-95] R. W. Mann, G. L. Miles, T. A. Knotts, D. W. Rakowski, L. A. Clevenger, J. M. E. Harper, F. M. D'Heurle and C. Cabral, Jr., Reduction of the C54-$TiSi_2$ phase transformation temperature using refractory metal ion implantation, Appl. Phys. Lett., 67(1995) 3729.

[May-90] J. W. Mayer and S. S. Lau, Electronic Materials Science: For integrated Circuits in Si and GaAs, (Macmillan, New York, 1990), p. 251,252,307,308.

[Nic-83] Marc-A. Nicolet and S. S. Lau, VLSI Electronics: Microstructure Science, edited by N. Einspruch (Academic Press, New York, 1983), p. 415

[Ohm-99] S. Ohmi and R. T. Tung, Effect of ultrathin Mo and $MoSi_x$ layer on Ti-silicide reaction, J. Appl. Phys., 86(1999) 3655.

[Pic-88] C. A. Pico and M. G. Legally, Kinetics of titanim silicide formation on single crystal Si: Experiment and modeling, J. Appl. Phys., 64 (1988) 4957.

[Pre-93A] R. Pretorius, T. K. Marais and C. C. Theron, Thin film compound phase formation sequence: An effective heat of formation model, Materials Science and Engineering, 10 (1993) 1.

[Pre-93B] R. Pretorius, C. C. Theron and T. K. Marais, Evaluation of anomalies during nickel and titanium silicide formation using the effective heat of formation model, Materials chemistry and Physics, 36 (1993) 31.

[Pre-97] R. Pretorius and J. W. Mayer, Silicide formation by concentration controlled phase selection, J. Appl. Phys., 81 (1997) 2448.

[Qui-99] A. Quintero and M. Libera, Mechanisms for enhanced C54-$TiSi_2$ formation in Ti-Ta alloy films on single-crystal Si, J. Mater. Res., 14 (1999) 4690.

[Raa-88] I. J. M. M. Raaijmakers, A. H. Reader and P. H. Oosting, The formation of an amorphous silicide by thermal reaction of sputter deposited Ti and Si layers, J. Appl. Phys., 63 (1988) 2790.

[Sab-00] A. Sabbadini, F. Cazzaniga and T. Marangon, Influence of $TiSi_2$ formation on film thermal stability, Microelectronic Engineering, 50 (2000) 159.

[She-96] Y.-L Shen, S. Suresh, and I. A. Blech, Stresses, curvatures, and shape changes arising from pattered lines on silicon wafers, J. Appl. Phys., 80 (1996) 1388.

[Via-00] F. La Via, S. Privitera, M. G. Grimaldi, E. Rimini, S. Quilici and F. Meinardi, Determination of C54 nucleation site density in narrow stripes by sheet resistance measurements and μ-Raman spectroscopy, Microelectronic Engineering, 50 (2000) 139.

[Vil-85] P. Villars and L. D. Calvert, Pearson's Handbook of Crystallographic Data for Inter-metallic Phases, American Society for metals (1985).

[Waa-99] H. S. de Waal, The effect of diffusion barrier, stress and lateral diffusion on Thin-film phase formation, PhD thesis, University of Stellenbosch (1999).

[Wei-85] C. S. Wei, J. Van der Spiegel and J. Santiago, Electrical characteristics of fast radiatively processed titanium silicides thin films, J. Vac. Sci. Technol. A, 3 (1985) 2259.

[Zha-01] S. –L. Zhang, Z. –B. Zhang, D. –Z. Zhu and H. –J. Xu, Differences between interfacial and surface molybdenum in the formation of $TiSi_2$, J. Appl. Phys., 89 (2001) 1641.